A NUMERICAL STUDY OF AN AUTOTHERMAL REFORMER FOR THE PRODUCTION OF HYDROGEN FROM ISO-OCTANE

by

Steven W.J. Sylvestre

A thesis submitted to the Department of Mechanical and Materials Engineering

In conformity with the requirements for

the degree of Master of Science (Engineering)

Queen's University

Kingston, Ontario, Canada

September, 2007

Abstract

The development of an auxiliary power unit (APU) capable of providing climate control and electricity in long haul trucks is of significant interest due to the expected economic and environmental benefits. A potentially efficient and environmentally friendly APU design is one based on the use of an autothermal fuel reformer that converts the liquid hydrocarbon truck fuel to a hydrogen rich product gas that directly fuels a solid oxide fuel cell unit. To assist in the development of such a unit a numerical study of the autothermal reforming of iso-octane in a compact tubular reactor has been undertaken. This was done to determine the reactor performance and the factors that potentially influence its performance. Variations in the wall thermal conductivity, the catalyst thermal conductivity, the catalyst porosity, the conditions of the inlet reactant gas, and the effectiveness factor of the chemical reaction mechanism have been studied to determine their effects on the properties of the product gas stream, the temperature distribution along the reformer, the fuel conversion and the dry hydrogen yield. It has been found that higher thermal conductivities of the outer wall and in the catalyst region gave increased dry hydrogen yield and fuel conversion. The study of the effects of inlet species concentration ratios indicated that maximum hydrogen yield was obtained with an oxygen-to-fuel ratio between 1.0 and 1.15 and a steam-to-fuel ratio of approximately 3.0. Results obtained with various inlet species temperatures and bed porosities showed only small changes in the reformer performance. While the results obtained here do provide useful information about the performance of the autothermal reformer, the model used has been re-assessed and it is recommended that an improved model be used in

future work. In particular, the assumed effectiveness factors for all of the chemical reactions occurring in the catalyst region need to be improved. This was highlighted by the fact that a brief study indicated a very strong dependence of the reformer product gas composition on the effectiveness factor. This indicates that while the present model is able to predict trends in the reformer performance, it is limited in its accuracy due to the fact that the effectiveness factor used is only approximately known.

Acknowledgements

Firstly I wish to thank the Mechanical Engineering Department of Queen's University for providing me with the opportunity to pursue graduate studies at this level of education.

I am particularly grateful to my supervisor, Dr. Patrick Oosthuizen for his guidance and support and continuous encouragement throughout this process.

I would also like to express my gratitude to Dr. Brant Peppley and Dr. Chris Thurgood of the Department of Chemistry and Chemical Engineering at the Royal Military College who were highly insightful and incredibly generous with their time.

I wish to thank my colleagues and friends in the Heat Transfer Lab and the Fuel Cell Research Centre who collaborated in the overall project and who helped me throughout my studies.

I would like to acknowledge the Auto 21 Network of Centres of Excellence for providing the funding necessary for me to conduct my research and for hosting events for student collaboration of innovative research.

Finally, I must thank my parents and Christine for motivating me and for giving me their love and support during this entire experience.

Table of Contents

List of Figures

List of Tables

Nomenclature

A	Arrhenius pre-exponential constant (units vary depending on reaction)
c_p	gas phase heat capacity (kJ/kg·K)
d_p	diameter of catalyst particle (m)
D_{eff}	effective diffusion coefficient (m^2/s)
D_k	knudson diffusion coefficient (m^2/s)
D_m	bulk diffusion coefficient (m^2/s)
E	Arrhenius activation energy (kJ/mol)
F_x	axial momentum source term (m/s^2)
F_r	radial momentum source term (m/s^2)
h	enthalpy (kJ/mol)
h_i^o	standard enthalpy of formation of species i (kJ/mol)
J	diffusion flux (kg/m·s)
k	thermal conductivity (W/m·K)
k_b	Boltzmann constant (kg·m^2/s^2·K)
k_f	fluid thermal conductivity (W/m·K)
k_s	solid thermal conductivity (W/m·K)
k_{eff}	effective thermal conductivity (W/m·K)
$k_{r,n}$	reaction rate constant for reaction n (units vary depending on reaction)
K_i	adsorption coefficient of species i (bar^{-1})
K_n	equilibrium constant of reaction n (units vary depending on reaction)
L	axial reactor length (m)
L_d	characteristic length (m)

M_i	molar mass of species *i* (kg/mol)
p_i	partial pressure of species *i* (bar)
Δp	pressure change (bar)
Pe	Peclet number (dimensionless)
Pr	Prandtl number (dimensionless)
r_i	rate of production of species *i* by chemical reaction (mol/m^3·s)
r	radial direction coordinate (m)
Re	Reynolds number (dimensionless)
R	universal gas constant (KJ/mol·K)
S	general source term (units vary depending on governing equation)
S_ϕ	general source term for flow variable (units vary depending on governing equation)
t	tortuosity (dimensionless)
T	absolute temperature (K)
T_{ref}	reference temperature (K)
u	axial direction velocity component (m/s)
U_s	superficial velocity (m/s)
v	radial direction velocity component (m/s)
x	axial direction coordinate (m)
Y_i	mass fraction of species *i* in mixture (dimensionless)

Greek Symbols

α	thermal diffusivity (m^2/s)
β	relaxation factor (dimensionless)
η	catalyst effectiveness factor (dimensionless)
σ	diameter of gas molecule (m)
ϕ	general flow variable (units vary depending on variable)
ϕ_f	face value of general flow variable (units vary depending on variable)
$\overline{\phi}_f$	arithmetic mean of general flow variable face value (units vary depending on variable)
ϕ_n	Thiele modulus (dimensionless)
φ	packed bed porosity (dimensionless)
θ	kinetic concentration function for catalytic and gas-phase reactions (units vary depending on reaction)
ρ	fluid density (kg/m^3)
μ	fluid kinematic viscosity (kg/m·s)
λ	mean free path (m)

Chapter 1
Introduction

1.1 Background

As the developing countries around the world continue to prosper, particularly countries of dense population in Asia and Central and South America, a steady exponential increase in the demand for energy has become an evident issue. The Energy Information Administration (2007) estimated that the world consumed 421 quadrillion British Thermal Units (BTU) of energy in 2003 (approximately 444 x 10^{21} KJ) with a projected 45% increase by 2030. The projected energy consumption in quadrillion BTU's from 1980 to 2030 is shown in figure 1.1:

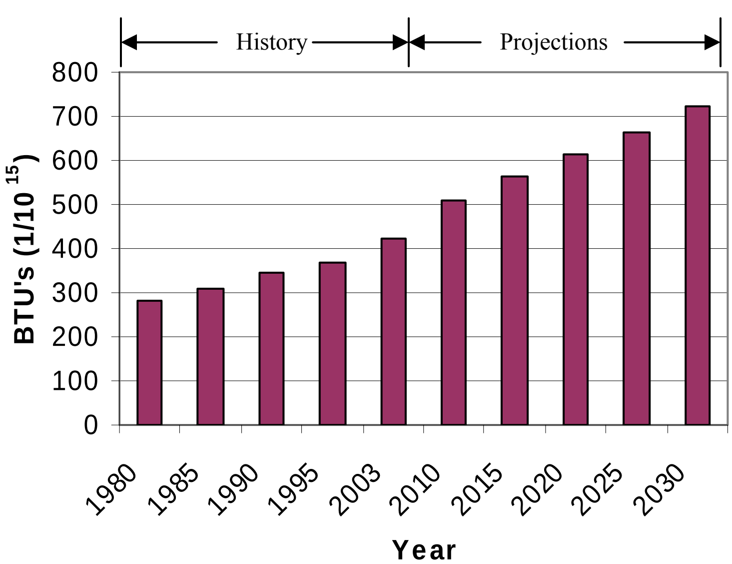

Figure 1.1: World marketed energy consumption per year from 1980-2030 (EIA, 2006)

This enormous growth in energy consumption is not sustainable from current energy production methods as almost 80% of this demand is satisfied by the use of fossil fuels (Asif and Muneer, 2007). It is believed that oil production has or will peak very shortly and that there will be a steady decline as the oil reserves run out. Perhaps more unfortunately is the environmental impact on the earth resulting from this consumption level. This energy crisis coupled with the growing awareness and evidence of global warming has promoted extensive research for alternative energy sources. It has often been said that a shift towards a hydrogen based economy will solve many of these issues, though there are many obstacles that make a solely hydrogen based economy nearly impossible.

Hydrogen is an abundant element on the earth but it does not naturally exist in its diatomic molecular form as H_2. It needs to be extracted from sources like water or hydrocarbons which can be a difficult and costly process to obtain pure hydrogen. In an ideal world, hydrogen would be produced by harnessing wind and solar energy to electrolyze water thus having an emission free production and consumption of hydrogen. Unfortunately, the enormous capital investment behind these projects has restricted its potential, and additionally the infrastructure required for the hydrogen distribution would require a tremendous expenditure. To aid the transition toward the use of hydrogen as an energy source, small changes must be made to achieve the environmental benefits while still being economically feasible. The transportation industry continues to provide funding for research and development in fuel cell vehicle technology and companies such as Honda, General Motors, Toyota, and Ford, to name a few, have already introduced commercially available vehicles that operate solely on hydrogen. Even with the growing popularity of hydrogen powered fuel cell vehicles, the near non-existent infrastructure for hydrogen fuel production and distribution limits its progress. For this reason, there has been a growth in interest in the production of hydrogen via an onboard hydrocarbon reforming process that could be suitable for powering a fuel cell stack in a variety of applications.

Larger vehicles such as transport trucks are high consumers of fuel and rarely turn off their engines. This is because they require power to heat or to cool the cabin areas and to power electrical systems for refrigerators, lighting, computers, or other electronic devices. When engines are running at idle, they are very inefficient and as a result produce higher amounts of emissions and particulate matter in the exhaust. Argonne National Laboratories (2007) has estimated that on average, a commercial long haul truck will idle 6 hours per day. With approximately 400 000 trucks in operation in the United States, this amounts to approximately 3 billion gallons of fuel usage during this idling periods. It was also estimated that about 10 million tons of CO_2, 50 000 tons of nitrogen oxides, and 2000 tons of particulate matter would be expelled as a result of these idling times over the course of the year. Engine idling is an undesirable yet unavoidable issue that transport trucks face. On-board reforming may provide a method of greatly reducing engine idling time. By designing a small scale reformer combined with a compact fuel cell stack, enough energy could be produced to power all the electrical needs of the truck therefore eliminating the need to remain in idle while at rest. The advantages of introducing such a system would be reduced overall fuel consumption, reduced emissions, and a longer engine life.

1.2 Overview of Thesis Development

In the present study, the development of a small scale autothermal reformer proposed by personnel at the Fuel Cell Research Centre has been considered. The purpose was to design a reformer that would produce a hydrogen rich product gas to power a solid oxide fuel cell unit. This device would be used as an auxiliary power unit in long haul trucks to eliminate the need for idling at rest stops when electrical power is still in demand. This project is a continuation of the work done by the Queen's/RMC Fuel Cell Research Group which included the initial design and construction of a concentric cylinder benchscale autothermal reformer for the conversion of iso-octane to hydrogen. The objectives of the design were to construct a prototype reactor that could facilitate heat transfer throughout the bed while meeting plug flow criteria, that was robust in design, and would produce high hydrogen yield. A concentric cylinder configuration was developed which had a central inlet cylinder where fuel oxidized in a catalyst bed to provide heat that would be conducted radially to an intermediate cylinder to promote the steam reforming reaction in a secondary catalyst region. Flow would then continue to pass through a non-catalytically active outer cylinder region before passing through the outlet tube. The proposed design that was manufactured is illustrated in figure 1.2 with the dimensions being given in Table 1.1:

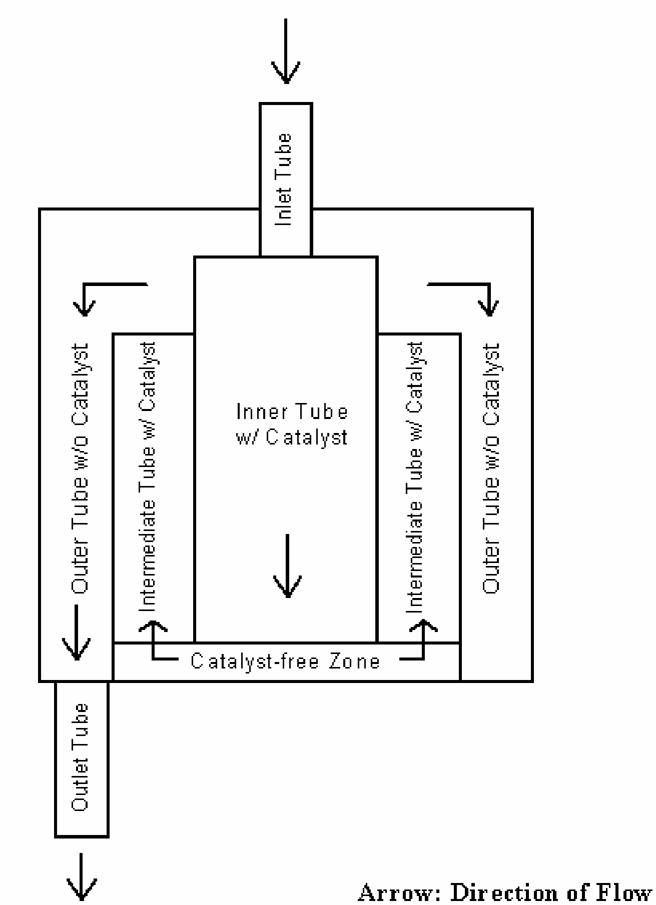

Figure 1.2: Cross-sectional view of concentric cylinder design proposed by Middleton (2004)

Table 1.1: Dimensions of the concentric cylinder design by Middleton (2004)

Region	Length (mm)	Inner Diameter (mm)	Outer Diameter (mm)
Inlet Pipe	51	13	17
Outlet Pipe	51	13	17
Primary Cylinder	127	51	60
Secondary Cylinder	114	111	114
Outer Cylinder	156	152	162

After construction of the design by Middleton (2004), testing was undertaken by Caners (2005) at the Fuel Cell Research Centre. Several tests were run varying the inlet species temperature and the oxygen-to-fuel and steam-to-fuel ratios, a wide range of results thus being obtained. Caners (2005) reported fuel conversion percentages that ranged from 69% to 97% and dry hydrogen output percentages that ranged from 26% to 62%. A gas chromatograph was used to accurately measure these outlet species concentrations, though determining the behaviour inside the reactor was evidently more difficult. A temperature profile inside the reactor was measured using fifteen thermocouples inserted along the fluid pathway. This showed large temperature gradients especially at the beginning of the catalyst region, indicating that the large heat release of the exothermic oxidation reaction was not being conducted effectively throughout the bed as desired. With the limited number of thermocouples used the actual temperature distribution was still in question as were the variations of the chemical reaction rates along the bed.

A computer model was developed to further understand the performance of the reactor and to provide a working mathematical model that could aid in future design improvements. A 1-dimensional model of this reactor was created by Li (2004) at Queen's University. This utilized a set of three chemical reactions; an oxidation reaction, a steam reforming reaction, and a water-gas shift reaction. First order Arrhenius-type rate expressions were developed for each reaction using standard gas phase kinetics, meaning rate expressions were developed only as a function of species concentrations, neglecting parameters such as adsorption coefficients and equilibrium constants. Activation energies and pre-exponential factors in the Arrhenius equation were found by fitting reaction rates at specific temperatures to experimental data provided by the catalyst manufacturer. This model produced results that were in accordance with the observed trends in the reactor behaviour and hydrogen yield could be estimated to within a 1% error, though the other predicted species concentrations were in error by as much as 35%. These results were therefore used to confirm the temperature trends of the experimental work and were intended to form the basis for the development of a more sophisticated model.

A basic 2-dimensional model was additionally proposed by Li (2004) that characterized the flow field of the reactor but neglected the chemical reaction scheme. This model was adopted by McIntyre (2005) and emphasis was placed on improving the chemical reaction mechanism and more accurately defining the physical properties of the reactor. Pacheco et al. (2003) performed a numerical and experimental study on the autothermal reforming of iso-octane over a platinum on ceria oxide based catalyst. A computational model was developed that accurately described the species concentrations of the reformate gas compared to experimental results. Since the catalyst used in the reformer proposed by Middleton (2004) was also a platinum on ceria oxide based catalyst, the Pacheco et al. (2003) model was adopted for the modeling work by McIntyre (2005). McIntyre (2005) was able to show that the predicted species concentrations of the outlet stream were accurate within a small margin of error, except the carbon monoxide concentration which was over-predicted and the carbon dioxide concentration which was under-predicted. It was concluded that the numerical results were in good agreement with the findings of Pacheco et al. (2003) model and that the results could be used for comparison to experimental work.

In accordance with the conclusions from the experimental results of Caners (2005), the results from McIntyre (2005) showed high temperature gradients at the catalyst bed entrance, and also showed a loss of heat to non-catalytically active areas of the reactor. It was also evident from the modeling work that majority of the steam reforming reaction had gone to completion before the end of the first catalyst bed, indicating the concentric cylinder design was not of benefit. The thermal conductivity of the reformer needed to be addressed as well as reducing the size of the reactor.

The new reformer design proposed by the personnel at the Fuel Cell Research Centre was greatly reduced in size by utilizing a single cylinder configuration. The previous reformer cylinder diameter was restricted to a minimum size that was 10 catalyst particles in length, which was a criteria necessary to achieve plug flow. To reduce the reformer diameter while meeting plug flow criteria, a new platinum on zirconia-ceria catalyst pellet averaging in diameter around 0.285mm was selected as compared to the previous catalyst pellet which had an average diameter of around 5mm. This allowed for the reactor diameter to be reduced to 9.5mm. In order to obtain better measurements of the temperature profile along the reformer bed provision was made for the inclusion of a multi-point thermocouple along the centreline of the bed. The configuration of the new reformer is shown in figure 1.3.

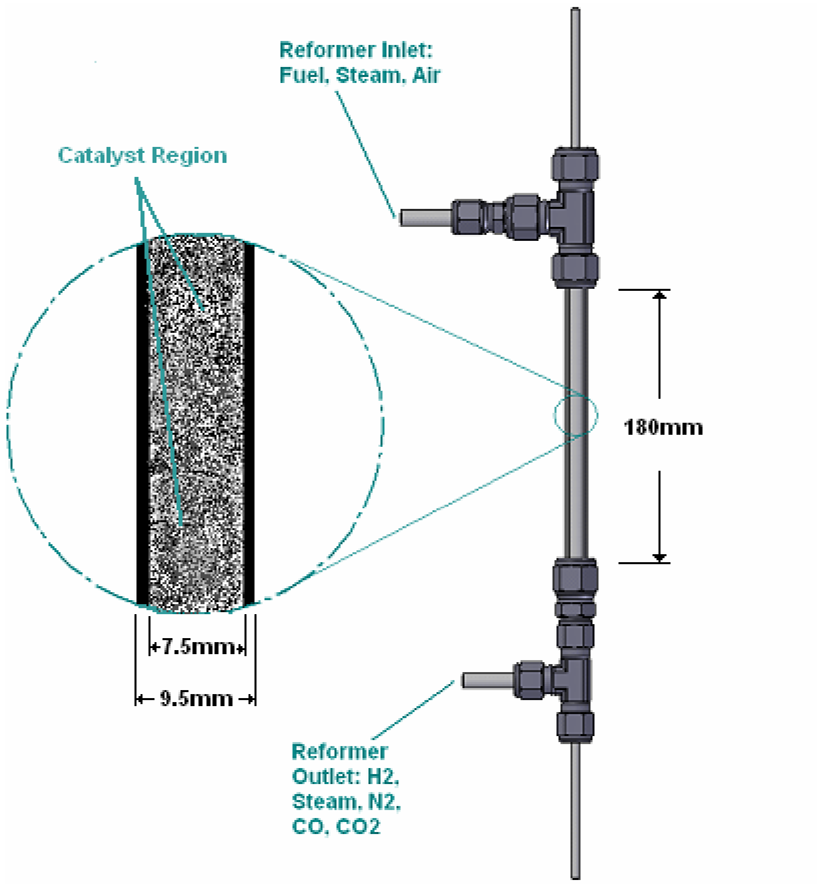

Figure 1.3: Cross-sectional diagram of the reformer proposed by personnel at the Fuel Cell Research Centre

1.3 Scope of Thesis

The present study is an adaptation of the work completed by McIntyre (2005) which describes a refined 2-dimensional, axis-symmetric, single cylindrical autothermal reformer and is chemically described by the Pacheco et al. (2003) mechanism. The objectives of the thesis are to:

- Investigate the effects of axial heat conduction by varying the wall thermal conductivity and the catalyst thermal conductivity
- Determine the change in flow characteristics and outlet species concentration with varying porosity
- Vary air-to-fuel and steam-to-fuel inlet stream ratios to determine the effect of these changes on the performance of the reformer
- Determine the fuel conversion and dry hydrogen yield with varying gas-hourly-space-velocities
- Analyze the effects of varying the effectiveness factor on the performance of the reformer

Chapter 2
Literature Review

2.1 Introduction

This chapter reviews the literature that describes potential methods of reforming hydrocarbons, fuels available for autothermal reforming, reaction mechanisms that describe the reforming process of these fuels, catalysts that are available for autothermal reforming, the operating conditions of autothermal reformers, and the applicability of autothermal reformers as components in auxiliary power units (APU's).

2.2 Reforming of Hydrocarbons

There are several possible methods of producing hydrogen by reforming, the most common methods including steam reforming, partial oxidation reforming, and auto-thermal reforming. Each of these methods has its advantages and disadvantages depending on the application and they are discussed briefly in the following section.

2.2.1 Steam Reforming

Steam reforming is a popular method of obtaining hydrogen since it can be done quite efficiently in large scale industrial applications. Ideally, a hydrocarbon will react with steam to produce hydrogen and carbon monoxide:

$$C_nH_m + nH_2O \rightarrow nCO + \left(n + \frac{m}{2}\right)H_2 \tag{1.1}$$

This is considered to be the most effective method of producing the highest hydrogen molar yield per mole of fuel. Steam reformers have been used for decades and can easily be scaled to any required size. The main drawback of steam reforming is that it is an endothermic process requiring the addition of heat to make the reaction proceed and this results in a relatively low overall system efficiency. The inlet gases must be preheated to high temperatures, around 700°C or higher, to ensure a high conversion rate of fuel to hydrogen. High temperature heat exchange equipment and pre-heaters can be very costly and quite inefficient for small scale applications such as vehicle APU's. Other issues are with the relatively long system startup time and the slow dynamic response when higher or lower hydrogen yields are required.

2.2.2 Partial Oxidation

Partial oxidation is a process where the overall reaction can be described as the reaction of a hydrocarbon fuel with oxygen over a catalytically active surface to produce hydrogen and carbon monoxide. The overall reaction is slightly exothermic which eliminates the need for pre-heating compared with a basic steam reformer. The basic partial oxidation reaction is assumed to be as follows:

$$C_nH_m + \frac{n}{2}O_2 \rightarrow nCO + \frac{m}{2}H_2 \tag{1.2}$$

Providing pure oxygen whether on a large scale or small scale is usually not a viable option. Therefore the reaction is fed with air to provide the oxygen which results in an overall decrease in reactor efficiency and dilutes the hydrogen product gas since nitrogen is a non-reactive molecule in the reaction (Rabe, 2007). Partial oxidation therefore will not produce as high of a yield of hydrogen rich gas compared to steam reforming, but it is considered a more simple system that does not require the addition of pre-heaters or heat exchange equipment.

2.2.3 Autothermal Reforming

Auto-thermal reforming is a process where fuel, air and steam are injected together over a catalytically active region where an oxidation reaction will occur followed by a steam reforming reaction. The oxidation reaction is highly exothermic and thus emits a large amount of heat. The elevated temperature promotes the reaction of the steam with the remaining fuel in a steam reforming reaction. In the ideal situation, the overall process can be described by the following chemical reaction:

$$C_nH_m + aO_2 + (2n-2a)H_2O \rightarrow \left(2n - 2a + \frac{m}{2}\right)H_2 + nCO_2 \qquad (1.3)$$

The oxygen content is typically supplied by using air containing nitrogen which dilutes the product gas. The advantage of autothermal reforming is that higher hydrogen yield rates are obtained from the steam reforming reaction compared to the hydrogen yield of the partial oxidation reaction. Also, the system requires much lower pre-heating temperatures of the inlet gas stream as compared with the high temperatures required with a basic steam reformer.

2.2.4 Water-Gas-Shift Reaction

In the process of steam reforming a secondary reaction will occur in the presence of a catalyst at elevated temperatures. Fortunately it is a desired process since it utilizes the undesirable carbon monoxide product gas of the steam reforming reaction to produce additional hydrogen and carbon dioxide by the water-gas-shift reaction:

$$CO + H_2O \Leftrightarrow CO_2 + H_2 \tag{1.4}$$

This reaction is an equilibrium reaction which means that once equilibrium is achieved, the reaction will stop and if equilibrium is exceeded, the reaction can occur in reverse, therefore the complete consumption of the carbon monoxide gas will not occur.

2.3 Reforming of Various Hydrocarbon Fuels

There are many fuels available for use in catalytic autothermal reforming. Unfortunately, some of these fuels may not be readily available, an example being iso-octane, the surrogate fuel of gasoline. For this reason, much interest has been directed at the reforming of more widely available commercial fuels such as gasoline, diesel, and natural gas. Unfortunately these commercial fuels are not homogeneous fuels and therefore result in added complexity to the reforming process. These fuels all contain a mixture of alkane, alkene, and aromatic hydrocarbons. Aromatics have been shown to reduce kinetic activity during the reforming process and to also increase carbon formation leading to catalyst deactivation (Kang, 2006). In addition, commercial fuels contain sulfur compounds that can also contribute to catalyst deactivation. Therefore selection of the fuel for the reformer will have significant affects on the reformer performance.

From a thermoneutral perspective, which is ideal in autothermal reforming, Ahmed and Krumpelt (2001) calculated the maximum theoretical efficiencies for many hydrocarbon fuels. They found that liquid methane could yield a lower-heating-value (LHV) efficiency of 93.9%, while gasoline had a LHV efficiency of 90.8%. An experimental analysis of several fuels was conducted and verified that heavier hydrocarbons resulted in lower overall maximum efficiencies. This was accredited to lower hydrogen to carbon ratios in heavier hydrocarbon molecules. Due to the higher maximum efficiency potential, methane or methanol fuels have primarily been used in the majority of the research conducted on autothermal reforming. Although these lighter fuels have the potential for higher efficiency, gasoline and diesel products are more widely available making them a more convenient choice of fuel, especially for the purpose of on-board fuel reforming.

More research on the use of gasoline and diesel for autothermal reforming as well as their surrogate fuels (C_8H_{18}, $C_{16}H_{34}$) has been conducted recently. Kang and Bae (2006) comparatively analyzed the use of gasoline and diesel versus their surrogate fuels to determine the differences in the product gas concentrations. Inlet temperatures were varied and product gas concentrations were measured for the commercial fuel versus its surrogate fuel. Figures 2.1 and 2.2 show the results obtained by Kang and Bae (2006).

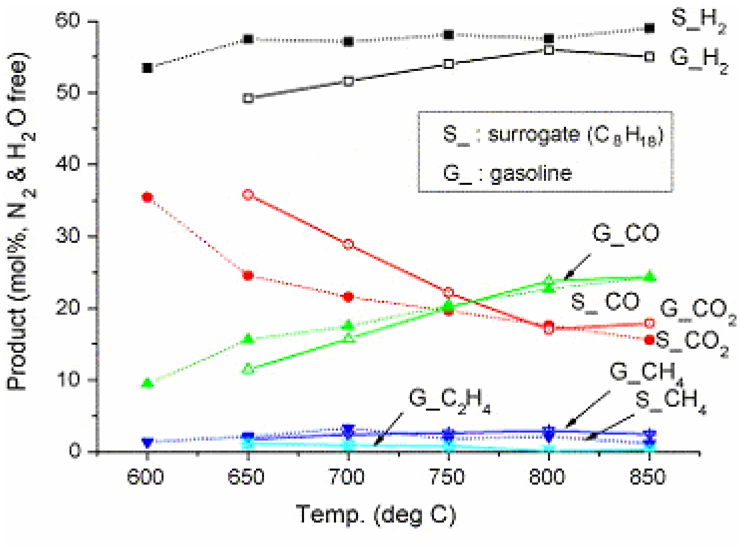

Figure 2.1: Comparison of product distributions obtained using gasoline and C_8H_{18}

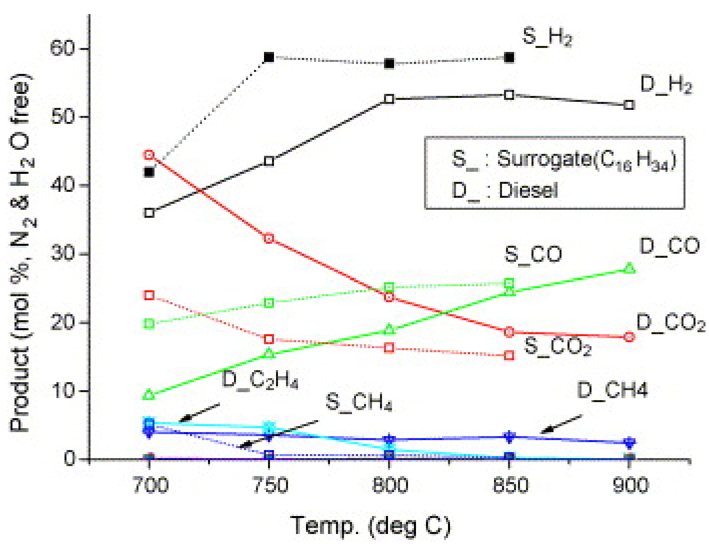

Figure 2.2: Comparison of product distributions obtained using diesel and $C_{16}H_{34}$

In both situations, there were obvious differences in the product gas concentrations of several species especially with the comparative study of diesel versus its surrogate fuel $C_{16}H_{34}$. Kang and Bae (2006) studied fuel conversion rates of different alkane and alkene hydrocarbons and used this information to create a mixture that would better simulate gasoline and diesel fuels. The synthetic fuels that were derived as a result of this work are listed below in Table 2.1.

Table 2.1: Composition of synthetic fuels with respect to volume

Simulated Gasoline ($C_7H_{13.9}O_{0.1}$)	Simulated Diesel ($C_{11.6}H_{19.5}$)
Iso-octane (C_8H_{18}): 50% by vol	*Dodecane ($C_{12}H_{26}$): 70% by vol*
Hexane (H_6H_{14}): 20% by vol	*Methyl Naphthalene ($C_{11}H_{10}$) 30% by vol*
Tolulene (C_7H_8): 10% by vol	
MTBE ($C_5H_{12}O$): 10% by vol	

The simulated fuels were determined to better match conversion behaviour of reactant fuel to product gas while maintaining an appropriate level of alkane and alkene hydrocarbons to aromatic hydrocarbons. The synthetic fuels were tested again against the commercial based fuels at different inlet temperatures to observe product gas concentrations. These results are given in figures 2.3 and 2.4.

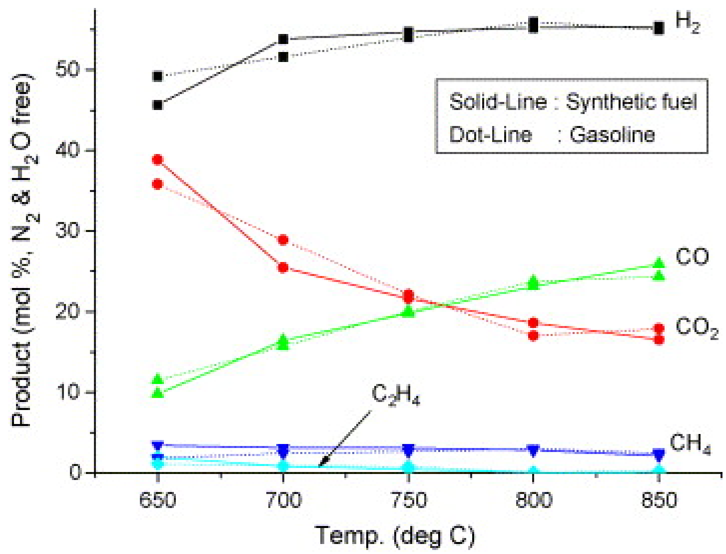

Figure 2.3: Product distribution obtained using synthetic and commercial gasoline

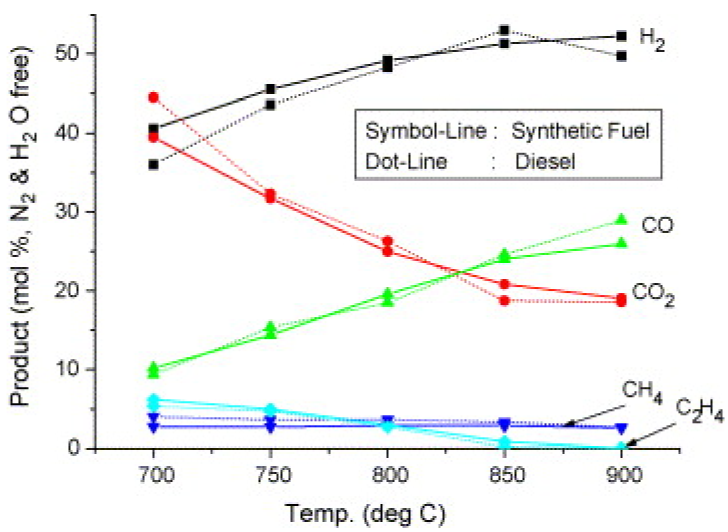

Figure 2.4: Product distribution obtained using synthetic and commercial diesel

The results of the study indicate a good correlation between the synthetic fuel results and the commercial fuel results for the concentrations of the outlet gases. By using synthetic fuels that mirror the performance of commercial fuels, researchers can perform a more indepth analysis of the chemical reforming process since all constituents of the reactant gas are known and improved chemical models can be developed for computational modeling purposes.

2.4 Chemical Reaction Mechanisms for Autothermal Reforming

The chemical reaction mechanism for describing the autothermal reforming process of any fuel can be difficult to accurately describe. This is due to the fact that the reforming process is not a simple one step reaction mechanism. In reality, it is comprised of several reaction steps or even hundreds to thousands of steps for fuels comprised of heavier hydrocarbons or mixtures of several hydrocarbons. Therefore determining an appropriate reaction mechanism for a surrogate fuel such as iso-octane can be a difficult process and disagreements exist between researchers on what is the common set of reactions.

Pacheco et al. (2003) developed a chemical reaction mechanism describing the autothermal reforming of iso-octane. This reaction mechanism was developed on the basis of methane steam reforming and methane partial oxidation by Xu and Froment (1989) and Jin et al. (2000) respectively. Pacheco et al. (2003) assumed that the reforming of methane closely reflected the behaviour of iso-octane reforming and that a similar chemical reaction mechanism could be derived from the methane reforming reaction mechanism. The reaction mechanism that was developed is as follows:

i) Oxidation: $C_8H_{18} + 12.5O_2 \rightarrow 8CO_2 + 9H_2O$

ii) Steam Reforming A: $C_8H_{18} + 8H_2O \rightarrow 8CO + 17H_2$

iii) CO_2 Reforming: $C_8H_{18} + 8CO_2 \rightarrow 16CO + 9H_2$

iv) Steam Reforming B: $C_8H_{18} + 16H_2O \rightarrow 8CO_2 + 25H_2$

v) Water-Gas-Shift: $CO + H_2O \rightarrow CO_2 + H_2$

This basic chemical reaction mechanism accounts for the primary reactions that occur in the autothermal reforming of iso-octane. Pacheco et al. (2003) were able to develop rate expressions for each reaction so that a computer model could be developed to describe the autothermal reforming of iso-octane. This was done by performing several tests on the autothermal reforming of iso-octane as different inlet temperatures and gas-hourly-space-velocities. However the values of these input variables were not given. This allowed new kinetic reaction constants to be determined so that the results of the mathematical model closely reflected the results of the experimental trials. Unfortunately this simple reaction mechanism does not account for the formation of lighter hydrocarbons that have been shown to be present in the product gas stream of autothermal reformers (Roychoudhury et al., 2005).

Villegas et al. (2005) performed a chemical kinetics and experimental study on the autothermal reforming of iso-octane. The thermodynamic study presented a detailed chemical reaction mechanism describing several additional reactions to those in the Pacheco et al. (2003) mechanism. The reaction mechanism that was described is as follows:

i) Total Oxidation:	$C_8H_{18} + 12.5O_2 \rightarrow 8CO_2 + 9H_2O$
ii) Partial Oxidation:	$C_8H_{18} + 4O_2 \rightarrow 8CO + 9H_2$
iii) Steam Reforming:	$C_8H_{18} + 8H_2O \rightarrow 8CO + 17H_2$
iv) Cracking:	$C_8H_{18} \rightarrow 8C + 9H_2$
v) CO_2 Reforming:	$C_8H_{18} + 8CO_2 \rightarrow 16CO + 9H_2$
vi) Water-Gas-Shift:	$CO + H_2O \rightarrow CO_2 + H_2$
vii) Methanation:	$CO + 3H_2 \rightarrow CH_4 + H_2O$
	$CO_2 + 4H_2 \rightarrow CH_4 + 2H_2O$
	$C + 2H_2 \rightarrow CH_4$
viii) Boudouard:	$2CO \rightarrow C + CO_2$
iv) Carbon Gasification:	$C + H_2O \rightarrow CO + H_2$

This chemical reaction mechanism provides a more detailed description of the chemical reactions that take place during the autothermal reforming of iso-octane. Unfortunately, Villegas et al. (2005) did not develop kinetic data for this reaction mechanism so rate expressions are not available and further experimental analysis would be required to develop this data. Xu and Froment (1989) considered some of these additional reactions for the steam reforming of methane, but reported that these reactions occur at a much slower rate than reactions such as the steam reforming and water-gas-shift reactions. As mentioned above, there are lighter hydrocarbons present in the reformate gas for the autothermal reforming of iso-octane and therefore these additional reactions that occur and in particular the methanation reactions should be considered in the modeling.

2.5 Catalysts for Autothermal Reforming

Catalysts for use in autothermal reforming continue to improve with technological advancements in production methods. It is common to find catalysts in autothermal reformers that are manufactured with transition metals supported on an oxide-ion-conducting substrate that has been doped with a small amount of a non-reducible element, which is the same technology on which solid oxide fuel cell catalysts are based. Krumpelt et al. (2002) conducted catalyst testing of several different transition metals doped on a ceria base. They examined the conversion rates of iso-octane at different temperatures for each metal. They were able to show that at a space velocity of 3000 h^{-1}, all transition metals tested exhibited a conversion of more than 95% at 600ºC, though, below this temperature, the conversion percentage of Ag, Ni, and Co all dropped rapidly. The results of this study are shown in figure 2.5.

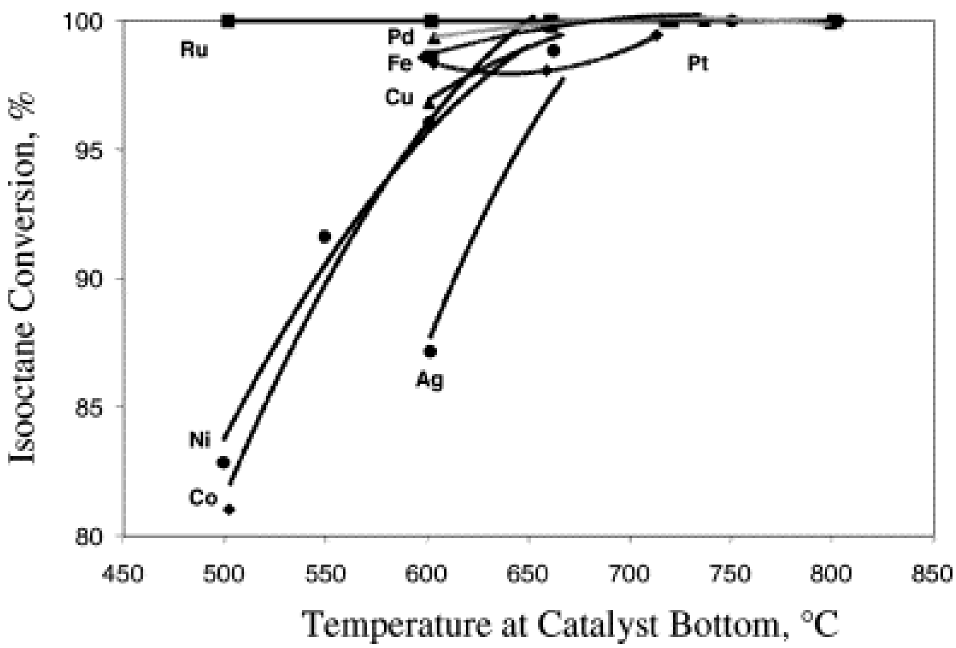

Figure 2.5: Conversion of isooctane exhibited by various transition metals supported on doped ceria. (O/C = 0.46, H_2O/C = 1.14, GHSV = 3000 h^{-1})

Of the metals tested, Ru, Pt, and Pd performed the best over the broadest range of temperatures. It is desirable to have a catalyst that is highly active at the lower range of temperatures so that less exotic materials can be used in the reformer design as well as to limit the high pre-heating temperatures. This is why metals such as Ru, Pt, and Pd are typically found in autothermal reformers (Tiemersma, 2005, Roychoudhury, 2005). Between these three metals, there are some notable differences in the properties of the product gas. At temperatures between 600 and 800ºC, the Pt catalyst yields small amounts of C_2H_x and CH_4 whereas the Ru and Pd catalysts had only small amounts of CH_4 and no traces of C_2H_x. Roychoudhury et al. (2005) also performed a study on the autothermal reforming of isooctane with a platinum and a rhodium catalyst. The platinum catalyst produced significant levels of CH_4, C_2H_4 and C_2H_6 while the rhodium catalyst only produced significant levels of CH_4. For the purpose of producing hydrogen by autothermal reforming, lighter hydrocarbons are not desired in the reformate gas and therefore these studies indicate that a rhodium or ruthenium catalyst may be better suited for the autothermal reforming of iso-octane.

2.5.1 Catalyst Deactivation

The active lifespan of a catalyst pellet can be limited by several factors. High temperature reactors are particularly vulnerable to catalyst deactivation due to thermal sintering, coking, poisoning, and masking (Gudlavalleti, 2007). Gudlavalleti et al. (2007) were interested in determining the long term effects of catalytic behaviour in autothermal reformers. For the study, desulfurized methane was used as the reactant fuel, this fuel passing over a commercially available monolithic precious metal catalyst. Thermocouples were placed throughout the autothermal reformer to record temperatures after 149, 279, 456, 560, and 581 hours of operation. It was found that there was a significant increase in temperature with time along specific lengths of the reactor bed suggesting a reduction in the endothermic steam reforming reaction. Data from this study was then used to develop a mathematical model to try to predict the effects of the catalyst aging process after 100,000 hours of operation. Using the results given by this model, estimates of the catalyst bed temperature with axial distance along the reactor were made. The results of the experimental temperature profiles along with a superimposed profile of the long term operation model are shown in figure 2.6.

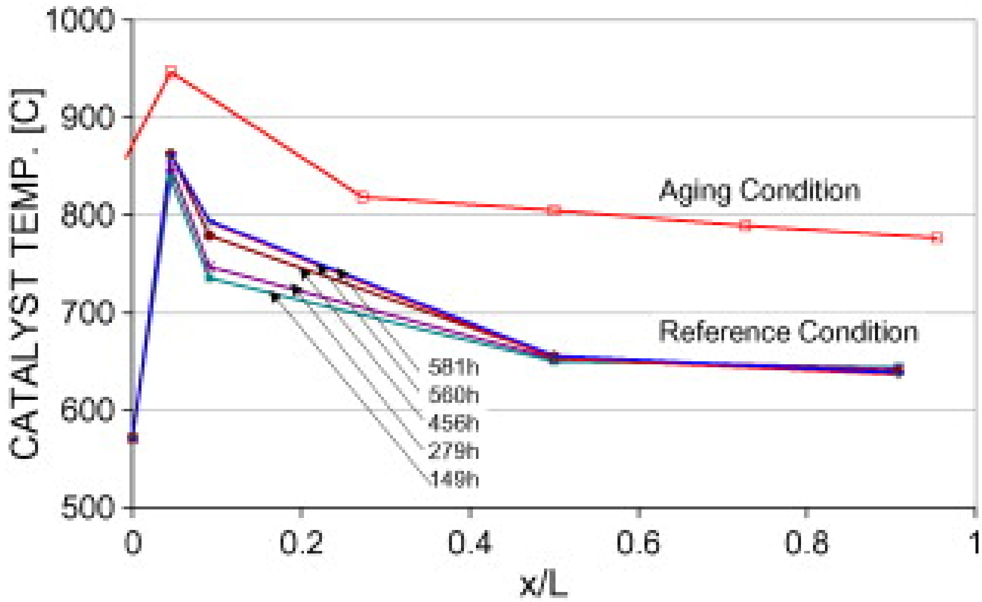

Figure 2.6: Temperature profile of catalyst bed after various durations of operation at reference conditions. (Accelerated aging condition model results are superimposed on the graph. Lines connecting the measurement points are meant for grouping and not to indicate the actual temperature profile)

The increase in temperature through the catalyst bed indicated by the experimental results is clearly visible in the experimental data in figure 2.6, and the hypothesized aging model suggests a dramatic increase in temperature throughout the entire bed and demonstrates the effects of the reduction in the steam reforming reaction rate with catalyst deactivation.

2.6 Reactor Operating Conditions

There are a number of independent variables that need to be chosen when defining the operating conditions of an autothermal reformer. The oxygen-to-fuel ratio, the steam-to-fuel ratio, the inlet stream velocity, the inlet stream temperature, the operating pressure and the type of catalyst all play key roles in determining the performance of the reformer and need to be selected appropriately depending on desired output.

In principle, autothermal reforming is conducted thermoneutrally to obtain a balance between heat produced and consumed by the reactions. While operating at a thermoneutrally balanced state may provide the highest overall efficiency, maximum hydrogen yield is typically of primary concern as hydrogen is the only desired by-product of the reaction. By varying the inlet species concentrations and operating conditions, higher hydrogen output levels can be achieved.

Several researchers have conducted experimental studies of autothermal reforming, though a rather limited amount of this research has been concerned with investigating the use of iso-octane as a fuel. Villegas et al. (2005) performed an experimental study of the catalytic autothermal reforming of iso-octane to determine optimal conditions for hydrogen production over a Pt/ceria-zirconia catalyst. Results of this study for varying the oxygen-to-carbon ratio are shown in figure 2.7.

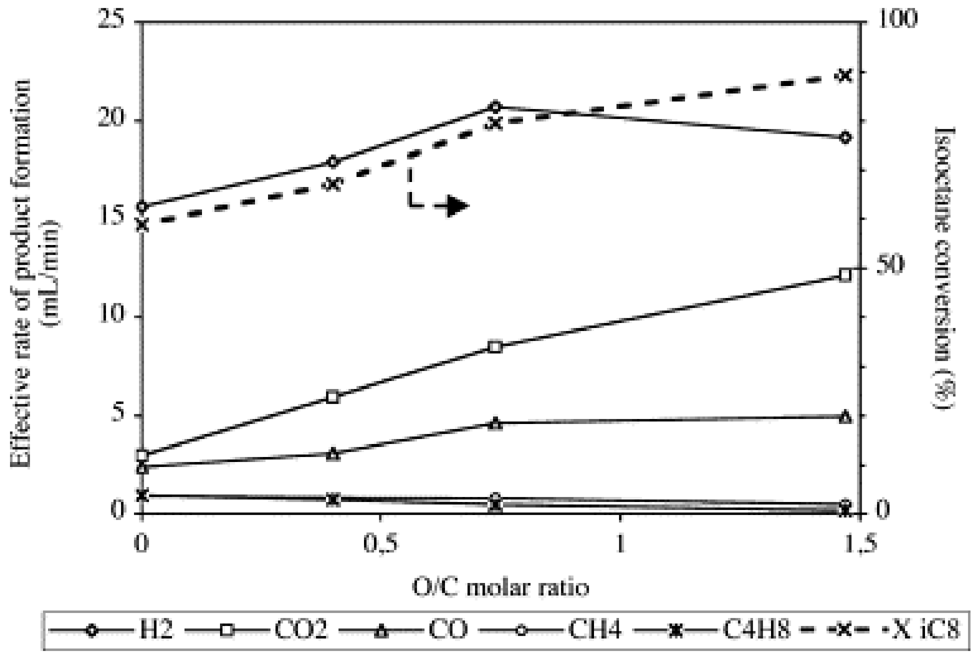

Figure 2.7: Iso-octane conversion and products distribution as a function of O:C ratio (conditions: 680 °C, 1.3 vol.% isooctane, H_2O:C = 1.5)

Figure 2.7 shows that with an inlet temperature of 680ºC and a space velocity of approximately 150000 h^{-1}, the highest rate of hydrogen production is obtained at an oxygen-to-fuel molar ratio of 0.75 and that iso-octane conversion is approximately 80%. The effects of varying the steam-to-fuel ratio were also considered and the results obtained are shown in figure 2.8.

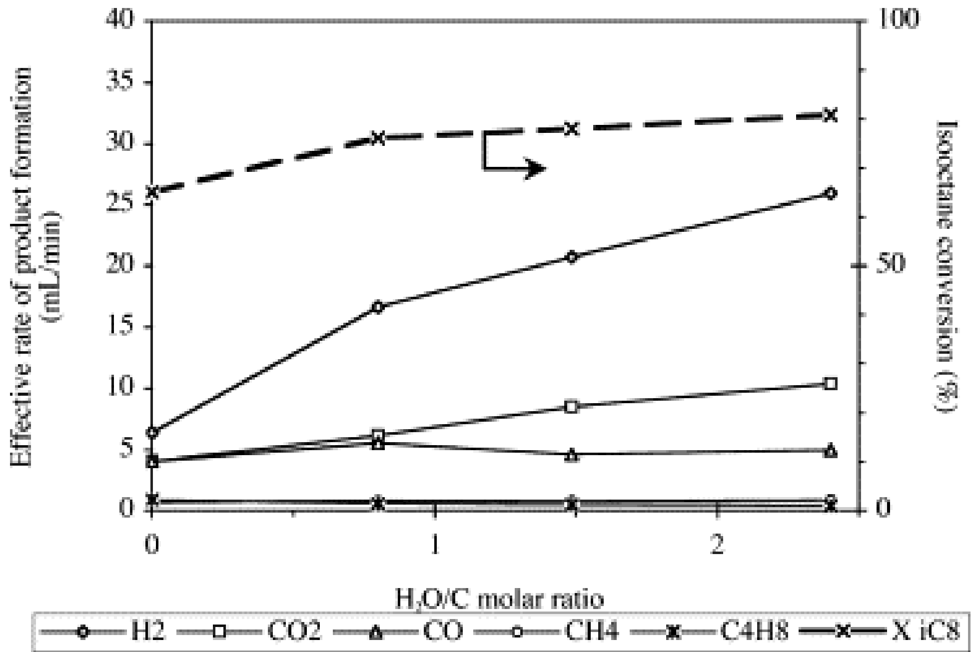

Figure 2.8: Influence of the H_2O:C ratio on the reformate composition and on isooctane conversion (conditions: 680 °C, 1.3 vol.% isooctane, O:C = 0.8, GHSV = 150 000 h^{-1})

Figure 2.8 indicates that the hydrogen yield is significantly increased at the higher steam-to-carbon ratios. Fuel conversion was not greatly affected which was claimed to be due to higher water-gas-shift reaction rates. It was also noted that with a steam to carbon ratio of 0.8, catalyst deactivation became evident. For these reasons, steam-to-carbon ratios above 2 were appropriate for the reformer.

Pacheco et al. (2003) and Roychoudhury et al. (2005) performed autothermal reforming experiments using iso-octane as a fuel, though different catalysts, inlet temperatures, space velocities and reactor sizes were utilized compared to those used in the work of Villegas et al. (2005). This prevents a direct comparison of the results, though it should be noted that Pacheco et al. (2003) determined optimal oxygen-to-fuel and steam-to-fuel molar ratios of 0.42 and 1.43 whereas Roychoudhury et al. (2005) determined optimal oxygen-to-fuel and steam-to-fuel molar ratios of approximately 1 and 2. This shows that optimal oxygen-to-fuel and steam-to-fuel molar ratios for maximum hydrogen production will vary greatly depending on the reformer design, type of catalyst, and operating conditions of the reformer and should be determined experimentally for each individual case.

2.7 Applicability of Autothermal Reformers in APU's

Compact auxiliary power units (APU's) provide a means of generating electrical power for a vehicle's electrical system instead of extracting power directly from the vehicle's engine. This concept of producing electricity from an auxiliary device is best utilized in large transportation vehicles that have a high electrical demand while the vehicle is in use. Long haul trucks for example remain idling even while at rest to provide the continuous electrical needs of the truck. When in idle, the engine operates at very low efficiencies resulting in poor fuel economy and higher levels of green-house-gas emissions. By introducing an APU, idling time can be significantly reduced providing both economic and environmental benefits.

Most transportation vehicles operate on liquid hydrocarbons such as gasoline or diesel. Since the fuel is already stored on-board the vehicle, it is convenient to use it as the fuel to operate the APU. Some current designs of APU's utilize a small combustion engine that is coupled with an electric generator to provide the auxiliary power. An alternative to this design is to pass the vehicle's fuel through a reformer to produce a hydrogen rich gas that can be fed to a fuel cell to generate electricity. Autothermal reformers when coupled with the appropriate fuel cell stack are very suitable for this type of application due to their compact design and relatively high efficiency.

When reforming any hydrocarbon, CO and CO_2 will be present in the product gas stream. The presence of CO especially effects the selection of the accompanying fuel cell stack in the APU. Many fuel cell technologies are available, but the most common types for use in an APU are proton exchange membrane fuel cells (PEMFC), molten carbonate fuel cells (MCFC), and solid oxide fuel cells (SOFC). High temperature fuel cells like MCFC's and SOFC's are a preferred choice as they can tolerate the presence of CO in the inlet stream and use it as fuel to actually further produce hydrogen whereas for PEMFC's, CO is extremely poisonous to its operation under all conditions. For PEMFC's, CO levels should not exceed 50ppm in the feed stream and should preferably be below 20ppm (Aicher, 2006). To reduce the CO concentration to acceptable levels, additional water-gas-shift reactors as well as preferential oxidation reactors are required by this type of system. Unfortunately, the manufacturing costs of high temperature fuel cells is currently much higher than that of the more common PEMFC's which brings an economic factor into the selection of design.

A major problem for all catalysts present in the system whether in the reformer, product gas treatment devices, or in the fuel cell stack, is the presence of sulfur compounds which ranges in concentration in commercial gasoline from 30 to 50ppm. Most suppliers of fuel cells recommend that sulfur content be below 1ppm to avoid catalyst deactivation (Aicher, 2006). The desulfurization of hydrocarbons is possible through rigorous chemical processing treatment though it is not an economically viable option for the process of on-board desulfurization. Preferably a regulation would need to be implemented demanding that commercial fuels be limited to sulfur levels between 1 and 10ppm, otherwise new methods will need to be developed to reduce the levels of sulfur or catalysts that are more tolerant to higher levels of sulfur will have to be developed.

Chapter 3
Numerical Modeling

3.1 Introduction

This chapter outlines the formulation of the numerical methods used in determining the performance of the reformer being considered. Descriptions of the assumptions, the conservation equations, the chemical reaction mechanism, the equations of flow in a porous media, and the boundary conditions are presented in this chapter.

3.2 Reformer Description

The autothermal reformer that has been analyzed was designed by the Fuel Cell Research Group. It operates on iso-octane which is a surrogate for gasoline. This fuel along with steam and air are preheated using a furnace and mixed before being injected into the reactor inlet. The inlet stream then proceeds through an inert porous region so that a fully developed plug flow or uniform velocity profile is achieved before the reactants reach the catalytically active porous region. In the presence of a catalyst, the inlet gas mixture chemically reacts to produce hydrogen, carbon monoxide, carbon dioxide, and steam. Nitrogen is also found in the product gas as it is present in the inlet air as well as trace amounts of unreacted fuel and lighter hydrocarbons that did not achieve complete decomposition. The product gas stream then flows through an additional inert porous region before exiting through the outlet, this second inert porous region being used to ensure that uniform velocity is maintained throughout the catalyst bed.

The minimum length of the catalytically active porous region that was required to achieve plug flow was 120mm. The specific criteria for plug flow conditions are discussed in section 3.6. Inert zones at the entrance and exit to the catalyst bed were chosen to be 30mm in length to avoid disturbances in the velocity profile due to the diameter change in the inlet and outlet tube regions of the reformer. The outer shell of the reformer was constructed of Inconel 625 with a length of 180mm, an outside diameter of 9.5mm and a wall thickness of 1mm. All fasteners, inlet/outlet tubing, screens, and the central 0.32cm diameter thermocouple tubing were constructed of Inconel 600. Figure 3.1 shows the basic design configuration of the reformer and figure 3.2 shows the experimental setup.

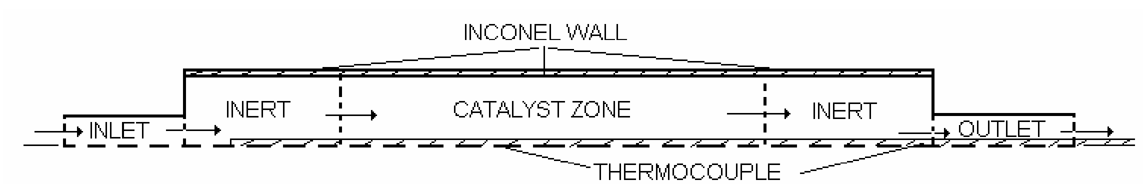

Figure 3.1: Basic design configuration of the reformer

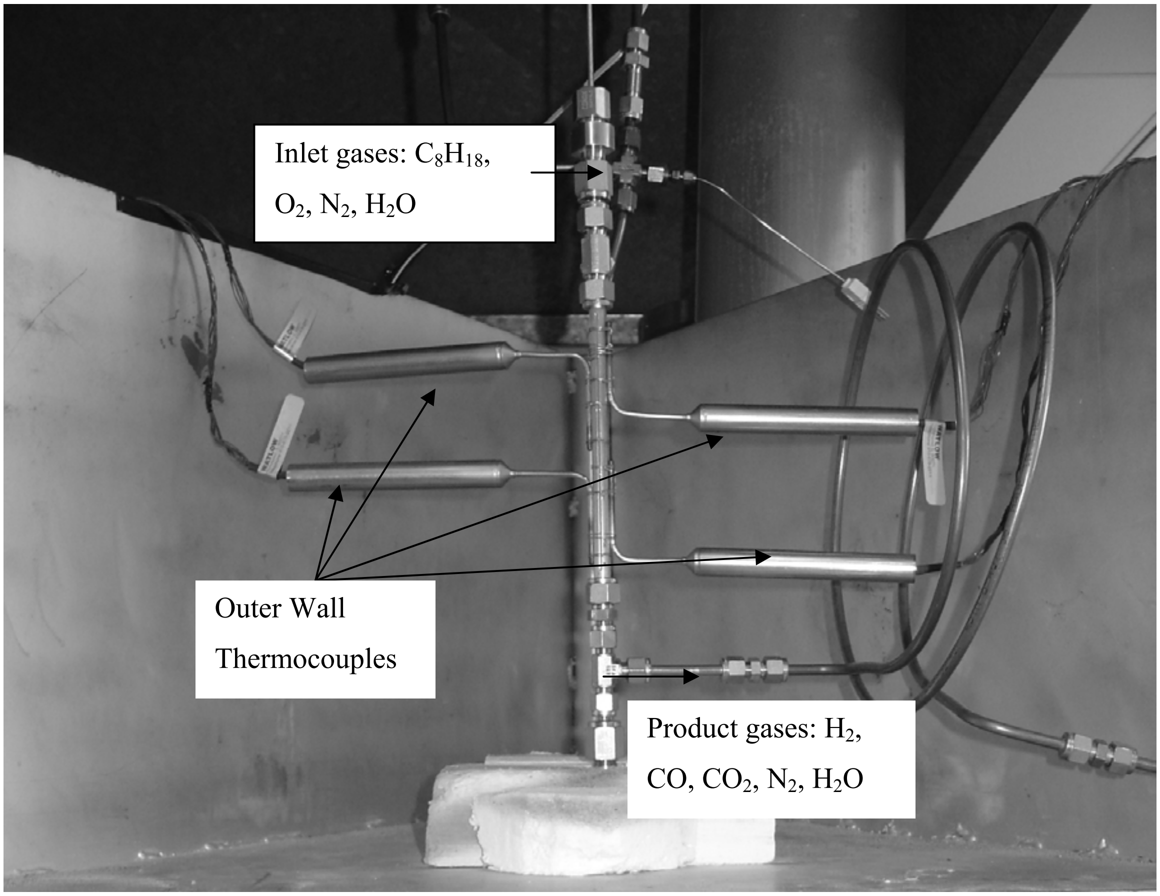

Figure 3.2: Photograph of the experimental reformer setup

3.3 Assumptions for Mathematical Model Development

In order to effectively describe the complex reforming process in the form of a computer model, a number of assumptions must be made about flow and other conditions. The assumptions used in the present work are as follows:

1. The flow is axis-symmetric, laminar, and steady
2. A pseudo-homogenous flow condition is imposed in the porous regions
3. Bed porosity is constant in the axial and radial bed directions

4. Molecular diffusion is assumed to be negligible relative to the bulk motion/momentum of the fluid
5. Thermal radiation is not considered
6. Outer walls are heavily insulated and therefore assumed adiabatic at their outer surface
7. Gases are assumed to be incompressible and to obey the ideal gas law
8. Catalyst deactivation has been neglected
9. Kinetic and pressure terms in the energy equation are negligible
10. The effect of viscous heating is negligible
11. Production of lighter hydrocarbons through chemical decomposition has been ignored

Packed bed reactor modeling work and the assumptions required to describe the pseudo-homogenous flow conditions as well as the diffusional effects are described in detail in section 3.6.

Heat transfer due to thermal radiation is not considered to occur inside the bed or to the ambient. Inside the porous region of the reformer, the presence of the inert and catalytically active pellets reduces the radiation mean beam length and, as a result, radiative heat transfer is negligible in comparison to the conductive and convective heat transfer occurring inside the bed (Olivieri, 2007).

The flow is considered incompressible which means there is no change in density with position. Therefore the bulk gas density is assumed to be constant. This is a reasonable assumption since the flow velocity is very low with Reynolds numbers between 70 and 1000, and a pressure drop across the reactor of approximately 4 kPa. The density of individual gases will change as a result of temperature change and are calculated using the ideal gas law to conserve mass and a constant bulk density.

Deactivation of the catalyst bed is an issue of concern that has not yet been addressed. Experimental investigation of catalyst deactivation due to coking, sintering, and poisoning will be conducted by the Fuel Cell Research Group in future experimental trials to determine its impact on hydrogen production and overall reformer efficiency. A computational model to predict catalyst deactivation is beyond the scope of this project.

Kinetic and pressure terms in the energy equation are neglected because they represent very small changes in energy in comparison to the thermal energy produced in species generation and consumption. Viscous heating effects can also be considered negligible in comparison to thermal energy generation.

3.4 Conservation Equations

The conservation of mass, momentum, energy and species transport equations are described here. The equations take into account the assumptions discussed in section 3.3. The conservation of mass equation in cylindrical coordinates is:

$$\frac{\partial}{\partial x}(\rho u)+\frac{\partial}{\partial r}(\rho v)+\frac{\rho v}{r}=0 \tag{3.1}$$

The conservation of momentum equations in cylindrical coordinates are:

$$\begin{aligned}\frac{1}{r}\frac{\partial}{\partial x}(\rho uu)+\frac{1}{r}\frac{\partial}{\partial r}(r\rho uv)=-\frac{\partial p}{\partial x}+\frac{1}{r}\frac{\partial}{\partial x}\left[r\mu\left(2\frac{\partial u}{\partial x}-\frac{2}{3}\left(\frac{\partial u}{\partial x}+\frac{\partial v}{\partial r}+\frac{v}{r}\right)\right)\right]\\+\frac{1}{r}\frac{\partial}{\partial r}\left[r\mu\left(\frac{\partial u}{\partial r}+\frac{\partial v}{\partial x}\right)\right]+F_x\end{aligned} \tag{3.2}$$

$$\begin{aligned}\frac{1}{r}\frac{\partial}{\partial x}(\rho uv)+\frac{1}{r}\frac{\partial}{\partial r}(r\rho vv)=-\frac{\partial p}{\partial r}+\frac{1}{r}\frac{\partial}{\partial r}\left[r\mu\left(2\frac{\partial v}{\partial r}-\frac{2}{3}\left(\frac{\partial u}{\partial x}+\frac{\partial v}{\partial r}+\frac{v}{r}\right)\right)\right]\\+\frac{1}{r}\frac{\partial}{\partial x}\left[r\mu\left(\frac{\partial u}{\partial r}+\frac{\partial v}{\partial x}\right)\right]-2\mu\frac{u}{r^2}+\frac{2}{3}\frac{\mu}{r}\left(\frac{\partial u}{\partial x}+\frac{\partial v}{\partial r}+\frac{v}{r}\right)+F_r\end{aligned} \tag{3.3}$$

where the terms F_x and F_r are momentum sink terms and represent the effects of pressure decrease due to the flow through a porous media. Their presence in the momentum equation and their magnitude are discussed in section 3.6.1. It should be noted that for non-porous regions, the values of F_x and F_r are effectively equal to zero.

The energy equation for steady state conditions and with negligible kinetic and potential energy changes can be written as follows:

$$\nabla\cdot(v\rho h)=\nabla\cdot(k\nabla T)+S \tag{3.4}$$

where S is a source term for the generation or consumption of heat from reaction. The presence of this source term is discussed further in section 3.5.2. k is the thermal conductivity and its value requires special attention since the porous region is modeled in a pseudo-homogenous gas phase instead of a two phase heterogeneous mixture. An effective thermal conductivity k_{eff} must be defined as a result and will be discussed in section 3.6.3.

The species transport equation used in the present model is:

$$\nabla \cdot (v\rho Y_i) = -\nabla \cdot J + r_i \tag{3.5}$$

where Y_i is the mass fraction of species i, J is the diffusion flux, and r_i is the rate of production or consumption of species i. Since molecular diffusion is considered negligible compared to the bulk motion/momentum of the flow, the diffusion flux term requires special attention which is discussed in section 3.6.2. The rate of production or consumption of each species r_i is calculated using the Pacheco et al. (2003) equations which describe the complex set of chemical reactions required to describe the reforming process of iso-octane. These equations are outlined in section 3.5.1.

3.5 Chemical Reactions

The rate of production of any species is dependent on the reaction mechanism that applies to the problem under consideration. As stated before, the Pacheco et al. (2003) mechanism was employed to model the extremely complex set of reactions that actually occur in the reforming of iso-octane. The general form to describe a reaction rate is as follows:

$$-r_i = k_r \cdot \theta \tag{3.6}$$

The reaction rate equation is a function of both temperature and concentration. k_r is the specific reaction rate constant which is dependent on temperature and θ is a concentration function based on species concentrations or inherently on their partial pressures. The value k_r can be expressed by an Arrhenius type function as follows:

$$k_r = Ae^{-\frac{E}{RT}} \tag{3.7}$$

For any Arrhenius type reaction there will be an associated pre-exponential factor A, and an activation energy E that can be determined from experimental results. These factors need to be carefully estimated when determining the rate constant since small differences can result in large changes in the results. For the present model, the work done by Xu and Froment (1989) and Jin et al. (2000) provided the values of A and E. The specific values used are discussed in section 3.5.1.

The concentration function θ needs to be defined for each of the reactions involved in the chemical process. The actual chemical mechanism for the reforming process of iso-octane is a highly complicated set of step functions where iso-octane will decompose to lighter hydrocarbons through multiple reactions before completely reforming to hydrogen, carbon monoxide, carbon dioxide and steam. Defining the complete reaction mechanism for the reforming of a heavy hydrocarbon such as iso-octane can be a near impossible challenge to accurately achieve, but can be simplified to a smaller set of reactions that closely describes the behaviour of the actual reaction mechanism. The set of reactions that was modeled was proposed by Pacheco et al. (2003) and is described below.

3.5.1 Pacheco Mechanism

Based on the studies conducted by Xu and Froment (1989) on methane steam reforming and by Jin et al. (2000) on methane partial oxidation, Pacheco et al. (2003) proposed a set of five chemical reactions to describe the reforming of iso-octane. Although the actual reaction mechanism for the reforming of iso-octane is much different than that of methane reforming, it was hypothesized by Pacheco et al. (2003) that the reaction mechanism and kinetic expressions could be adapted for other heavier hydrocarbons by performing a regression on the kinetic parameters in the chemical reactions to match experimental data of iso-octane reforming. The reaction mechanism consists of the following reactions:

i) Oxidation:	$C_8H_{18} + 12.5O_2 \rightarrow 8CO_2 + 9H_2O$
ii) Steam Reforming A:	$C_8H_{18} + 8H_2O \rightarrow 8CO + 17H_2$
iii) Carbon Dioxide Reforming:	$C_8H_{18} + 8CO_2 \rightarrow 16CO + 9H_2$
iv) Steam Reforming B:	$C_8H_{18} + 16H_2O \rightarrow 8CO_2 + 25H_2$
v) Water-Gas-Shift:	$CO + H_2O \rightarrow CO_2 + H_2$

For these reactions a set of rate expressions for the change in concentration of iso-octane was adopted and modified from the work of Xu and Froment (1989) and Jin et al. (2000) as stated before and are given below:

1) $r_{oxidation} = k_{r1} p_{iC_8H_{18}} p_{O_2}$

2) $r_{steam\ reforming\ A} =$

$$\frac{k_{r2}}{p_{H_2}^{2.5}}\left(p_{iC_8H_{18}} p_{H_2O} - \frac{p_{H_2}^3 p_{CO}}{K_2\left(1 + K_{CO}p_{CO} + K_{H_2}p_{H_2} + K_{iC_8H_{18}}p_{iC_8H_{18}} + K_{H_2O}(p_{CO}/p_{H_2})\right)^2}\right)$$

3) $r_{carbon\ reforming} = k_{r3} p_{iC_8H_{18}} p_{CO_2} \left(1 - \frac{p_{CO}^2 p_{H_2}^2}{K_3 p_{iC_8H_{18}} p_{CO_2}}\right)$

4) $r_{steam\ reforming\ B} =$

$$\frac{k_{r4}}{p_{H_2}^{3.5}} \left(p_{iC_8H_{18}} p_{H_2O}^2 - \frac{p_{H_2}^4 p_{CO_2}}{K_4 \left(1 + K_{CO} p_{CO} + K_{H_2} p_{H_2} + K_{iC_8H_{18}} p_{iC_8H_{18}} + K_{H_2O}(p_{CO} / p_{H_2})\right)^2} \right)$$

5) $r_{water\text{-}gas\text{-}shift} =$

$$\frac{k_{r5}}{p_{H_2}} \left(p_{CO} p_{H_2O} - \frac{p_{H_2} p_{CO_2}}{K_5 \left(1 + K_{CO} p_{CO} + K_{H_2} p_{H_2} + K_{iC_8H_{18}} p_{iC_2H_{18}} + K_{H_2O}(p_{CO} / p_{H_2})\right)^2} \right)$$

where $k_{r,n}$ = the reaction rate constant defined in equation (3.7) of reaction n

p_i = the partial pressure of species i

K_n = the equilibrium constant of reaction n

K_i = the adsorption constant for species i

Rate expressions 2 through 5 are given in a Langmuir-Hinshelwood-Hougen-Watson (LHHW) second order form meaning that the adsorption and reaction of species on active catalyst sites is considered in the reaction rate. Rate expression 1 is of first order and is not represented in a LHHW form, therefore it does not account for adsorption of species at active catalyst sites. The inconsistency between the oxidation reaction and the other four reactions originates from using the oxidation reaction described by Jin et al. (2000) and simply adding it to the steam reforming mechanism described by Xu and Froment (1989) to create a reaction mechanism appropriate for autothermal reforming. Work by Villegas et al. (2005) describes a more detailed set of chemical reactions for the reforming of iso-octane as discussed in section 2.4, though there is no discussion in this work of the kinetic parameters necessary to describe the reaction rate constants for this mechanism. Kinetic parameters will vary widely depending on the selection of catalyst and therefore adapting the results of other experimentation will introduce some uncertainty in the kinetic rate expressions. While obtaining kinetic data for the specific catalyst used in the reformer is desired, this experimentation is beyond the scope of the present project and since Pacheco et al. (2003) used a similar proprietary platinum catalyst, the regressed kinetic data was assumed to be adequate for the present modeling purposes.

Pacheco et al. (2003) used experimental data from research on autothermal reforming of iso-octane conducted at Argonne National Laborartory (ANL) for the determination of the kinetic parameters and model validation. Several tests were run in which the inlet temperature and the gas-hourly-space-velocity were varied. However details of the conditions under which these tests were run at were not stated. A sensitivity analysis was conducted to determine which parameters had the most influence on the results. Six parameters were found to have a significant effect on the performance of the reformer, those being the five pre-exponential factors for the Arrhenius rate constants k_1 through k_5 and the dissociative adsorption constant for water vapour at the catalyst active sites, K_{H2O}. New values of these parameters were determined from the experimental results from ANL and are listed in Table 3.1. It should be noted that Pacheco et al. (2003) made the assumption that the activation energies and the enthalpy of adsorption of water were the same as values reported in the literature by Xu and Froment (1989) and Jin et al. (2000).

Table 3.1: Values of the pre-exponential factors determined from experimental data and the kinetic parameters used from the literature

Parameter	Pre-exponential Factor, *A*	Activation Energy, *E* (KJ/mol)	Enthalpy of Adsorption (KJ/mol)
k_1 (mol/(g_{cat} s bar^2))	2.58×10^8	166.0	-
k_2 (mol $bar^{0.5}$/(g_{cat} s))	2.61×10^9	240.1	-
k_3 (mol/(g_{cat} s bar^2))	2.78×10^{-5}	23.7	-
k_4 (mol $bar^{0.5}$/(g_{cat} s))	1.52×10^7	243.9	-
k_5 (mol/(g_{cat} s bar))	1.55×10^1	67.1	-
K_{H2O} (dimensionless)	1.57×10^4	-	88.7

The dissociative adsorption constants for all other species were taken from the literature. The sensitivity analysis showed that the water dissociative adsorption constant was approximately a full order of magnitude larger in value compared to all other dissociative adsorption constants and therefore the values from the literature were considered acceptable.

3.5.2 Heat of Reaction

There are both exothermic and endothermic reactions in the Pacheco et al. (2003) mechanism and the heat generated or consumed by these reactions needs to be accounted for in the energy equation. A source term S as introduced in equation (3.4) was briefly described in section 3.4 as the generation or consumption of heat from a reaction. This source term can further be described as the sum of the change in enthalpy of each species multiplied by the rate of consumption or production of that species and can be expressed as:

$$S = -\sum_i \left(\frac{h_i^o}{M_i} + \int_{Tref}^{T} c_{p,i} dT \right) r_i \tag{3.8}$$

This equation accounts for the exothermic energy release of the oxidation and water-gas-shift reactions and sums them together with the energy consumption of the steam and carbon reforming reactions to account for the overall change in energy along the reactor bed.

3.6 Packed Bed Reactor Modeling

As mentioned in section 3.3 the presence of a porous media in the reformer requires special attention in the computer model. The bed is filled with inert and catalytically active particles in separate regions with an average diameter of 0.3mm. These particles randomly distribute themselves to fill the reactor leaving a non-symmetrical void space distribution between particles due to the random nature of their packing. Representing the exact distribution of the particles is nearly impossible especially since they are not perfect spheres but more an assortment of randomly shaped rough surfaced particles that increases the complexity of the packing.

The combination of solid and gas phases in one region can be referred to as a heterogeneous mixture where the two phases exist separately. In a heterogeneous reactor model, the chemical reactions occur only at the surface of the catalyst pellets. Heterogeneous reactor models have been developed that can randomly generate the packing nature of spherically shaped particles and therefore the chemical reactions can be defined to only occur at these surfaces. Unfortunately these models require an immense amount of computing power and are only appropriate for basic flow models in small geometries and are therefore not suitable for this application.

To simplify the problem of accounting for the two phases in the flow, the packed bed of the reactor can be considered pseudo-homogeneous. This essentially means that the mass of the catalyst is assumed to be uniformly distributed throughout the packed bed and the chemical reactions can be represented as occurring everywhere in the bed. The flow is then assumed to only have the gas phase present. This eliminates dispersion of the gas phase in the radial direction and therefore a uniform velocity profile is obtained which can be described as plug flow. For an actual reformer that has non-uniformities in the catalyst mass distribution, plug flow is said to be achieved when the ratio of the reformer diameter to the catalyst pellet diameter is greater than 10 (Rase, 1977) and when the ratio of the reformer bed length to the catalyst pellet diameter is greater than 600 (Mears, 1976). For the present reformer, these ratios are 25 and 630 respectively, satisfying the conditions for plug flow. Modifications to the momentum equations and the thermal conductivity must be made when assuming a pseudo-homogeneous gas phase. Source terms are added to the momentum equations and an effective thermal conductivity is calculated. Both of these changes require that the porosity of the packed bed be known before these values can be determined. The catalyst manufacturer NexTech reported that a porosity of 0.6 is an appropriate value to describe the amount of void space in the packing of the catalyst.

3.6.1 Momentum Source Terms

For flow through a porous media, there is an associated pressure drop that needs to be accounted for as a momentum loss in equations (3.2) and (3.3). The terms F_x and F_r are added to the momentum equation to account for the pressure decrease that would be induced as a result of the inert and catalytically active stationary particles. These terms were derived from the well known Ergun's law that describes pressure decrease per unit length in porous media (Ergun, 1952):

$$\frac{\Delta p}{L} = \frac{150(1-\varphi)^2}{\varphi^3 d_p^2}\mu u + \frac{3.5(1-\varphi)}{\varphi^3 d_p}u^2 \tag{3.9}$$

where d_p represents particle size, and φ represents porosity. Assuming that the porosity value is 0.6 as stated by the catalyst manufacturer and that average catalyst particle size is 0.3mm, F_x and F_r can be written to describe the pressure decrease in the axial and radial directions in the porous media the results being given in equations (3.10) and (3.11) respectively.

$$F_x = 1.234x10^9 \mu u + 21605u^2 \tag{3.10}$$

$$F_r = 1.234x10^9 \mu v + 21605v^2 \tag{3.11}$$

3.6.2 Species Diffusion

The assumption that molecular diffusion is negligible relative to the bulk motion/momentum of the fluid requires that special consideration is given to the diffusion flux term J in equation (3.5). An effective species diffusion term, denoted D_{eff}, was derived from the dimensionless number called the Peclet number which relates the mass transport by convection to the mass transport by diffusion:

$$Pe = \frac{VL_d}{\alpha} \tag{3.12}$$

where V = velocity

L_d = characteristic length

α = thermal diffusivity

The thermal diffusivity term α can be replaced with the effective diffusion term D_{eff}. The characteristic length L_d refers to the catalyst particle diameter and can therefore be replaced with the variable d_p. The physical velocity of the flow field in the porous media is not known since the pseudo-homogeneous gas phase assumption was made and therefore the velocity is calculated using the equations for the superficial velocity:

$$U_s = \varphi\sqrt{u^2 + v^2} \tag{3.13}$$

Using these in equation (3.12) then gives:

$$D_{eff} = \frac{U_s d_p}{Pe} \tag{3.14}$$

The Peclet number for mass transfer in packed beds has been found to be between 4 and 12 as reported by Thurgood (2003). Due to the absence of experimental data for the actual reformer, only a range of possible values could be provided for the Peclet number and a mean value of 8 was therefore selected for the present study. The resulting effective species diffusion D_{eff} is applied to all of the chemical species present in the reformer.

3.6.3 Thermal Conductivity

The value of the thermal conductivity is required in the solution of the energy equation. In the inlet and outlet regions, only the gas phase is present and the thermal conductivity is calculated by a mass-weighted-mixing-law function utilizing the known thermal conductivities and masses of the species in the mixture to determine the overall thermal conductivity. For the inert and catalytically active porous regions, a different approach must be used to account for the conductivity of solid particles. An effective thermal conductivity can be defined that accounts for both the fluid and solid conductivities. This is done by multiplying the porosity value or void space with the thermal conductivity of the fluid and adding it to the remaining solid volume multiplied by the solid thermal conductivity. This is the default method used by the CFD code of FLUENT to determine effective thermal conductivity when modeling porous media. The effective thermal conductivity k_{eff} is thus given by the following equation:

$$k_{eff} = \varphi k_f + (1-\varphi)k_s \tag{3.15}$$

3.7 Effectiveness Factor

When designing a catalytic reformer, maximizing active catalyst surface area or essentially the number of available catalyst sites for reactions to occur at is of main consideration. Catalyst particles are porous in nature meaning they allow gases to diffuse internally thus providing pathways to access all active catalyst sites. This phenomenon is commonly referred to as intraparticle diffusion as opposed to inter-particle diffusion which is the diffusion of particles in the void spaces of packed particles. The ability of reactant gases to diffuse to all available catalyst sites varies due to species concentrations and as a result the rate of reaction can vary dramatically depending on the ability of reactant gases to reach the active catalyst sites. A term referred to as the effectiveness factor is commonly used in reactor modeling to account for these diffusion limitations. The effectiveness factor η is defined as:

$$\eta = \frac{\text{actual overall reaction rate}}{\text{rate existing if entire catalyst surface was exposed to bulk concentration}}.$$

An effectiveness factor can be defined for each reaction in a chemical reaction mechanism and is simply multiplied by the rate of reaction r_i to obtain an effective value for the rate of reaction. Its value is known to vary along the length of the reactor for each reaction due to rapidly changing species concentrations that affect intraparticle diffusion rates. In order to calculate the effectiveness factor of a reaction, a quantity known as the Thiele modulus must first be determined. The Thiele modulus ϕ_n is a ratio of the surface reaction rate to the diffusion reaction rate. Determining the Thiele modulus requires knowledge of a number of parameters and information about the catalyst pellet such as catalyst pellet porosity, average pore diameter, pore tortuosity, as well as the reactant surface concentrations. These values can be very difficult to measure or to estimate and were not provided by the catalyst manufacturer. Further discussion of the theory necessary to calculate the Thiele modulus is given in Appendix A.

For the above reasons, a rigorous evaluation of the effectiveness factor was not considered and approximate values were estimated. Pacheco et al. (2003) used a proprietary platinum on ceria-oxide based catalyst and conducted a study to estimate the effectiveness factor. They determined that the effectiveness factors for the reactions ranged from 0.0003 to 0.002 at the start of the catalyst bed where reaction rates were the highest. Reaction rates rapidly drop with distance along the catalyst bed due to reduced reactant concentrations. This results in an increase of the effectiveness factor since intraparticle diffusion limitations are no longer restricting reaction rates. Since the highest reaction rates are expected to occur at the beginning of the bed where the highest temperature region occurs, a constant effectiveness factor of 0.001 was chosen for majority of the simulations. A brief study of the effect of changing this value was conducted to determine the sensitivity of the outlet species concentrations to the assumed effectiveness factor. It should be noted that although Pacheco et al. (2003) reported results for a platinum on ceria-oxide based catalyst of different average pellet size, it was assumed that the catalyst would perform similarly to the platinum on zirconia-ceria based catalyst used in the present study.

Chapter 4
Computational Fluid Dynamics Modeling

4.1 Introduction

In this chapter, a description of the methods used in the computational fluid dynamics modeling of the reformer will be given. This will include a discussion of the software packages used, the geometry and grid generation, the numerical solution process and the parameters that were used in obtaining the solution.

4.2 CFD Background

The use of computational fluid dynamics software (CFD) for the purpose of modeling transport phenomena and heat transfer within a given geometry has become a common approach for aiding in design and for providing detailed solutions to complex operational problems. With continuous advancements in computer technology, commercial CFD software packages have become much more readily available and they have also become much more user friendly. The CFD software package that was chosen for this study is FLUENT 6.2.16 which is widely used by academia and industry.

The FLUENT software package can be utilized for any 1-dimensional, 2-dimensional or 3-dimensional geometry for a wide variety of applications. Before the

FLUENT software is initialized a step called *pre-processing* is required where a mesh geometry is created by another program that can then be passed to FLUENT. For this purpose, the program GAMBIT 2.2.30 was used here to map the geometry of a physical object and to define the domain of discretized cells to generate a "mesh" of the geometry. Furthermore, boundary conditions can then be applied to the geometry to characterize inlet and outlet regions, presence of walls, axes of symmetry, fluid and solid regions, etc.

FLUENT imports the mesh and uses a discretized solution algorithm to solve the governing equations for the problem through an iterative process until a converged solution is obtained. This is done using the finite-volume method for representing and evaluating the governing equations in an algebraic form as partial differential equations. The finite volume method is a standard approach used in most CFD software. One benefit of the finite volume method is that it allows an unstructured mesh to be used due to its integral formulation process.

Post-processing provides a method for the interpretation of the rendered solution given by the FLUENT solver. The software used has a built in post-processor to generate results such as surface fluxes, surface averaged data, contour and vector plots, and scaled graphs to aid in reporting results.

4.3 Modeling Assumptions

A 2-dimensional, axis-symmetric flow was chosen to represent the geometry of the reformer. A number of assumptions were made in order to proceed to simplify the model and those assumptions are as follows:

- gradients in the angular direction of the reactor are zero
- porosity is constant throughout the porous regions of the reformer
- the presence of the Inconel mesh screen required to contain the inert and catalyst pellets is ignored
- the presence of the thermocouple along the centreline of the reformer is not being considered

4.4 Grid Generation

An unstructured mesh was utilized in the computational model taking advantage of the flexibility of the finite volume method which allows for unstructured meshes as stated in section 4.2. For the grid generation, a number of considerations were taken into account to create a mesh that would be suitable for the reactor conditions. These considerations were:

1) Gradients in species concentrations and temperature are expected to be high at the start of the catalyst region due to the high reaction rates in this region
2) Reaction rates are highest at the start of the catalyst region and approach zero towards the end of the catalyst bed

The mesh that was created as a result of these considerations is shown in figure 4.1

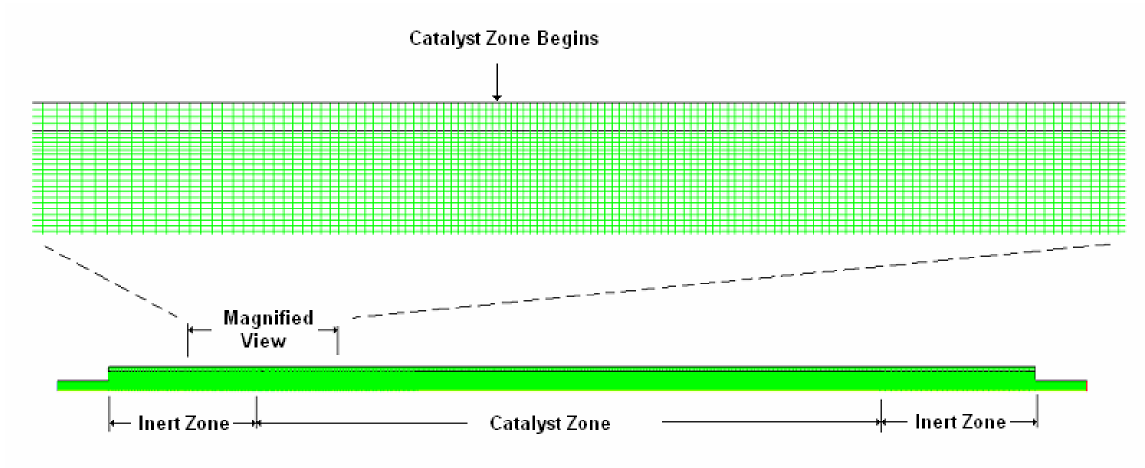

Figure 4.1: Magnified view of mesh topology for the inlet region of the geometry

The grid used involved 11854 quadrilateral cells and 24725 faces. A grid sensitivity analysis indicated that this grid size gave results that were grid independent to an acceptable degree. The grid independence testing involved several trials with different axial and radial grid spacing to determine when an effectively grid independent solution was obtained. The species outlet mole fractions for each trial as well as the outlet temperatures and the maximum reactor temperatures obtained in these trials are given below in Table 4.1.

Table 4.1: Results of mesh sensitivity analysis

Trial	*# of Cells*	*nH_2*	*nC_8H_{18}*	*nCO*	*nCO_2*	*Max Temp. (K)*
1	5898	0.1622	0.0041	0.0648	0.0546	1953.6
2	8328	0.1553	0.0054	0.0665	0.0559	1910.1
3	11854	0.1505	0.0067	0.0670	0.0561	1899.7
4	15212	0.1504	0.0067	0.0670	0.0561	1899.9

By examining the changes in outlet species concentration between trials, it was determined that a grid with 11854 cells was accurate enough to account for the conditions of the reactor without any noticeable change in the solution with an increased number of cells.

4.5 Solution Technique

A description of the solution techniques used in the finite volume method is presented in this section.

4.5.1 Overview

Once a mesh is generated by the pre-processor, the mesh is imported into FLUENT where the conditions of the reactor are implemented. All physical properties, boundary conditions and user-defined functions are applied as well as the discretization schemes used to solve the governing equations, any under-relaxation factors, and an initial guess to the solution. A control volume based technique known as the finite volume method is used that divides the domain into discrete control volumes over which the conservation equations of mass, momentum, energy, and molecular species can be solved. These governing equations are integrated over each control volume to construct a set of algebraic equations of all the dependent variables such as the velocity, pressure, temperature, and any scalar variables. The first iteration begins with the initially prescribed solution and the results of this iteration are compared against the previous values to the next set of values for the next iteration. This process is continued until a converged solution is declared.

4.5.2 Discretization

FLUENT uses a control volume based technique in determining the numerical solution to a problem. Around each node in the geometry, a control volume is defined that is to be non-overlapping with adjacent control volumes and an integration of the governing equations over the control volume is performed. This gives a set of algebraic equations involving the values of the unknown flow variables ϕ at specific grid points. The value of the flow variable ϕ is influenced only by neighbouring grid points. FLUENT uses an interpolation scheme between neighbouring grid points to determine a cell face value that lies on the plane where the control volumes meet. There are a number of different interpolation schemes that can be utilized for determining the cell face values. FLUENT will always use a central-differencing scheme to determine the diffusion flux term at a face value while the convective flux term has many differencing schemes to choose from.

The central-differencing scheme is used for determining diffusion flux across a face since it determines the face value of the flow variable ϕ_f from the centroid values of neighbouring cells upwind and downwind of the face. It is a basic method of determining the cell face value and it can be considered the natural outcome of a Taylor-series formulation (Patankar, 1980). While the central-differencing scheme is suitable in determining the diffusion flux term, if it is used for determining the convective flux term unrealistic results may be produced leading to divergence of the solution. The central differencing has been shown to be unstable particularly when the Peclet number (ratio of convection to diffusion) is greater than 2 (Pollard, 1982). For this reason, upwind-differencing schemes were created for determining the convective flux term as a computationally economical and convenient solution.

Upwind-differencing schemes differ from the central differencing scheme in a basic manner; upwind-differencing schemes calculate cell face values only from grid points upwind of the face whereas the central-differencing scheme calculates the cell face value from grid points upwind and downwind of the face. The advantage of the upwind differencing scheme is that the face value ϕ_{f} is derived from the centroid value of the cell upstream relative to the direction of flow in the geometry. With Peclet numbers of 2 or higher, the cell face value approaches the value of the upwind grid point value and therefore assigning the upwind grid point value to the cell face value gives a better approximation of the exact value rather than an interpolation between upwind and downwind grid points.

The process of simply assigning the value of the upwind grid point to the cell face value is known as a first-order-upwind-differencing. In order to improve accuracy, the second-order-upwind-differencing scheme can be utilized. Rather than simply setting the face value to the upwind grid value, the second-order-upwind-differencing scheme accounts for a flow variable gradient over a given displacement and adds this value to the grid point value before determining the cell face value. Another differencing scheme commonly used is QUICK (Quadratic Upstream Interpolation for Convective Kinematics). This differencing scheme uses a weighted average of the second order upwind differencing scheme and the central differencing scheme. It is typically more beneficial to use when a structure grid is used that is aligned with the flow.

The second-order-upwind-differencing interpolation scheme was used in the present study. This was an appropriate interpolation scheme for the given problem since the flow is considered to be laminar, the geometry is small, an unstructured mesh was used, and large gradients are expected within the geometry therefore higher-order accuracy was desired. Trials were run using a first-order-upwind-differencing scheme which showed variation in species outlet concentrations as compared to a second-order-upwind-differencing scheme. The QUICK scheme was also tested and was found to produce nearly identical results to the second-order-upwind-differencing scheme but with a larger computational expense most likely due to the unstructured mesh, therefore the second-order-upwind-differencing scheme was determined to be appropriate.

4.5.3 Solution Algorithm

The pressure-based segregated solution algorithm was used for the given problem. It can be simply described as the process of solving the governing equations in a sequential order as opposed to simultaneously as with a coupled solver. The segregated solution algorithm is memory efficient since it only needs to store the discretized equations in memory sequentially. The segregated solver is appropriate for the problem to be solved since the benefits of a coupled solver are only necessary when pressure-velocity coupling is strong as with transonic or supersonic fluid flow. The methodology of the segregated solver that is executed in each iterative step is illustrated in figure 4.2 and is outlined as follows:

1) All fluid properties such as density, specific heat, viscosity, etc., are updated
2) Each individual momentum equation is solved using the previously updated pressure and fluxes
3) A pressure correction is obtained using the previously updated velocity and mass fluxes
4) Mass fluxes, velocity and pressure are updated using the obtained pressure correction
5) Conservation equations are solved for energy and species terms

6) Source terms are evaluated for the generation/depletion of energy and species due to chemical reaction

7) Convergence is checked to determine if more iterations are required

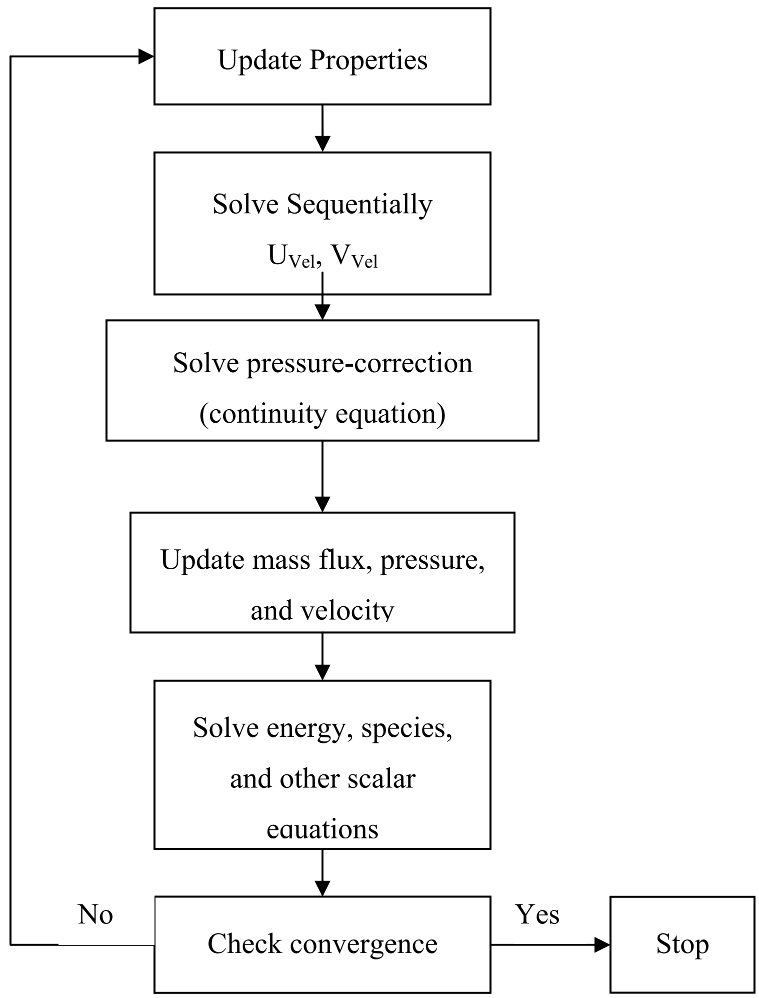

Figure 4.2: Overview of segregated solver approach

When solving the momentum equations the pressure values are set to fixed values. The iterative process will return pressure values that show an inconsistent pressure drop between cells along the reformer. To reduce this error, FLUENT uses a pressure correction interpolation scheme. The two interpolation schemes available are the standard and PRESTO! (PREssure Staggering Option) schemes. The PRESTO! interpolation scheme was chosen since it uses a staggered selection of control volumes to determine the average pressure drop. This method is recommended when dealing with porous media since the standard interpolation scheme tends to overshoot/undershoot cell velocity in porous media (Fluent, 2005). The SIMPLE pressure-velocity solution algorithm is then necessary to provide a relationship between the pressure and velocity so that they can be corrected to conserve mass and momentum. A detailed description of the SIMPLE algorithm can be found in Patankar (1980).

Once a solution is obtained the temperature, reaction rates, species concentrations, and other property dependent variables are updated. Initially, the solution will be highly inaccurate due to the presence of multiple species and highly temperature dependent reaction rates that can result in instability in the solution algorithm. For this reason, relaxation factors are used in the iterative process to dampen the magnitude of change of field variables between iterations. The new field variable is found by adding the previous value of the field variable with the change in the field variable multiplied by a dampening factor.

$$\phi_{updated} = \phi_{old} + \beta\Delta\phi \tag{4.10}$$

where β = relaxation factor

$\Delta\phi$ = change in field variable

Relaxation factors are chosen manually by the user if divergence in the solution is detected. Values range from as high as 0.9 to as low as 0.05. Lower relaxation values were necessary for temperature and species concentrations due to the high reaction rates.

4.5.4 Solution Initialization

To begin the iterative process of the solution algorithm, an initial guess to the solution can be provided for the flow variables in the domain. This can aid in the speed of convergence if appropriate values are assigned. Temperature, velocity and species concentrations were given initial values and are described below.

Temperature

The temperature in the reformer varies largely due to the highly exothermic oxidation reaction that takes place primarily at the beginning of the catalytically active porous region. High temperature gradients will exist in the reactor since the thermal conductivity of the bed is not adequate enough to quickly disperse the large amount of heat released by the oxidation reaction. Due to these large temperature gradients and the fact that the oxidation reaction is highly temperature dependent, a conservative initial guess of the temperature was given. The temperature of the inlet stream was set to 773K, so a value of 1100K was used for the present study which was an approximation of the average bed temperature inside the reactor instead of peak temperatures.

Velocity

Flow velocity was set to reflect a gas-hourly-space velocity (GHSV) of $30{,}000^{-h}$ matching the conditions of the experimental setup. GHSV is a measure that is inversely related to the residence time a gas species will occupy at a given catalyst site. A GHSV of 30,000 requires an inlet velocity of 2.0m/s so the initial velocity was set to 1m/s since the flow reduces in velocity over the packed bed region.

Species

Species concentrations vary highly throughout the reactor bed with six of seven species in the mixture being reactive. Product species yield of CO_2, CO, H_2, N_2 and H_2O as well as unreacted C_8H_{18} was determined from previous experimental data by Caners (2005) and these values were initialized while O_2 was set to zero since complete consumption of O_2 is to be expected due to high inlet temperatures.

Pressure

The operating conditions of the reformer are set to atmospheric pressure. In order to maintain plug flow across the porous regions in the reformer, a very small pressure drop is required. The porosity of the porous media was indicated to be 0.6 which is relatively large in value so that a minimal pressure drop is expected. For these reasons, pressure initialization was left at atmospheric pressure.

4.5.5 Convergence

Determining convergence is not a trivial issue especially when dealing with complex chemically reacting problems. Residuals of the field variables can be monitored during the iteration process to report a converged solution when residuals are very small, but to confirm convergence it is recommended that other integrated quantities be examined (Fluent, 2005). During the iteration process, once residuals were of the magnitude of 10^{-6} or lower, specific properties such as temperature and species concentrations were more closely examined which were still found to be changing with time. In order to confirm convergence, the criteria that were monitored were as follows:

- Maximum temperature and its location
- Average temperature of exit stream boundary
- Mole fractions of outlet stream species
- Rate of species conversion for each reaction

4.6 User-Defined Functions

In order to implement the complex chemical reactions of the Pacheco et al. (2003) mechanism into FLUENT's "user-defined functions" a computer code must be written to describe them in a fashion that FLUENT can compile. Though FLUENT is able to define a volumetric reaction involving several species in several chemical reactions, the rate expression is limited to the Arrhenius type or power law definitions. The chemical mechanism chosen is the Pacheco mechanism, as described in section 3.5.1, which is in a Langmuir-Hinshelwood-Hougen-Watson form and cannot be input directly into

FLUENT's rate expression. A code written in C++ language was chosen and compiled by FLUENT to become accessible as a user-defined function via a window library. This can be done to overwrite any expression that the user wishes to change enabling more flexibility over the controls and input of the program.

4.7 Post Processing

Post processing of a converged solution is done with FLUENT's post processor which was mention earlier in section 4.1. Post processing can provide useful information about the obtained solution and present it a user friendly graphical manner. The types of post processing that were utilized are:

Surface averaging – primarily used at reformer outlet to monitor species mole fractions to determine the composition of the reformate gas stream

Contour plots – used to show temperature, velocity, and pressure profiles as well as rate of reaction throughout the reformer and consumption/production of species

Point variables – used to find information at a specific location of interest within the reformer (ie. location of thermocouple points)

Chapter 5
Results and Discussion

5.1 Introduction

In this chapter, the results obtained using the two-dimensional axis-symmetric computational fluid dynamics model are presented and discussed. FLUENT's built-in post-processor was used to calculate mass-averaged conditions at the reformer outlet, and to produce graphs and contour plots for the entire solution. Results were compared to previous results obtained at Queen's University.

5.2 Selection of Cases

The present study was performed to determine the influence of a number of parameters on the operation of the reformer. In particular, investigations into the effects of wall thermal conductivity, catalyst thermal conductivity, packed bed porosity, inlet species concentration ratios, inlet temperatures, gas-hourly-space-velocity (GHSV), and effectiveness factor were conducted. The results of these calculations will be used to suggest possible design improvements for future prototypes, as well as generating results to be compared with experimental data once obtained. A base case was chosen so that the effects of varying individual parameters could be compared against a basic solution. While all results were considered and analyzed, hydrogen yield was of primary concern in all of the modeling work.

5.3 Base Case

The base case was chosen to represent the experimental reformer and the conditions under which it will be operated. Previous work by Caners (2005) was used to determine an appropriate and conservative operating inlet temperature, GHSV, and inlet species concentration ratios. This provided a benchmark with which the results obtained using various values of the thermal conductivity, porosity, inlet conditions and effectiveness factor could be compared. The base case parameters were set as follows:

1) The outer wall of the reformer is made from Inconel 625 and is 1mm in thickness
2) Inert zones of the packed bed exhibit the thermodynamic properties of silicon carbide and have a local porosity of 0.6
3) The catalyst zone exhibits the thermodynamic properties of a 2% Pt-ZrCe based catalyst with a local porosity of 0.6
4) The GHSV is approximately 30,000h^{-1} at the entrance to the catalytically active region
5) The inlet species concentrations molar ratios (mol/mol) of O_2:C_8H_{18} and H_2O:C_8H_{18} are 0.5 and 2 respectively
6) The inlet air stream consisted of 21% oxygen and 79% nitrogen on a molar basis.
7) The inlet temperature is 773K or 500ºC
8) The effectiveness factor is 0.001 for the entire catalyst bed

A solution was obtained with these base conditions to determine the conversion rate of fuel, the dry hydrogen yield (steam and unreacted fuel has been condensed out), the molar concentration of the product species, the pressure drop along reactor bed, the temperature and velocity profiles, and the local rate of reaction.

The conversion rate of fuel can be expressed as the ratio of the fuel molar flow rate at the inlet minus the ratio of the fuel molar flow rate at the outlet to the fuel molar flow rate at the inlet and expressed as a percentage, hence;

$$\%conversion C_8H_{18} = 1 - \frac{(mol/\sec_{C_8H_{18}})_{outlet}}{(mol/\sec_{C_8H_{18}})_{inlet}} x100 \qquad (5.1)$$

The dry hydrogen yield expresses on a percentage basis the amount of dry hydrogen that is produced as a percentage of the maximum amount of hydrogen yield possible. Considering the steam reforming B reaction, for one mole of fuel the maximum amount of hydrogen yield possible is twenty five moles of hydrogen. The dry hydrogen yield is then expressed as the ratio of the molar flow rate of hydrogen at the outlet in the absence of steam and fuel over the maximum hydrogen molar flow rate possible if one mole of fuel is converted to twenty five moles of hydrogen and is calculated as a percentage as follows:

dry hydrogen yield =

$$\frac{(mol/\sec_{H_2})_{outlet} / [1 - (mol/\sec_{H_2})_{outlet} - (mol/\sec_{C_8H_{18}})_{outlet}]}{25 \cdot (mol/\sec_{C_8H_{18}})_{inlet}} x100 \qquad (5.2)$$

A summary of the results obtained is given in Table 5.1 and in figures 5.1 to 5.4.

Table 5.1: Summary of results from base case

Conversion rate of fuel (%)	40.5
Dry hydrogen yield (%)	8.1
Mole fraction of C_8H_{18} at outlet	0.0932
Mole fraction of O_2 at outlet	1.4×10^{-10}
Mole fraction of CO_2 at outlet	0.0437
Mole fraction of CO at outlet	0.1264
Mole fraction of N_2 at outlet	0.3296
Mole fraction of H_2 at outlet	0.2746
Mole fraction of H_2O at outlet	0.1375
Pressure drop along bed (kPa)	3.5

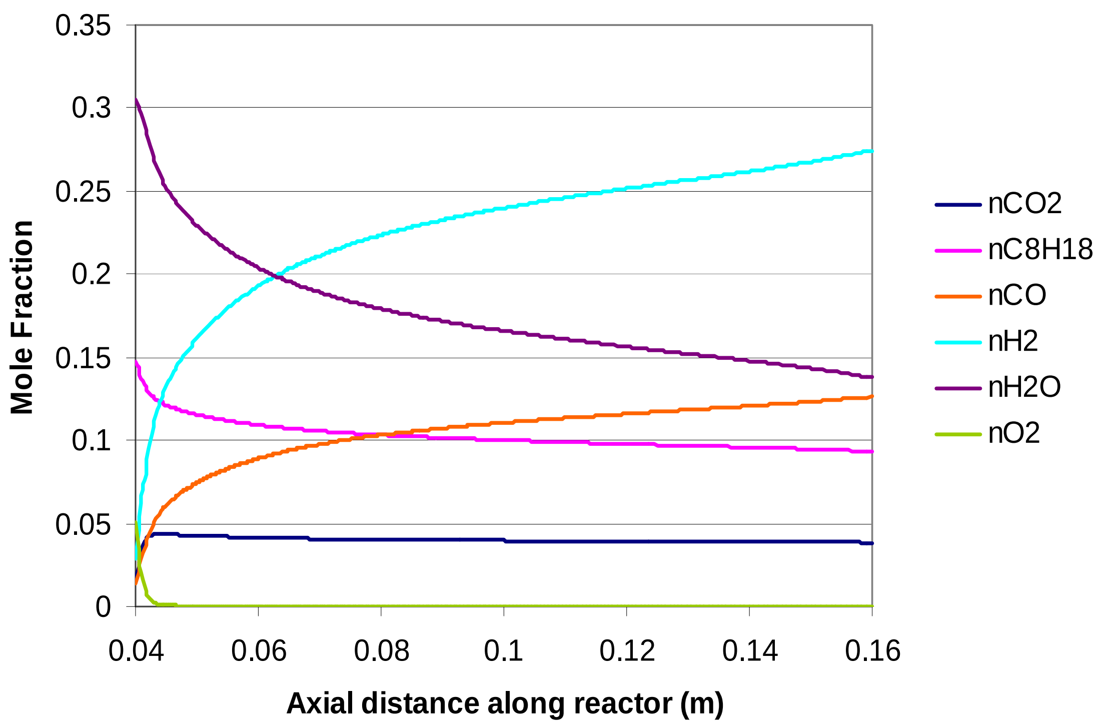

Figure 5.1: Predicted mole fractions along reformer bed for base case

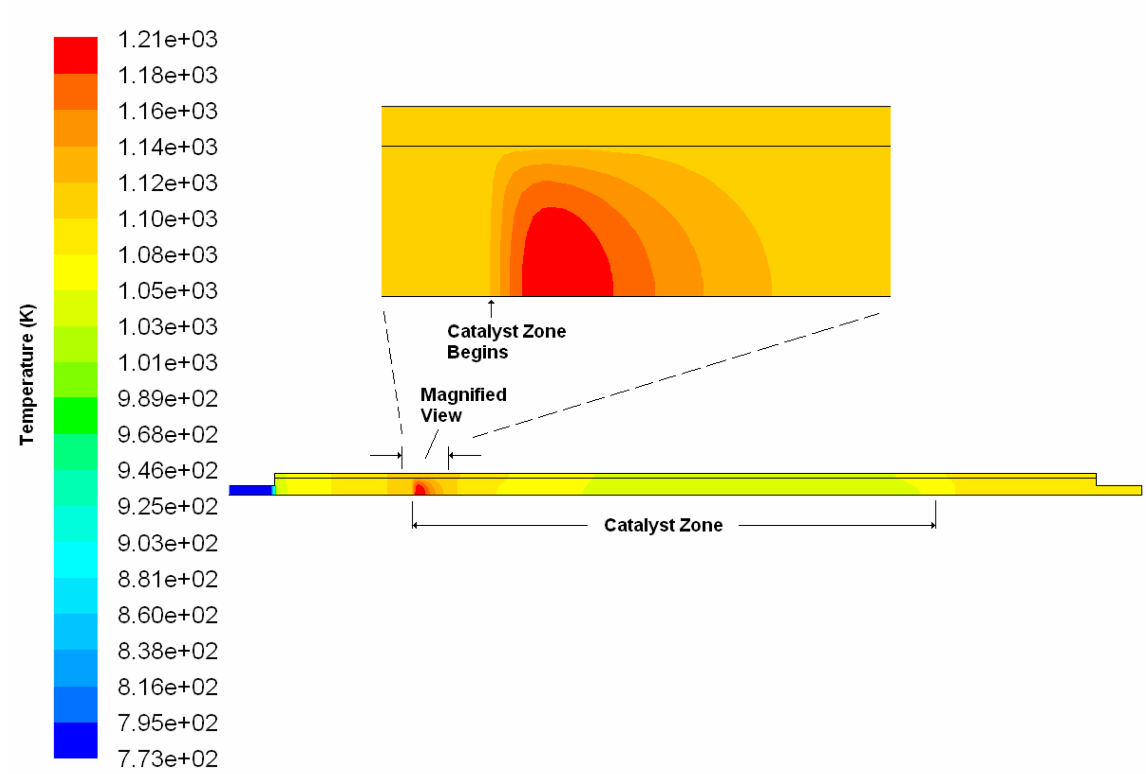

Figure 5.2: Temperature profile for base case

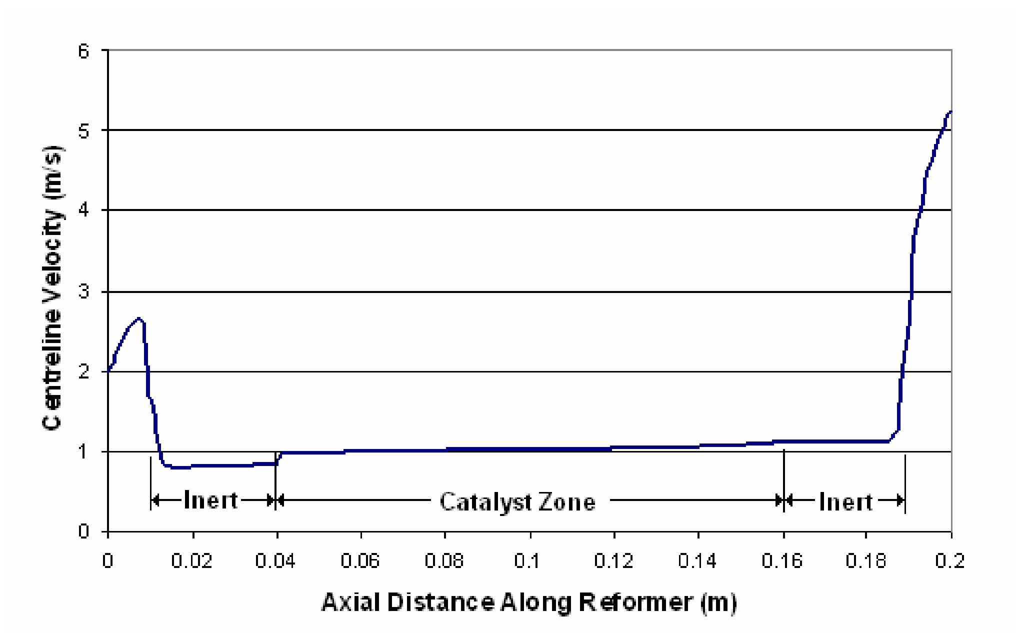

Figure 5.3: Velocity profile for base case

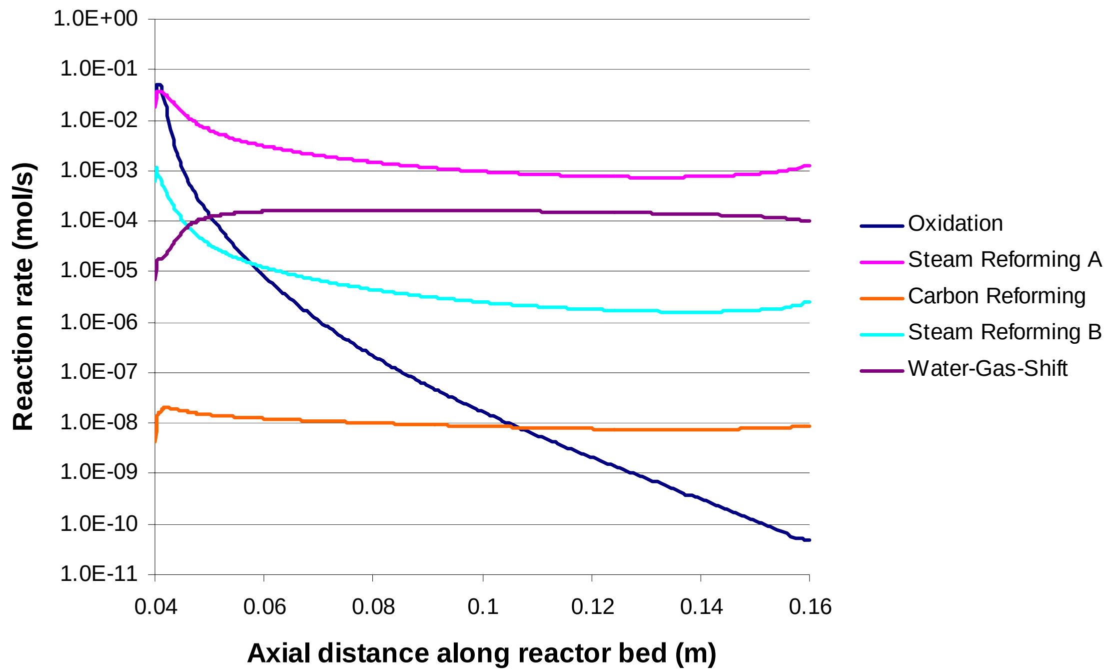

Figure 5.4: Reaction rates along the active catalyst region

Figure 5.2 shows a contour plot of the temperature distribution along the reformer. At the beginning of the catalyst region, there is a large temperature gradient. This is due to the large heat release of the exothermic oxidation reaction. It can be seen that the temperature is at its highest towards the center of the reformer in this region. Closer to the outer wall, heat is being conducted away from this large concentration of heat along the reformer walls to other regions of the reformer bed.

Figure 5.3 shows the velocity profile of the packed bed along the centreline of the reformer. Initially, the velocity profile is set to be uniform once the flow enters the reformer. This entranceway allows for the flow to begin developing which is why there is an increase in the velocity profile initially. Once the flow reaches the beginning of the packed bed, there is a dramatic drop in the velocity. Once the flow leaves the final porous inert zone, the flow rapidly increases in velocity as it flows through the exit tube.

5.4 Wall Treatment

The outer casing of the reactor was assumed to be fabricated from Inconel 625 with an outer diameter of 9.53mm and a wall thickness of 1mm. This material was selected due to its ability to withstand elevated temperatures and for its corrosion resistance. One of the design criteria of the new reformer was that it have better thermal conductivity throughout the catalyst bed to conduct heat away from the exothermic oxidation region occurring primarily at the beginning of the catalyst bed. An investigation into the effects of changing the outer wall thermal conductivity was conducted to determine if heat could be effectively transferred axially through the wall and into the catalyst bed to further promote the steam reforming reactions.

The thermal conductivity of Inconel 625 ranges from 17.5 W/mK at 538ºC to 25.3 W/mK at 982ºC which is the range of typical operating temperatures of the reformer. Trials were run for thermal conductivity values between 10 W/mK to 100 W/mK. This was done to determine how the thermal conductivity of the wall material affects the performance of the reformer.

Centreline temperature profiles were obtained for thermal conductivities of 10, 30, 50 and 100 W/mK and were compared against the temperature profile of the base case. Plots are shown for each case in figure 5.5.

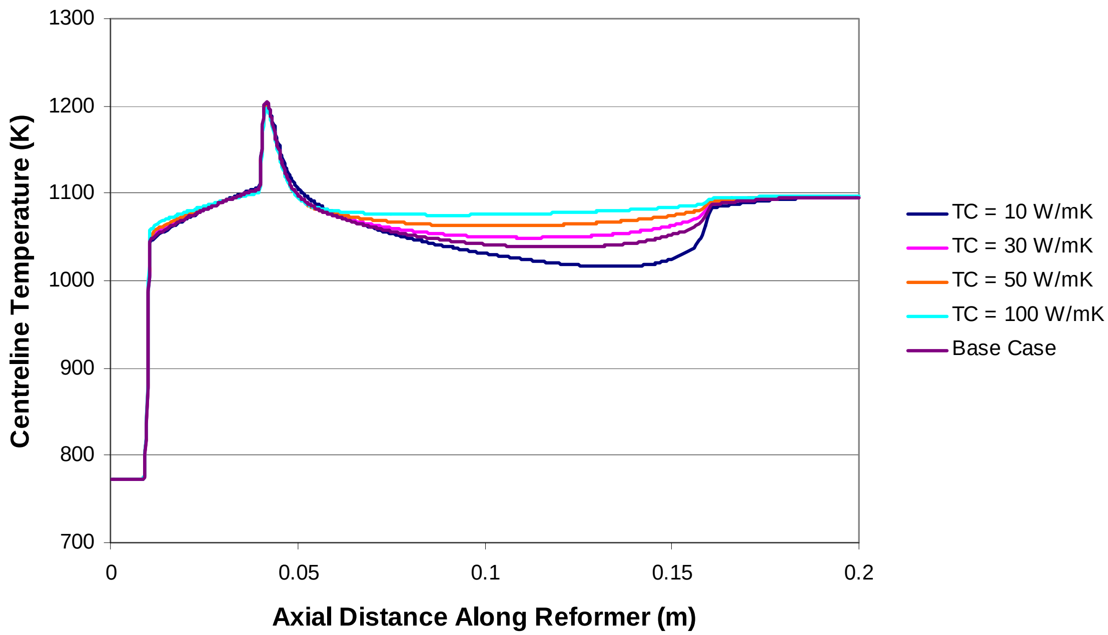

Figure 5.5: Temperature profiles of varying wall thermal conductivity

The centreline temperature distribution along the bed varies significantly with changes in the wall thermal conductivity as seen from figure 5.5. There is a noticeable increase in the average centreline temperature along the catalyst bed region from 0.05 to 0.16m with increased wall thermal conductivity. To demonstrate the impact of the increased average bed temperature on the performance of the reformer, the fuel conversion and hydrogen yield changes with thermal conductivity are shown in figure 5.6.

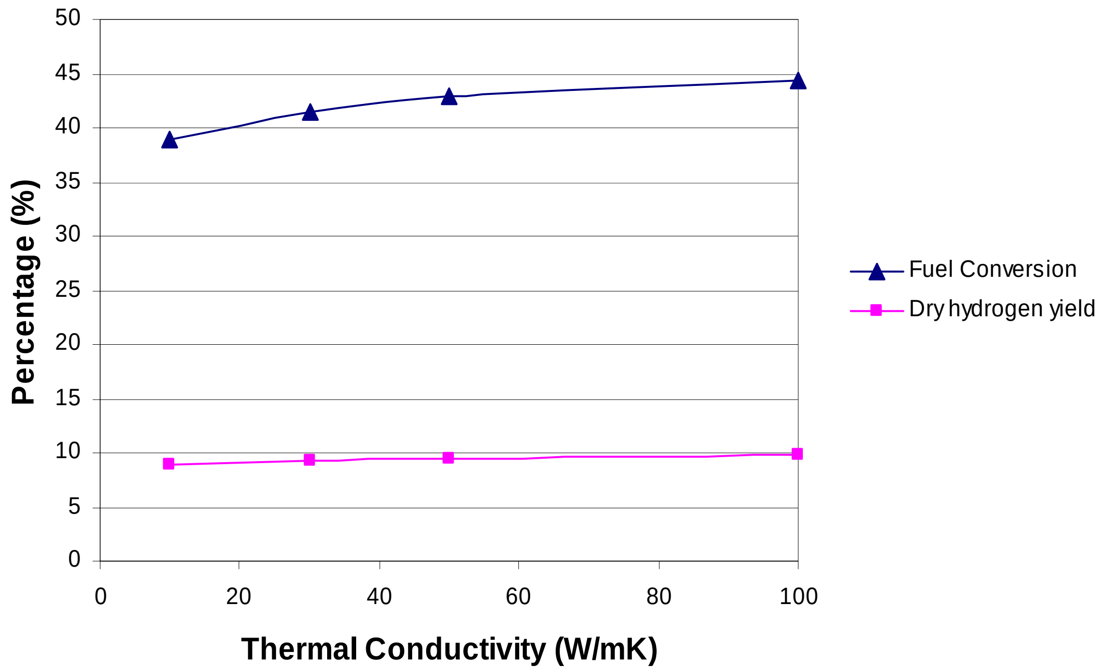

Figure 5.6: Fuel conversion and dry hydrogen yield for varying wall thermal conductivity

The results given in figure 5.6 show that increasing the wall thermal conductivity will promote higher fuel conversion and higher dry hydrogen yield. However the magnitude of these increases is relatively small considering the increase in thermal conductivity necessary to produce this change. The increase in fuel conversion and dry hydrogen yield is accounted for by the steam reforming A reaction rate increase, which was expected with higher average bed temperatures. With an increase in average bed temperature there will be an increase in the steam reforming reaction rate which is illustrated in figure 5.7:

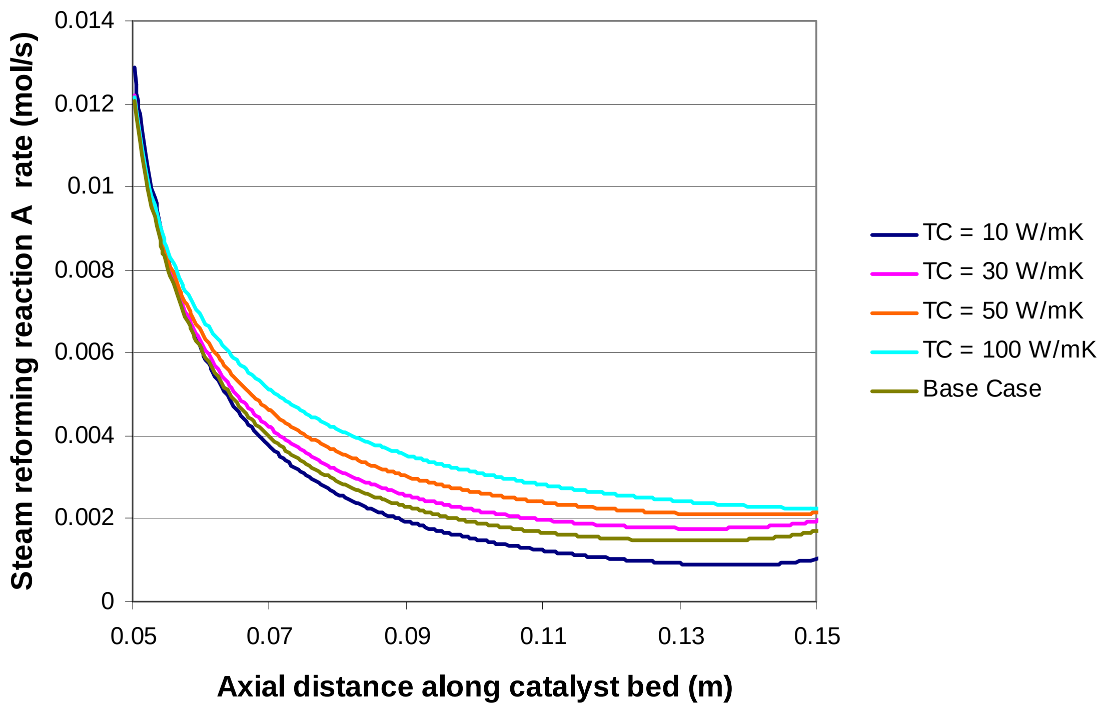

Figure 5.7: Rate of steam reforming reaction A along catalyst bed

Figure 5.7 shows the increase of the steam reforming reaction A that accounts for the higher fuel consumption and hydrogen yield. Although higher fuel conversion and hydrogen yields are attainable by selecting a material with a higher conductivity, very few materials are available that can withstand the very high operating temperatures of the reformer and are also robust and corrosion resistant while having a thermal conductivity of the maximum values considered. Most stainless steels suitable for an autothermal reformer have thermal conductivities very similar to that of Inconel 625. More exotic materials such as platinum or rhodium have thermal conductivities as high as 77W/mK and 150W/mK respectively, but are very expensive and do not show dramatic enough increases in performance to justify their use. The selection of Inconel 625 for the construction of the outer casing of the reformer may therefore be considered suitable considering the economic restrictions on the project and in almost all autothermal reformer designs, although if hydrogen yield is to be maximized, more exotic materials with higher thermal conductivities should be considered.

5.5 Catalyst Conductivity

The catalyst that was selected for use in the reformer was 2% platinum supported on a zirconia-ceria base that was reported to have a thermal conductivity of approximately 2 W/mK by the catalyst manufacturer NexTech (Schwarz, 2007). The low thermal conductivity is due to the ceramic zirconia-ceria base that the platinum is impregnated in. An investigation into the influence of the thermal conductivity of the catalyst was undertaken to determine if increasing the catalyst conductivity would greatly improve reactor performance. Trials were therefore run varying the thermal conductivity of the catalyst from 1 W/mK to 20 W/mK to determine if an increase in fuel conversion and hydrogen yield could be obtained.

Centreline temperature profiles were obtained for thermal conductivities of 1, 3, 10 and 20 W/mK and compared with the temperature profile for the base case where the thermal conductivity was 2 W/mK which is shown in figure 5.8. The variation of fuel consumption and dry hydrogen yield with thermal conductivity is shown in figure 5.9.

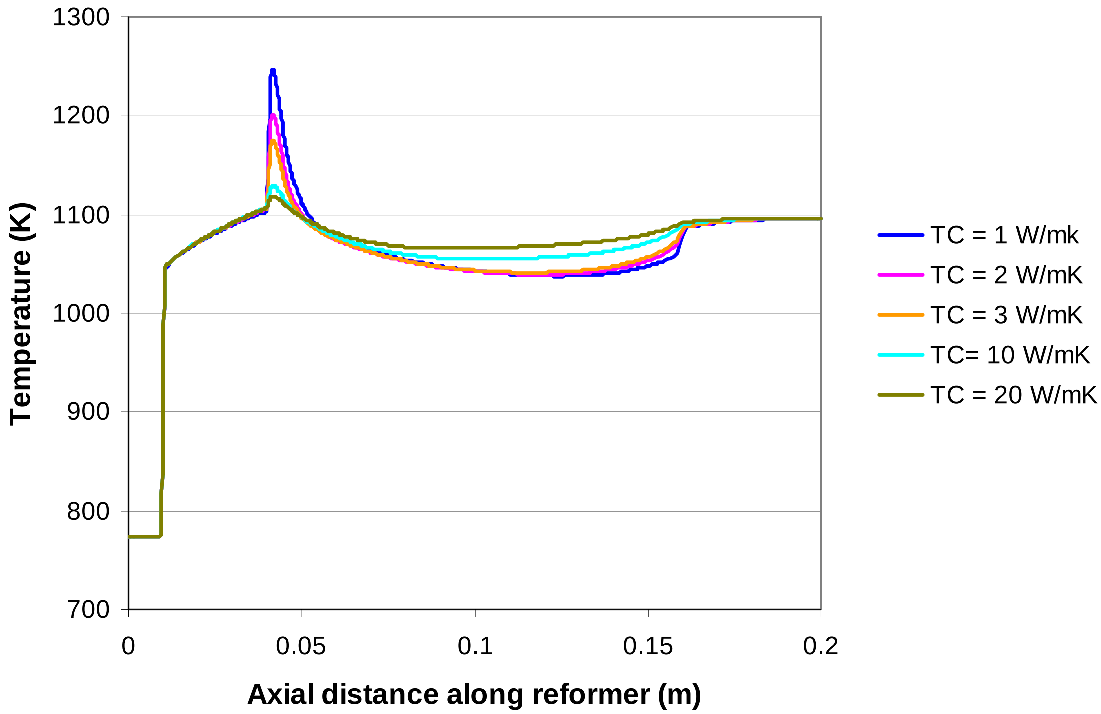

Figure 5.8: Temperature distribution along centreline of reformer for varying catalyst thermal conductivity

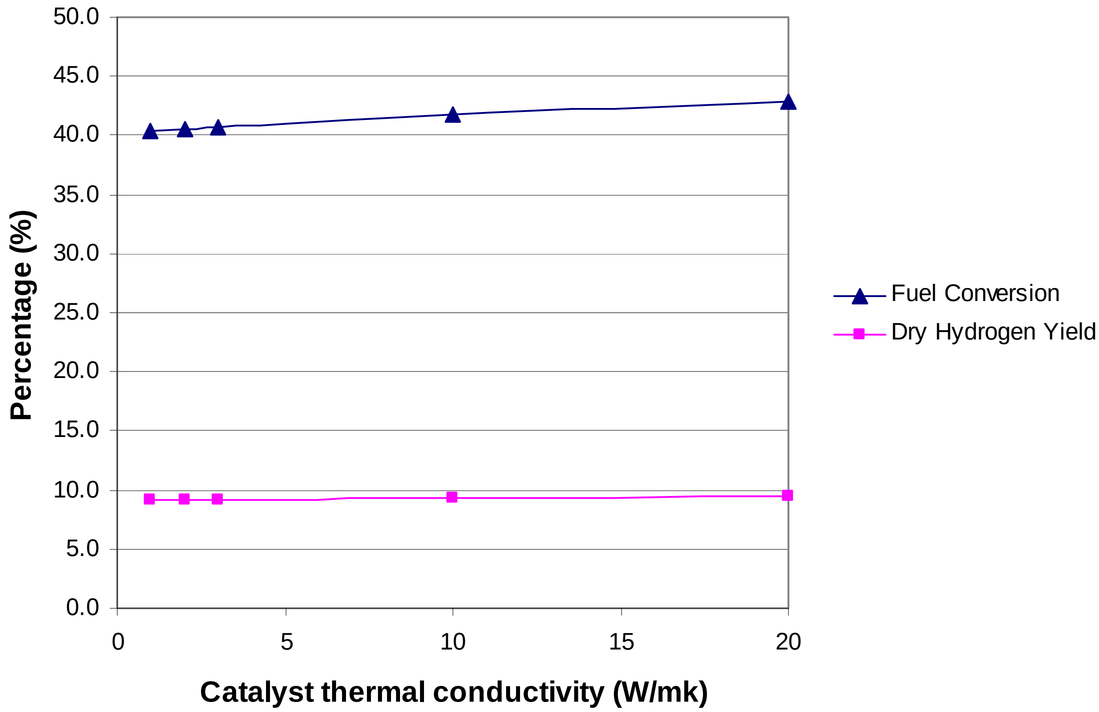

Figure 5.9: Fuel conversion and dry hydrogen yield percentages for varying catalyst thermal conductivity

Figure 5.8 shows that there are significant variations in the centreline temperature distribution with varying catalyst conductivity. However, even with these temperature changes, only small changes in the fuel conversion and dry hydrogen yield are obtained as was seen figure 5.9. By increasing the catalyst thermal conductivity from 2 W/mK to 20 W/mK, the fuel conversion rate only increases by 2.4% and the dry hydrogen yield only increases by 0.9%. The effects of the catalyst bed thermal conductivity on the steam reforming A reaction rate along the active catalyst region are shown in figure 5.10.

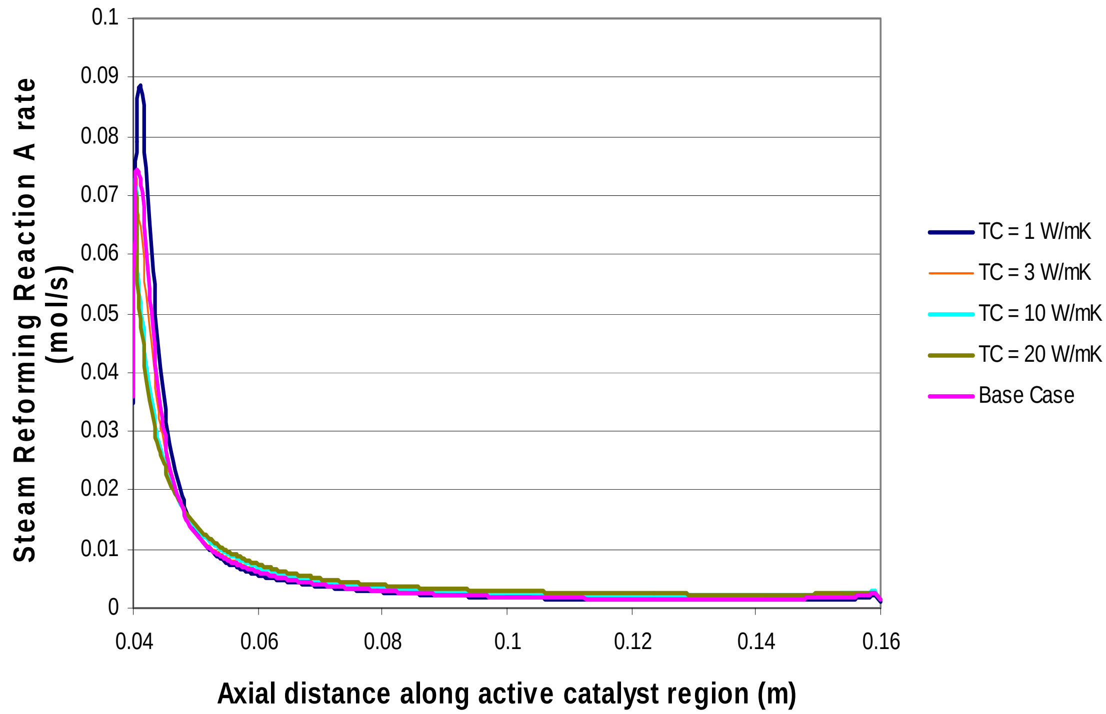

Figure 5.10: Rate of steam reforming reaction A along active catalyst region for varying catalyst thermal conductivity

With varying catalyst thermal conductivity, there is a change in the behaviour of the stream reforming reaction rate, there being a decline in the peak reaction rate with increased thermal conductivity and a slight increase in the overall reaction rate along the bed. When the catalyst thermal conductivity is increased, small increases in fuel conversion and hydrogen yield are obtained which indicates that the slight increase in the average reaction rate along the bed does not provide a means to significantly improve reactor performance.

5.6 Porosity of Packed Bed

The porosity of a packed bed has an influence on the pressure drop, the thermal conductivity, and the reaction kinetics of the catalyst bed. If the porosity is decreased and the volume of the catalyst particles is increased, higher reaction rates may be achieved due to the increase in the mass of catalyst. Consequently, a reduction in porosity will result in a larger pressure drop which can affect the velocity profile causing non-uniformities in the flow and making the plug flow assumption invalid. This will also have an impact on the heat transfer rate within the packed bed which will affect the reformer performance.

Trials were run to determine if there are significant pressure drop changes with varying bed porosity and to determine if the variation in the thermal conductivity of the bed will significantly affect the fuel conversion and the dry hydrogen yield. The average porosity of the packed bed was indicated to be 0.6 by the catalyst manufacturer although this is known to vary slightly due to the random packing of the catalyst pellets. Calculations were undertaken for porosity values of 0.4, and 0.5 and compared against the base case where the porosity was 0.6. It should be noted that the effect of changes in porosity on the effectiveness factor have not been accounted for. Therefore the benefits of an increase in mass of catalyst have not been accounted for in the reaction kinetics.

Figure 5.11 shows the variation of pressure along the reactor bed for various porosity values.

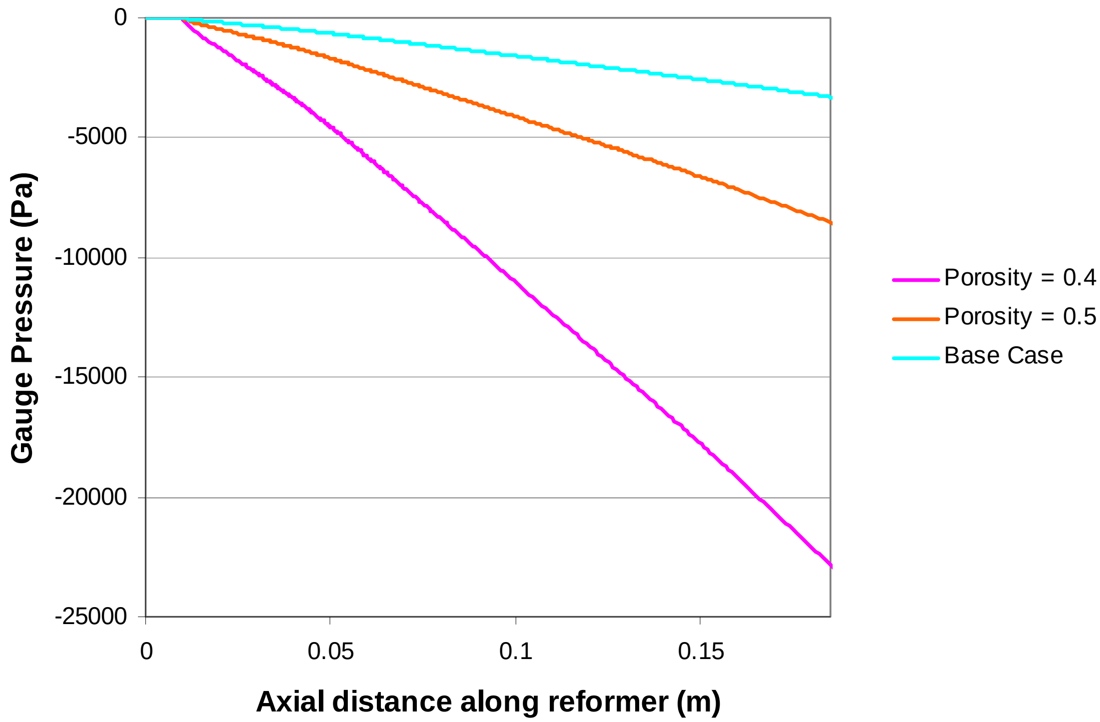

Figure 5.11: Pressure drop along axial reformer length

From figure 5.11, it can be seen that as the porosity is decreased, the pressure drop along the bed will increase. The change in porosity also has an effect on the bed thermal conductivity as mentioned above. Figure 5.12 shows the temperature profile along the bed with varying porosity values.

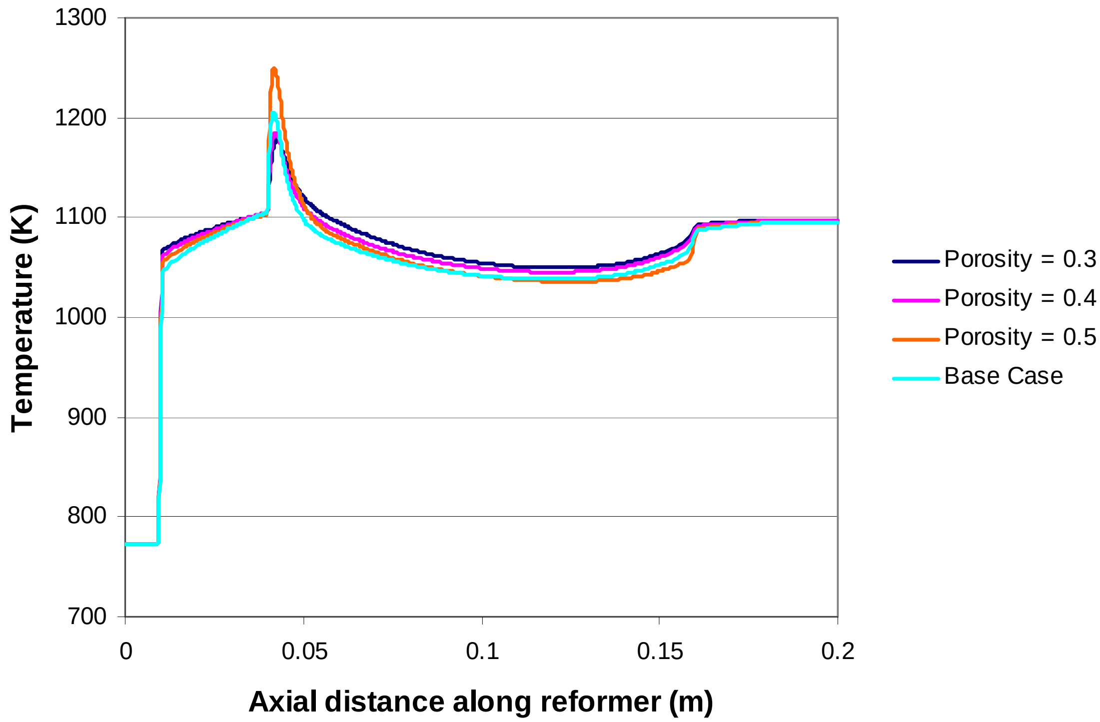

Figure 5.12: Centreline temperature profile along reformer for varying porosity

Decreasing the porosity of the reformer bed will be seen to produce relatively small changes in the temperature distribution. This is due to the fact that changes to the porosity will affect the heat transfer in the bed which will affect the performance of the reformer. To illustrate the effects of this change in heat transfer characteristics, the variation of the fuel conversion rate and dry hydrogen yield are shown figure 5.13.

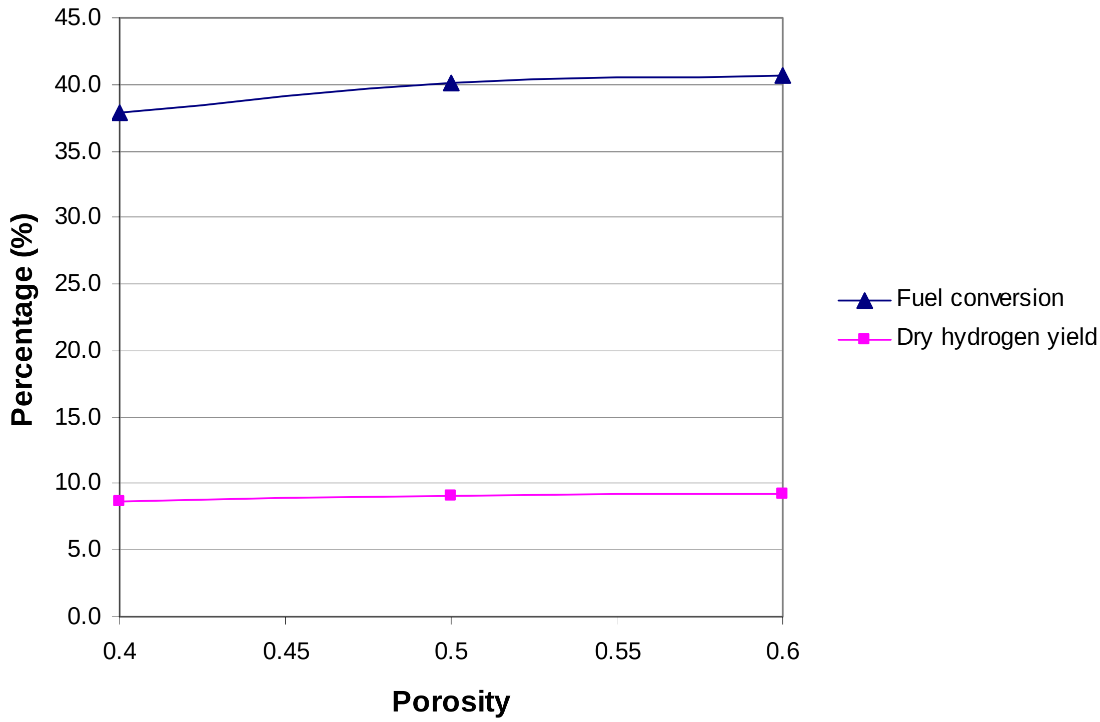

Figure 5.13: Fuel conversion and dry hydrogen yield for varying porosity

Figure 5.13 shows that lower porosity values result in a reduction in fuel conversion and dry hydrogen yield. Varying the porosity of the packed bed from 0.6 which is the porosity of the base case will be seen to produce a small reduction in fuel conversion and dry hydrogen yield. This indicates that reducing the porosity has a small influence on the performance of the reactor. As was stated earlier, the results do not to account for changes in the reaction kinetics due changes in porosity. In order to account for changes in the reaction kinetics, changes would need to be made to the value of the effectiveness factor, which for this study, was set to a constant value. The results therefore provide information about the pressure drop incurred by a change in porosity, and also illustrate the effects on the performance due to a change in the heat transfer rates in the bed.

5.7 Inlet Species Concentrations

Inlet concentrations ratios of O_2 to C_8H_{18} and H_2O to C_8H_{18} were varied to attempt to determine optimal inlet conditions for fuel conversion and dry hydrogen yield. O_2 to C_8H_{18} ratios were varied from 0.35 to 0.65 and H_2O to C_8H_{18} ratios were varied from 1.0 to 3.0 which is consistent with typical values discussed in the literature. The ratios were selected to match the trials intended for the prototype reformer. Figure 5.14 shows the fuel conversion for varying O_2 to C_8H_{18} and H_2O to C_8H_{18} inlet ratios.

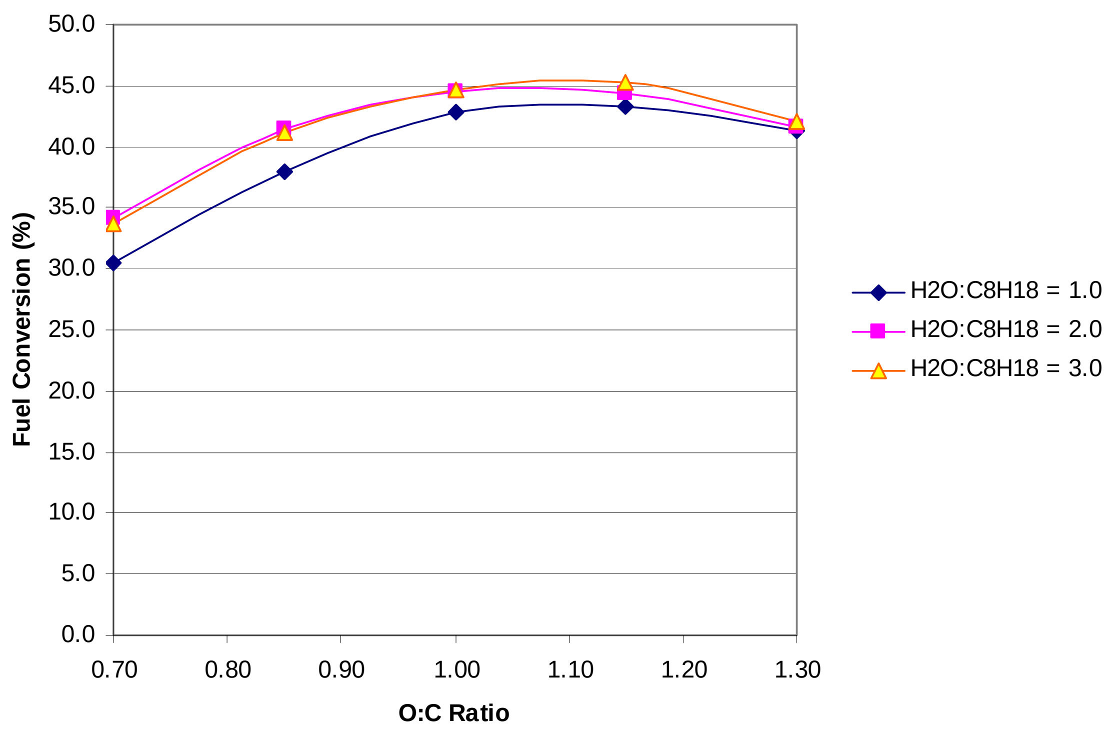

Figure 5.14: Fuel conversion for varying oxygen-to-carbon and steam-to-carbon ratios

Figure 5.14 shows that maximum fuel conversion is achieved when the oxygen-to-fuel ratio is between 1.0 and 1.15. It also shows that increasing the steam-to-fuel ratio from 1.0 to 2.0 yields a significant increase in fuel conversion, but increasing the steam-to-fuel ratio from 2.0 to 3.0 yields almost identical results. Of more interest is the dry hydrogen yield which is shown in figure 5.15 for varying oxygen-to carbon and steam-to-carbon inlet ratios.

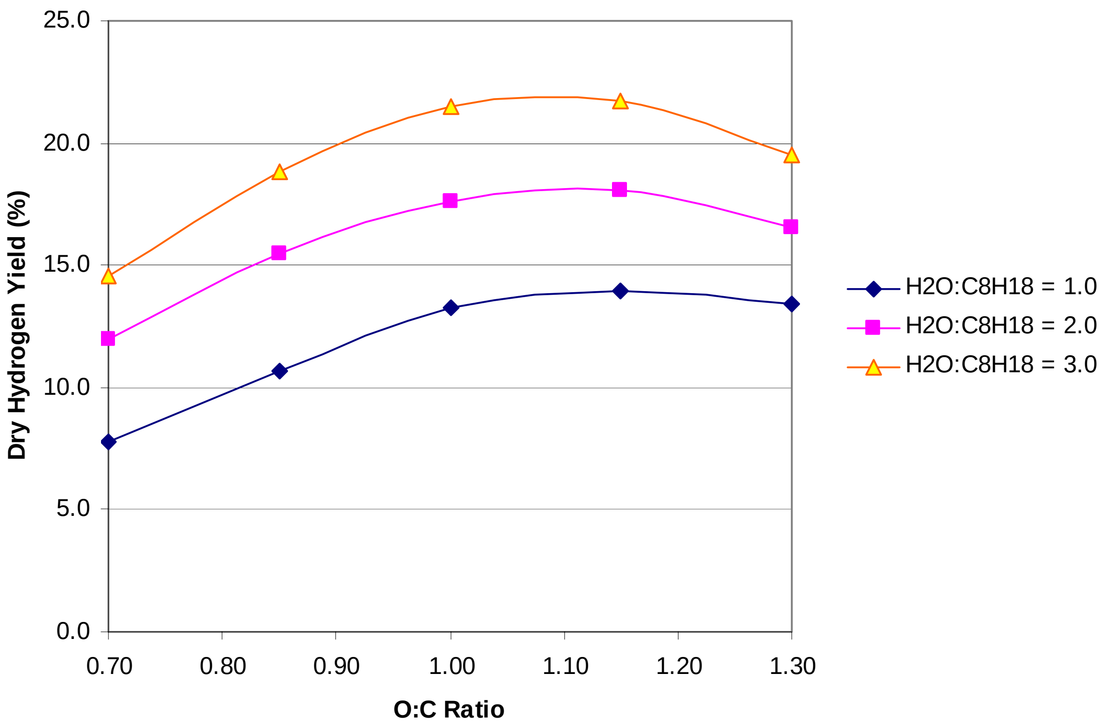

Figure 5.15: Dry hydrogen yield for varying oxygen to carbon and steam to carbon ratios

Figure 5.15 clearly show that a steam-to-carbon ratio of 3.0 with an oxygen-to-carbon ratio between 1.0 and 1.15 yields the maximum dry hydrogen yield. While figure 5.14 shows minimal differences in the fuel conversion from an increase in the steam-to-fuel from 2.0 to 3.0, figure 5.15 shows a significant increase in the dry hydrogen yield. An explanation for this is that although the fuel conversion performance is unchanged due to additional steam content beyond a steam-to-fuel ratio of 2.0, higher steam concentration levels may promote further production of hydrogen due to the water-gas-shift reaction. Figure 5.16 shows the variation in the water-gas-shift reaction along the reformer for varying the steam-to-fuel ratios when the oxygen-to-fuel ratio is set to 1.15.

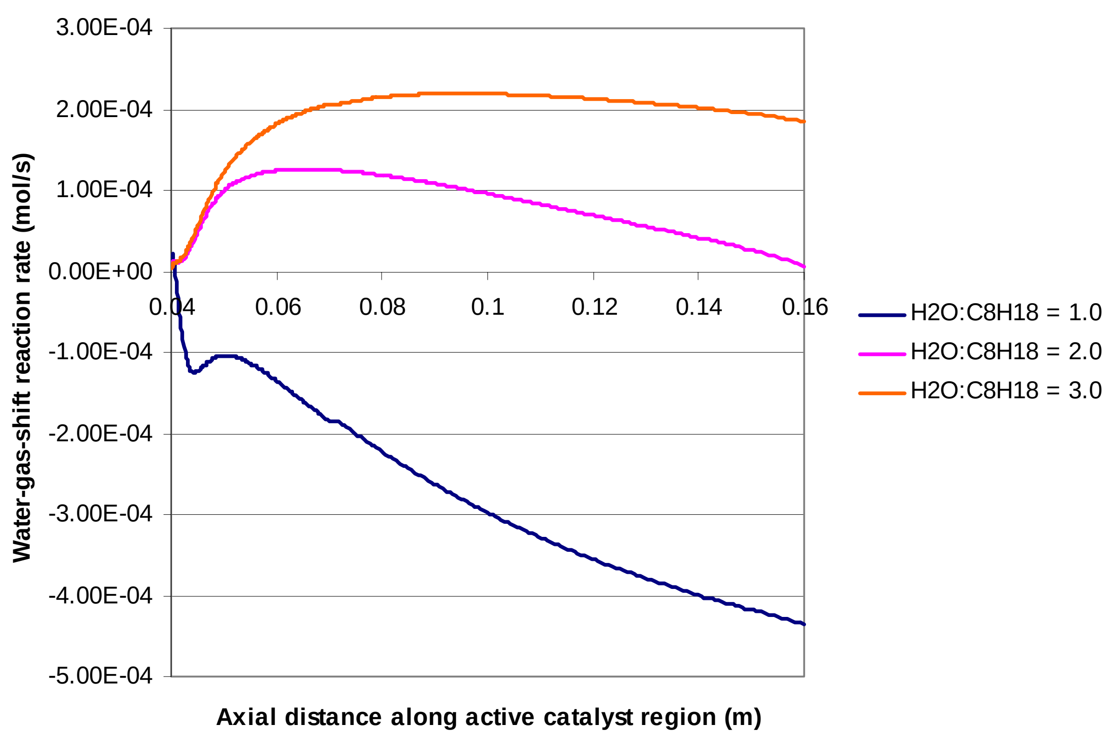

Figure 5.16: Rate of water-gas-shift reaction for varying steam-to-carbon ratios with an oxygen-to-carbon ratio of 1.15

Figure 5.16 shows an interesting result indicating that the highest WGS reaction rates occur at a steam-to-carbon ratio of 3.0 and that the reaction actually proceeds in reverse when the steam-to-carbon ratio is 1.0. Increasing the steam-to-carbon ratio effectively will result in a higher dry hydrogen yield. Additional benefits of increasing the steam-to-carbon ratio are in reduced coking and catalyst deactivation which was discussed in section 2.5.1.

5.8 Inlet Temperature

Gas inlet temperatures were varied to determine if preheating to higher inlet temperatures would significantly increase reactor performance, and to determine if lower inlet temperatures would significantly affect the results. Inlet temperatures were varied from 673K to 973K and product species concentrations were determined for these cases. The variation of fuel conversion and dry hydrogen yield with inlet temperature is shown in figure 5.17.

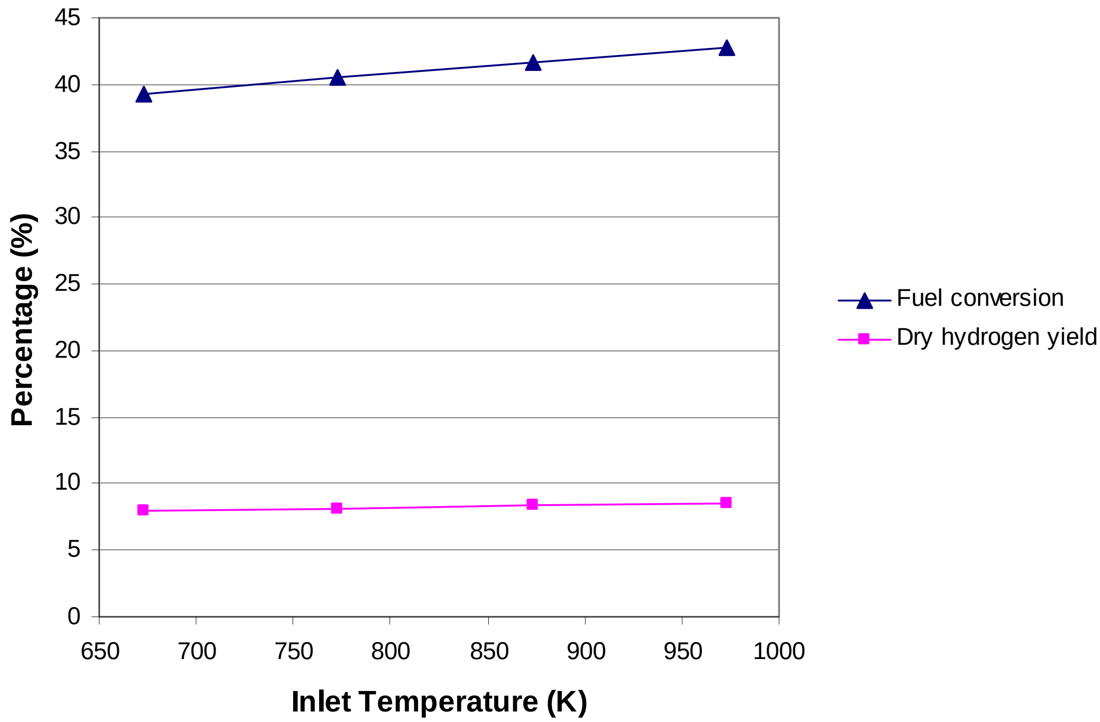

Figure 5.17: Fuel conversion and dry hydrogen yield percentages for varying inlet temperature

Figure 5.17 shows that varying the inlet temperature does not have a large influence on the fuel conversion and dry hydrogen yield of the reformer. The temperature profile variation with various inlet temperatures is shown in figure 5.18

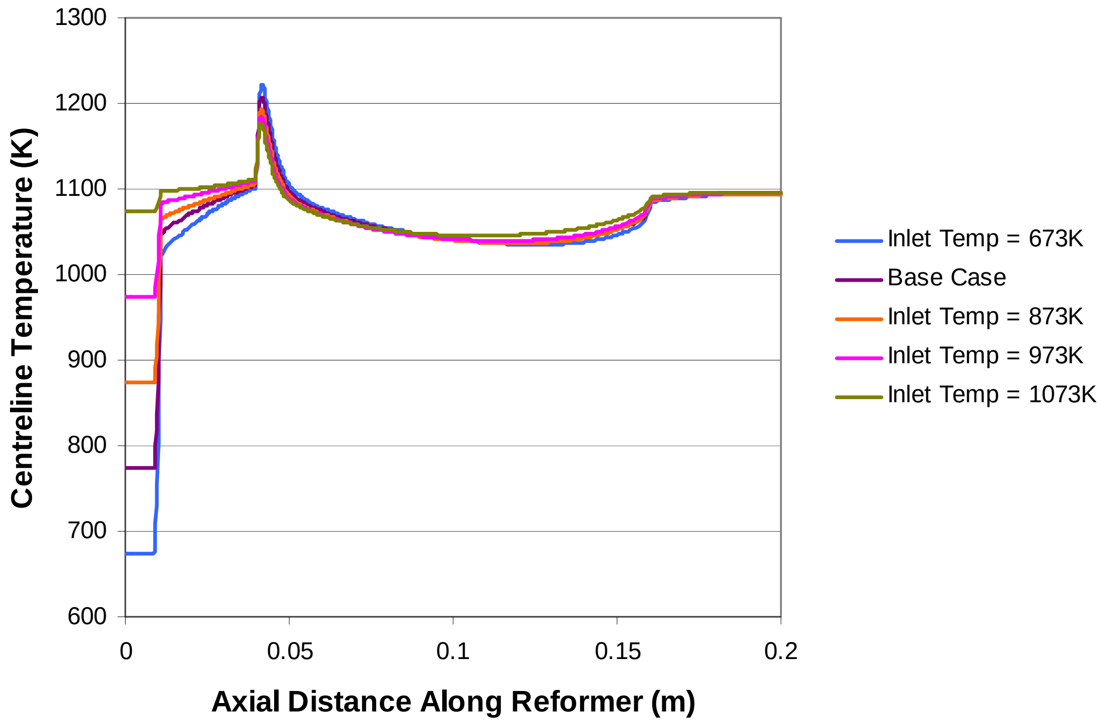

Figure 5.18: Centreline temperature profile for varying inlet temperatures

Figure 5.18 shows that the large variations in the inlet temperature do not greatly affect the overall temperature profile along the reformer. This indicates that inlet temperature does not have a strong influence on the rate of reaction in the catalyst region since the reactant gas is already at elevated temperatures. There are some small differences in the temperature profile which confirms the small changes in fuel conversion and dry hydrogen yield. This can be seen by looking at the overall reactions rates along the reformer for each case which are shown in figure 5.19.

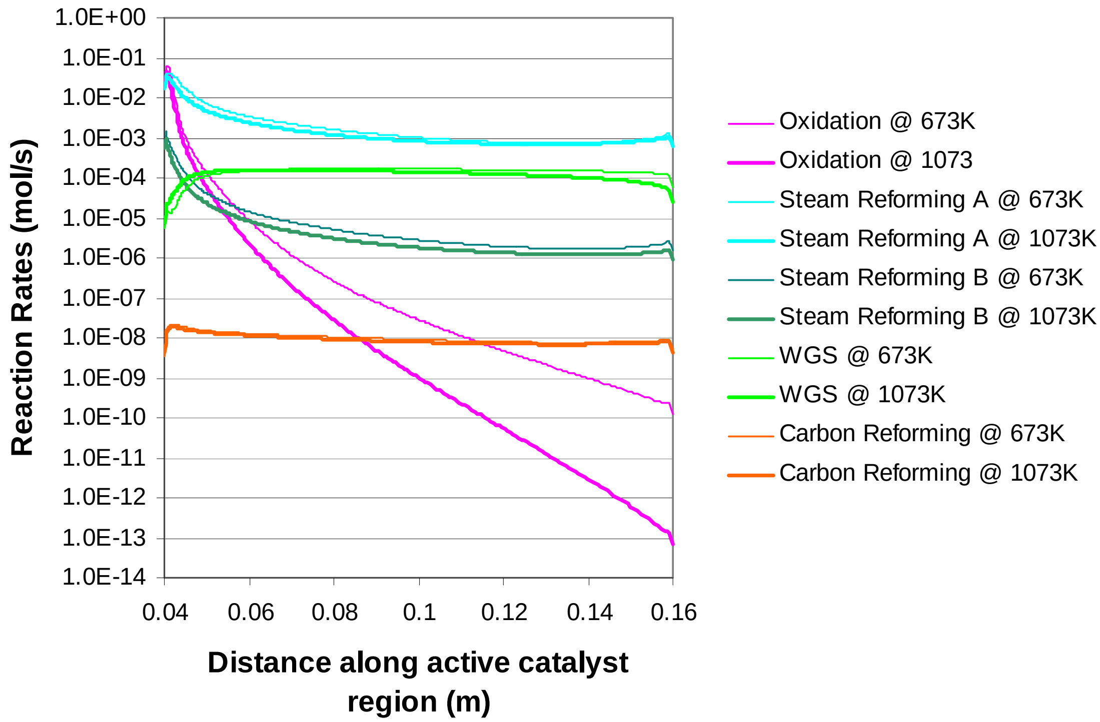

Figure 5.19: Reaction rates along the active catalyst region

Figure 5.19 shows that inlet temperature variation has a small influence on the overall reaction rates. Kang (2006) performed an experimental investigation on the autothermal reforming of iso-octane and found that for operating temperatures between 973K to 1123K, the concentrations of the product gas stream were relatively constant, though for temperatures below 973K, the reduction in fuel conversion and hydrogen yield was significant. Larger variations in product gas concentrations and reaction rates were expected for varying inlet temperature between 673K and 1073K. This indicates that the Pacheco et al. (2003) model may be limited in its range of operating temperatures for predicting the kinetic data of the reformer. Pacheco et al. (2003) reported that the data regression performed to determine the kinetic parameters of the chemical reaction mechanism considered three different operating temperatures, though these temperatures were never discussed. Without knowledge of these temperatures, it is unclear whether the Pacheco et al. (2003) model is appropriate for determining the performance of the reformer when there are such large variations in temperature.

5.9 Gas-Hourly-Space-Velocity

As stated before, the gas hourly space velocity (GHSV) is a measure that is inversely related to the residence time of a reactant gas at an active catalyst site. With a longer residence time, more reactant gas is able to convert to product gas due to longer exposure to the catalyst zone. In the development of the reformer, it is beneficial to know the relationship between the fuel conversion rate and GHSV since this governs the quantity of hydrogen produced. To determine this relationship, several calculations were run in which the GHSV was varied from 8000 to 150000 h^{-1}. The results obtained are plotted in terms of fuel conversion against GHSV in figure 5.20.

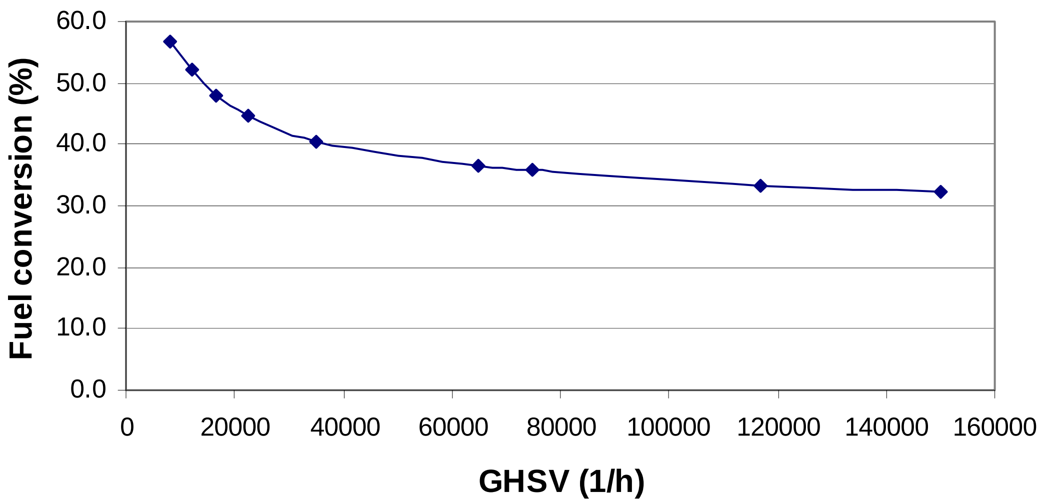

Figure 5.20: Fuel conversion percentage for varying catalyst residence time

The results in figure 5.20 provide the information necessary to determine by how much the conversion efficiency will suffer when hydrogen production is required at higher rates. To examine the difference in product gas yield, a plot of species concentrations at the outlet for various GHSV's is given in figure 5.21.

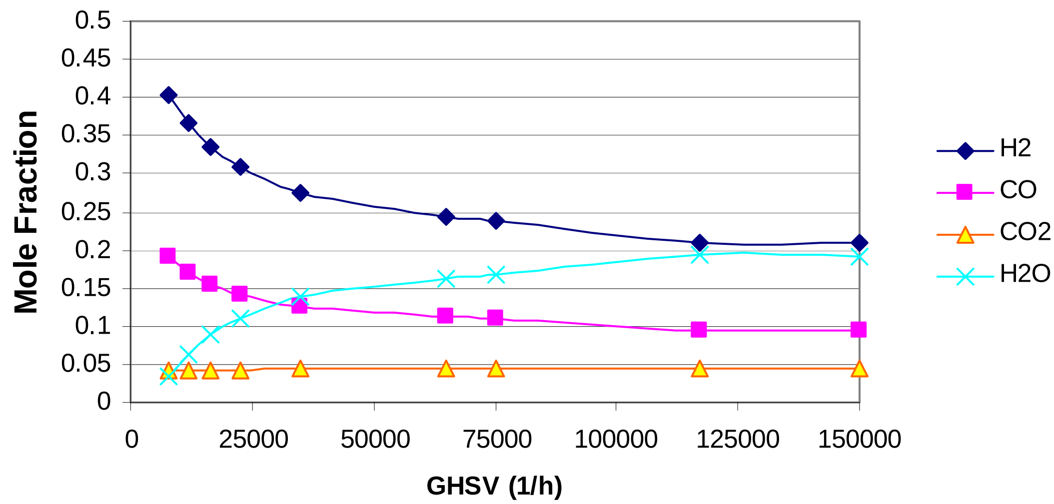

Figure 5.21: Mole fraction of product species for varying GHSV

Figure 5.21 clearly shows that as the GHSV is increased, the hydrogen yield decreases, though carbon monoxide yield also decreases. When the GHSV is very high, product gas concentrations approach a constant value.

5.10 Effectiveness Factor

For the present study, it has been assumed that the effectiveness factor has a constant value throughout the catalyst bed. However, it is well know that the effectiveness factor is not constant, rather it varies as species concentrations change along the length of the catalytically active region. To determine how influential the effectiveness factor is on the rate of reaction, as well as on the fuel conversion rate and the hydrogen yield, results were obtained with several different effectiveness factors ranging in value from 0.0001 to 0.01. Figure 5.22 shows the fuel conversion and dry hydrogen yield with varying the effectiveness factor.

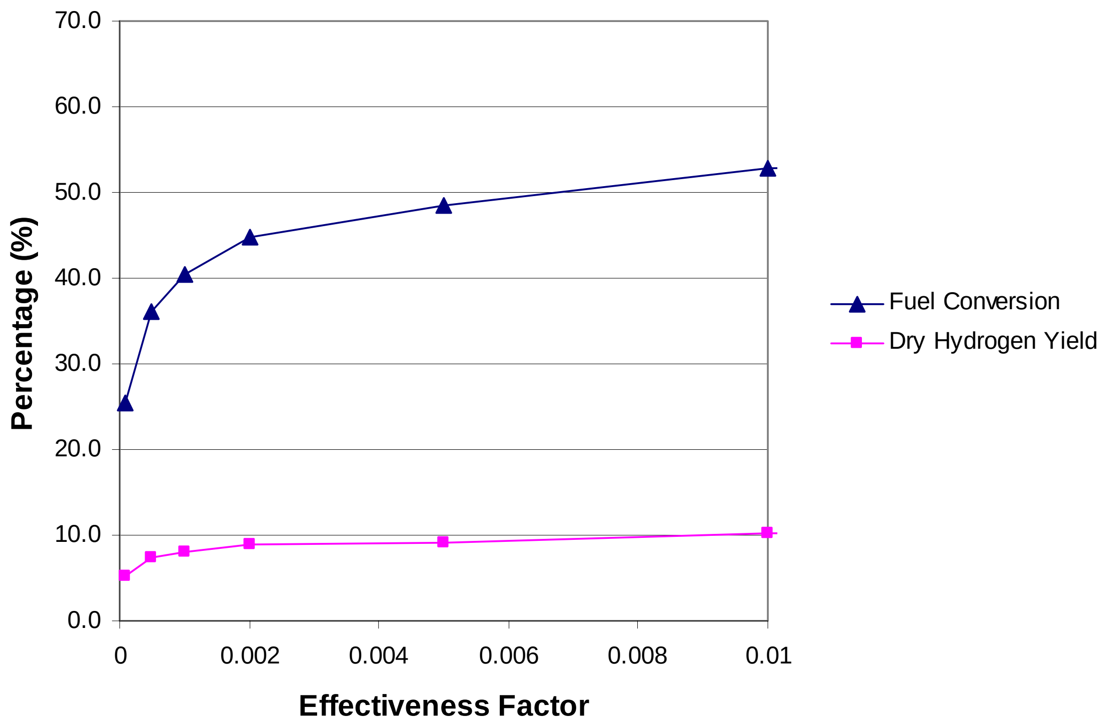

Figure 5.22: Fuel conversion and dry hydrogen yield for varying effectiveness factor

Figure 5.22 clearly indicates that varying the effectiveness factor has a large effect on the fuel conversion and dry hydrogen yield of the reformer. To further examine the affects of changing the effectiveness factor, a plot of the rate of steam reforming reaction A for various effectiveness factors is shown in figure 5.23.

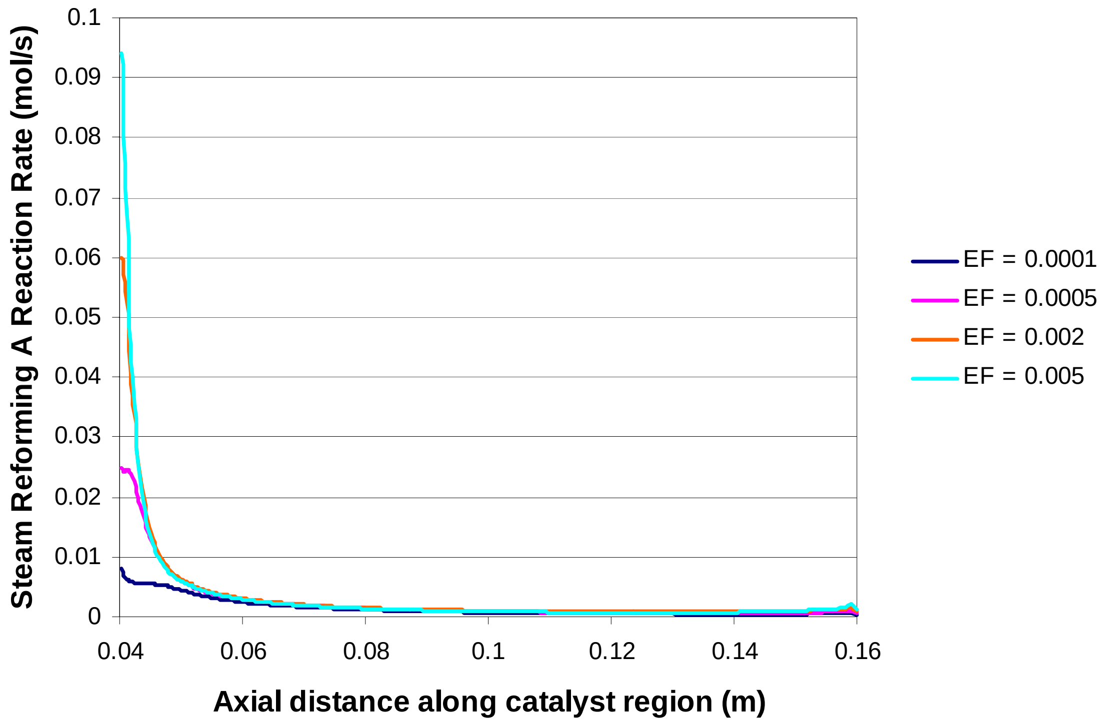

Figure 5.23: Steam reforming A reaction rate for varying effectiveness factors

Figure 5.23 shows large variations in the peak reaction rate with effectiveness factor. After roughly 1cm beyond the entrance to the catalytically active region, reaction rates attain a near constant value for the rest of the reformer in all cases. The impact on the product gas hydrogen concentration is shown in figure 5.24.

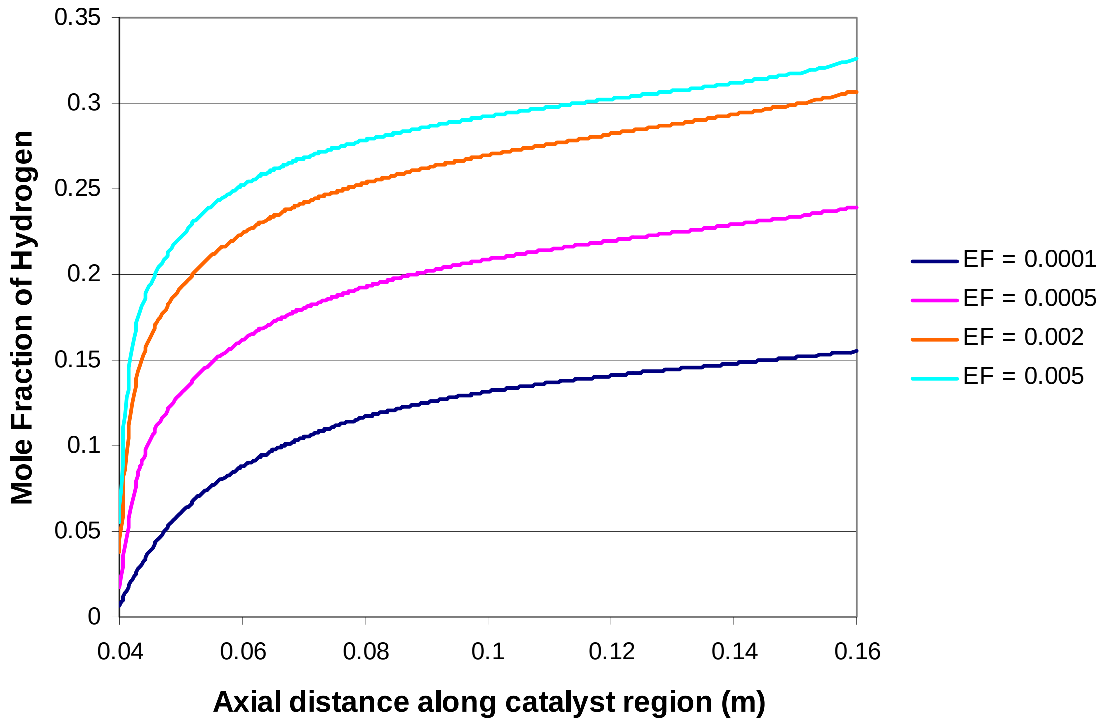

Figure 5.24: Mole fraction of hydrogen product gas for varying effectiveness factors

Figure 5.24 shows that the majority of the hydrogen production occurs in the first 2cm of the catalyst bed. Higher effectiveness factor values result in higher hydrogen yield which is consistent with the higher reaction rates of the steam reforming reaction A shown in figure 5.23. To further illustrate, the impact of effectiveness factor on all of the product gas outlet concentrations is shown in figure 5.25.

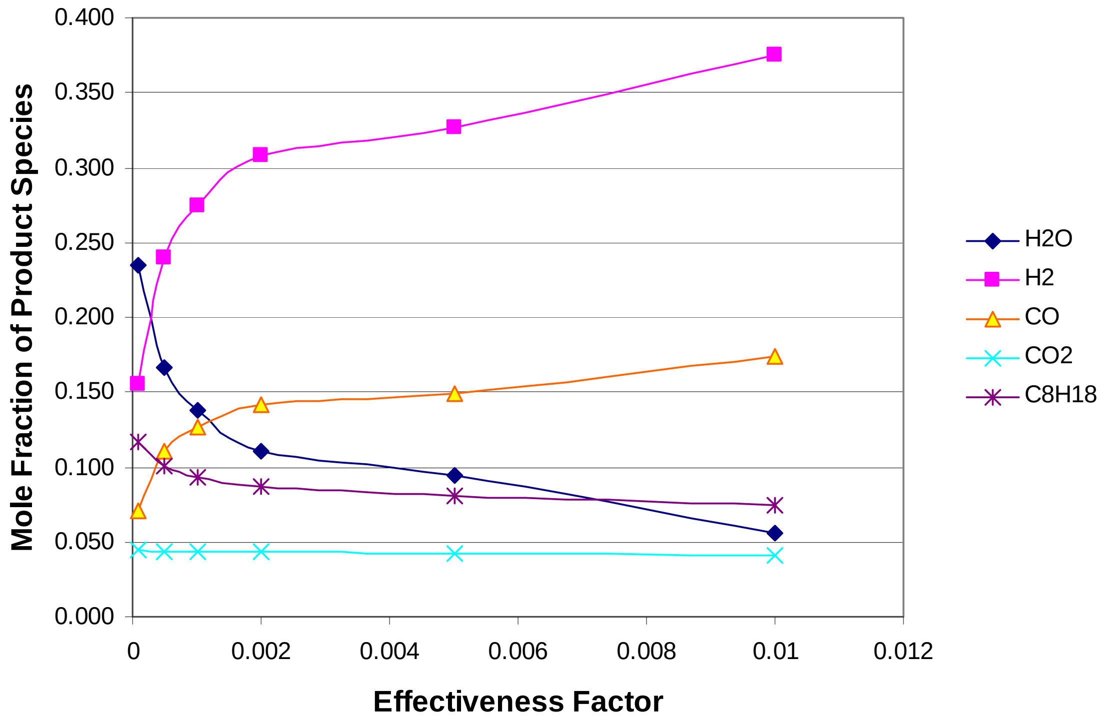

Figure 5.25: Product species mole fraction for varying effectiveness factors

Figure 5.25 shows the large variation in all product species with varying effectiveness factor. This confirms that use of a constant value for the effectiveness factor may lead to significant discrepancies between the computed results and the experimental results. A further investigation into the formulation of the effectiveness factor is required to obtain a better estimate of its value. This is discussed in Appendix A.

Chapter 6
Conclusions and Recommendations

6.1 Conclusions

An autothermal reformer using a proprietary platinum on zirconia-ceria base catalyst for the purpose of reforming of iso-octane was evaluated using a computational fluid dynamics software package. This was done in order to study the performance and product gas yield of the reformer and to determine the effects of varying the operating conditions and the material properties of the reformer. Results obtained show areas for potential improvements in for the reformer design as well as indicating the optimal operating conditions for the present reformer. The main findings of the study are:

- The dry hydrogen yield and the fuel conversion efficiency of the base case considered were found to be 9.2% and 40.6% respectively.
- By increasing the wall thermal conductivity, a more evenly distributed temperature distribution can be achieved along the catalyst bed resulting in higher chemical reactivity and higher hydrogen yield.
- Improving the catalyst thermal conductivity greatly reduces the large temperature gradients in the catalyst bed that result from the highly exothermic oxidation reaction by conducting the heat more evenly throughout the catalyst bed. This results in higher average reaction rates that contribute to a higher hydrogen yield and a better overall fuel conversion efficiency.

- Decreasing the porosity of the packed bed in the reformer from 0.6 to 0.4 results in a small increase in the pressure drop along reformer. It also affects the heat transfer along the bed where higher temperature gradients exist for lower porosity bed values.
- Variations in the inlet temperature were found to have a small influence on the fuel conversion and dry hydrogen yield of the reformer.
- A steam-to-fuel molar ratio of 3.0 and an oxygen-to-fuel ratio between 1.0 and 1.15 will yield maximum fuel conversion and dry hydrogen yield
- Increasing the gas-hourly-space-velocity results in a higher hydrogen production rate at the expense of a reduced fuel conversion and hydrogen yield on an output percentage basis.
- There are variations in the product species concentrations with varying effectiveness factors which indicates that the use of a constant value for the effectiveness factor may not adequately predict the reformer performance.

6.2 Recommendations for Future Work

While the results provided much information about the performance of the reformer, it is recommended that a number of steps should be taken to improve the numerical model so that a more accurate prediction of the reactor performance can be obtained. To improve the model, a number of steps should be considered, these being:

- Undertaking an investigation into available catalysts that have a higher thermal conductivity to significantly reduce the large temperature gradients in the packed bed and to increase the average bed temperature thereby increasing the rate of the steam reforming reaction.

- Incorporating the intraparticle diffusion effects into the computational model by obtaining measurements or better estimates of the catalyst porosity, pore diameters and pore tortuosity.
- With inclusion of diffusional effects into the model, improvements can be made in the prediction of the effectiveness factors for each reaction of the chemical reaction mechanism.
- Further experimental work examining the actual reaction kinetics of the current reformer under its operating conditions using the selected catalyst can provide better estimates of the reaction constants in the Pacheco et al. (2003) model to improve the accuracy of the results given by this model.
- Conduct a numerical study of the reformer performance when varying multiple parameters such as wall thermal conductivity, catalyst thermal conductivity and inlet temperature simultaneously and use the results to optimize the design.
- The results indicate that the performance of the reformer will increase with reformer length. Therefore a study should be undertaken to determine the costs associated with increasing the length of the reformer so that a comparison can be made between the increase in the cost and the benefits of an increase in length of the reformer.

References

Ahmed, S., Krumpelt, M., "Hydrogen from hydrocarbon fuels for fuel cells" International Journal of Hydrogen Energy, Vol. 26, pp. 291-301, (2001)

Aicher, T., Lenz, B., Gschnell, F., Groos, U., Federici, F., Caprile, L., Parodi, L., "Fuel processors for fuel cell APU applications" Journal of Power Sources Vol. 154, pp. 503-508, (2006)

Asif, M., Muneer, T., "Energy supply, its demand and security issues for developed and emerging economies", Renewable and Sustainable Energy Reviews, Vol. 11, pp. 1388-1413, (2007)

Argonne National Laboratories (ANL), www.anl.gov, (2007)

Beretta, A., Baiardi, P., Prina, D., Forzatti, P., "Analysis of a catalytic annular reactor for very short contact times" Chemical Engineering Science, Vol. 54, pp. 765-773, (1999)

Caners, C. "The experimental evaluation of a compact autothermal gasoline reformer for fuel cell applications" MSc, Queen's University, (2005)

Dixon, A.G., Nijemeisland, M., "CFD as a design tool for fixed-bed reactors" Industrial Engineering Chemistry, Vol. 40, pp. 5246-5254, (2001)

Dixon, A.G., Nijemeisland, M., "CFD study of fluid flow and wall heat transfer in a fixed bed of spheres" AIChE Journal, Vol. 50, pp. 906-921, (2004) Docter, A., Lamm, A., “Gasoline fuel cell systems” Journal of Power Sources, Vol. 84, pp. 194-200, (1999)

Energy Information Administration (EIA), www.eia.doe.gov/oiaf/ieo/world.html, (2006)

Ergun, S., “Fluid flow through packed columns” Chemical Engineering Programming Vol. 48, pgs. 89–94 (1952)

Ferziger, J.H., “Estimation and reduction of numerical error” ASME Winter Annual Meeting, CA, (1989)

Fogler, S.,H., “Elements of Chemical Reaction Engineering” Prentice-Hall, Inc., NJ, (1999)

Hoang, D.L., Chan, S.H., “Modeling of a catalytic autothermal methane reformer for fuel cell applications” Applied Catalyst A: General, Vol. 268, pp. 207-216, (2004)

Fluent User’s Guide, Fluent Documentation 6.2, www.fluent.com, Lebanon, NH (2005)

Ibrahim, H.H., Idem, R.O., “Kinetic studies of the partial oxidation of iso-octane for hydrogen production over a nickel-alumina catalyst” Chemical Engineering Science, Vol. 61, pp. 5912-5918, (2006)

Incropera, F.P., DeWitt, D.P., “Introduction to Heat Transfer 3rd Edition” John Wiley & Sons, NY, (1985)

Jin, W., Gu, X., Li, S., Huang, P., Xu, N., Shi, J., “Experimental and simulation study on a catalyst packed tubular dense membrane reactor for partial oxidation of methane to syngas” Chemical Engineering Science, Vol. 55, pp. 2617-2625, (2000) Kaila, R.K., Krause, A.O.I, "Autothermal reforming of simulated gasoline and diesel fuels" International Journal of Hydrogen Energy, Vol. 31, pp. 1934-1941, (2006)

Kang, I., Bae, J., Bae, G., "Performance comparison of autothermal reforming for liquid hydrocarbons, gasoline and diesel for fuel cell applications" Journal of Power Sciences, Vol. 163, pp. 538-546, (2006)

Krumpelt, M., Krause, T.R., Carter, J.D., Kopasz, J.P., Ahmed, S., "Fuel processing for fuel cell systems in transportation and portable power applications" Catalyst Today, Vol. 77, pp. 3-16, (2002)

Krishna, R., "Problems and pitfalls in the use of the fick formulation for intraparticle diffusion" Chemical Engineering Science, Vol. 48, pp. 845-861, (1993)

Larminie, J., Dicks, A., "Fuel Cell Systems Explained" John Wiley & Sons, LTD., Chichester, England (2000)

Latimer, B.R., Pollard, A., "Comparison of pressure-velocity coupling solution algorithms" Numerical Heat Transfer, Vol. 8, pp. 635-652, (1985)

Leonard, B.P., "A Stable and accurate convective modeling procedure based on quadratic upstream interpolation" Computational Methods and Applications in Mechanical Engineering, Vol. 12, pp. 59-98, (1979)

Li, V.C., "Development of a basic numerical model of an iso-octane catalytic autothermal reformer for an automobile" MSc, Queen's University, (2004) Maestri, M., Beretta, A., Groppi, G., Tronconi, E., Forzatti, P., "Modeling of fixed bed reactors for the catalytic partial oxidation of methane to syngas: a comparison among structured and packed bed reactors" Chemical Engineering Transactions, Vol. 6, pp. 13-18, (2005)

Mears, D.E., "On criteria for axial dispersion in non-isothermal packed bed catalytic reactors" Industrial Engineering Chemistry, Vol. 15, pp 20-27, (1976)

Mears, D.E., "Tests for transport limitations in experimental catalytic reactors" Industrial Engineering Chemistry, Vol. 10, pp. 541-547, (1971)

McIntyre, C., "Development of a numerical model of a compact autothermal reformer for the production of hydrogen from iso-octane" MSc, Queen's University, (2005)

Middleton, C., "Design and construction of an autothermal gasoline reformer" MSc, Royal Military College of Canada, (2004)

Moran, M.J., Shapiro, H.N., "Fundamentals of Engineering Thermodynamics" John Wiley & Sons, Inc., NY, (1988)

Murata, K., Saito, M., Inaba, M., Takahara, I., "Hydrogen production by autothermal reforming of sulfur containing hydrocarbons over re-modified Ni/Sr/ZrO2 catalysts" Applied Catalysis B: Environmental, Vol. 70, pp. 509-514, (2007)

Olivieri, A., Personal Communication, (2007)

Oosthuizen, P., Naylor, D., "Introduction to Convective Heat Transfer Analysis" WCB/McGraw Hill, NY, (1999) Pacheco, M., Sira, J., Kopasz, J., “Reaction kinetics and reactor modeling for fuel processing of liquid hydrocarbons to produce hydrogen: iso-octane reforming” Applied Catalyst A: General, Vol. 250, pp.161-175, (2003)

Patankar, S.V., “Numerical Heat Transfer and Fluid Flow” Hemisphere Publishing Corporation, NY, (1980)

Praharso, Adesina, AA, Trimm, D.L., Cant, N.W., “Kinetic study of iso-octane steam reforming over a nickel-based catatlyst” Chemical Engineering Journal, Vol. 99, pp. 131-136, (2004)

Pollard, A., Siu, A., “The calculation of some laminar flows using various discretisation schemes” Computer Methods in Applied Mechanics and Engineering, Vol. 35, pp. 293-313, (1982)

Rabe S., Truonga T., and Vogel F., “Catalytic autothermal reforming of methane: Performance of a kW scale reformer using pure oxygen as oxidant” Applied Catalyst A: General, Vol. 318, pp. 54-62, (2007)

Raithby, G.D., “Skew upstream differencing schemes for problems involving fluid flow” Computer Methods in Applied Mechanics and Engineering, Vol. 9, pp. 153-164, (1975)

Rioux, R.M., Marsh, A.L., Gaughana, J.S., and Somorjai, G.A.”Oxidation and reforming reactions of CH4 on a stepped Pt(5 5 7) single crystal”, Catalysis Today, (2007)

Roychoudhury, S., Castaldi, M., Lyubovsky, M., LaPierre, R., Ahmed, S., “Microlith catalytic reactors for reforming iso-octane based fuels into hydrogen” Journal of Power Sciences, Vol. 152, pp. 75-86, (2005) Schwarz, S., NexTech Materials, personal communication, (2007)

Thurgood, C., Amphlett, J., Mann, R., Peppley, B., “Methanol-steam reforming in a packed-bed reactor: inclusion of radial porosity”, AIChE Spring National Meeting, New Orleans, LA, (2003)

Tiemersma, T.P., Patil, C.S., van Sint Annaland, M., Kuipers, J.M. “Modeling of packed bed membrane reactors for autothermal production of ultrapure hydrogen”, Chemical Engineering Science, Vol. 61, pp. 1602-1616, (2006)

Transport Canada, http://www.tc.gc.ca/pol/en/Report/anre2005/5_e.htm, (2003)

Villegas, L., Guilhaume, N., Provendier, H., Daniel, C., Masset, F., Mirodatos, C., “A combined thermodynamic/experimental study for the optimization of hydrogen production by catalytic reforming of isooctane” Applied Catalyst, Vol 281, pp. 75-83, (2005)

Wakao, N., Kaguei, S., “Heat and mass transfer in packed beds” Gordon and Breach Science Publishers, NY, (1982)

Xu, J., Froment, G.F., “Methane steam reforming, methanation and water gas shift: I. Intrinsic kinetics” AIChE Journal, Vol. 35, pp. 88-96, (1989)

Xu, J., Froment, G.F., “Methane steam reforming: II. Diffusional limitations and reactor simulation” AIChE Journal, Vol. 35, pp. 97-103, (1989)

Appendix A
Improvements to Numerical Model

Consideration of the results obtained in this study that were discussed in chapter 5 suggests that consideration should be given in further reformer modeling work to improve some aspects of the model. In particular, improvements to the modeling of the packed bed should be considered. Some such improvements will be discussed in this appendix. The effectiveness factor and the Pacheco et al. (2003) chemical reaction mechanism have been used in the present work with several assumptions that need re-evaluation. The theory and parameters required to improve upon these aspects of the modeling are discussed in this appendix.

In the present work, the effectiveness factor which was defined as the ratio of the actual overall reaction rate to the maximum rate possible if the entire catalyst surface was exposed to bulk gas concentration was set to a constant value of 0.001 for all calculations discussed. This served as a conservative approximate value since the determination of the actual effectiveness factor was made difficult by several factors. The effectiveness factor is known to actually vary along the length of the reactor bed. To describe the effectiveness factor in mathematical terms, the dimensionless parameter called the Thiele modulus is commonly used, which can be described as the ratio of the surface reaction rate to the diffusion reaction rate. The Thiele modulus will vary depending on the reaction order and the reaction kinetics of the chemical reaction mechanism it is describing. Pacheco et al. (2003) reported the Thiele modulus for a pseudo-first order reaction as follows:

$$\phi_n = \frac{r_p}{3}\sqrt{\frac{k_i^{'}(K_{eq,i}+1)}{D_{eff}K_{eq,i}}} \tag{6.1}$$

where r_p = catalyst particle radius

$k_i^{'}$ = pseudo-first order reaction constant for chemical reaction i

$K_{eq,i}$ = pseudo-first order equilibrium constant for chemical reaction i

D_{eff} = effective diffusivity

This form of the Thiele modulus is for a first-order reaction rate as stated above. Reactions ii-v as defined in section 3.5.1, are second order rate equations. Defining the effectiveness factor using first order equations is much easier than with second order equations, therefore rewriting the second order equations in a pseudo-first order form provides a simplified approach to determining the effectiveness factor. An example of the pseudo-first order reaction rate, the pseudo-first order reaction rate constant and the pseudo-first order equilibrium constant for the steam reforming A reaction are:

$$r^{'}_2 = k_2^{'}\left(P_{C_8H_{18}} - \frac{P_{CO}}{K_{eq2}}\right) \tag{6.2}$$

where $k_2^{'} = \left(\dfrac{k_2 P_{H_2O}}{P_{H_2}^{2.5}\left(1 + K_{CO}p_{CO} + K_{H_2}p_{H_2} + K_{iC_8H_{18}}p_{iC_8H_{18}} + K_{H_2O}(p_{CO}/p_{H_2}\right)}\right)$

and $$K_{eq2} = \frac{K_1 P_{H_2O}}{P_{H_2}^3} \tag{6.3}$$

Once the Thiele modulus is determined a correlation for the effectiveness factor to the Thiele modulus can be obtained again assuming spherical catalyst pellets. Pacheco et al. (2003) reported this correlation to be as follows:

$$\eta = \frac{1}{\phi_n} \frac{(3\phi_n)\coth(3\phi_n) - 1}{3\phi_n} \tag{6.4}$$

The effectiveness factor is commonly obtained by this method of relating it to the Thiele modulus. In all instances of determining the Thiele modulus, a reaction rate constant as well as an effective diffusivity must be determined. The reaction rate constant is derived from the Arrhenius equation as described in section 3.5. The effective diffusivity refers to the interparticle diffusion of reactant gases into the void spaces between catalyst particles as well as the intraparticle diffusion of reactant gases into the catalyst pellet. In the present work it was assumed that molecular diffusion is negligible relative to the bulk motion of the fluid and as a result the effective diffusivity term only accounts for convective species interactions in the void spaces of the catalyst bed and not the interparticle or intraparticle diffusion effects. This assumption also then implies that the reaction mechanism is reaction rate limited and not diffusion rate limited. While the chemical reaction mechanism is limited by the rate of reaction for the majority of the catalyst bed, at the entrance region to the catalyst bed, diffusion limitations play a larger role since reaction rates are very high. In order to correctly determine the effectiveness factor along the bed, interparticle and intraparticle species diffusion must be determined for the entire catalyst bed and incorporated into the model.

In order to account for molecular diffusion the effective diffusivity term requires some attention. Diffusion is commonly described as either molecular or bulk diffusion, Knudsen diffusion, or a combination of the two depending on the relative magnitude of the mean free path of the molecules and the catalyst pore radius. Bulk diffusion refers to the collision of molecules with other molecules and Knudsen diffusion refers to the collision of molecules with any surface. Knudsen diffusion will dominate when catalyst pore diameters are very small compared to the mean free path of the molecules. With larger pore diameters, molecules will have a higher probability of colliding with each other and Knudsen diffusion effects become negligible. There is a range over which both molecular diffusion and Knudsen diffusion are dominate and is referred to simply as the transition regime. To determine the dominate mechanism Zalc et al. (2003) reported a range for the ratio of the mean free path of molecules to catalyst pore radius as follows:

Bulk Diffusion: $\lambda / r_p < 0.05$

Transition regime: $0.05 < \lambda / r_p < 30$

Knudsen Diffusion: $\lambda / r_p > 30$

The mean free path (λ) is the average distance traveled between collisions for a gas molecule and can be derived from the kinetic theory of gases that gives the following.

. $$\lambda = \frac{k_b T}{P\sqrt{2}\pi\ \sigma^2} \tag{6.5}$$

where T = temperature (K)

σ = diameter of gas molecule (m)

k_b = Boltzmann constant

P = total pressure (Pa)

Although the mean free path for gas molecules can be calculated quite easily, determining catalyst pore radii is not easily done. This is because catalyst pores are extremely small channels and vary in length, shape, and diameter that poses a problem for determining average values. Information about the catalyst pores was not provided by the catalyst manufacturer and measurements or estimates of pore length and diameter could not be conducted at the FCRC. Pacheco et al. (2003) made estimates of the catalyst pore diameter, but did not discuss in detail how it was determined. Although this value is an estimate for a different catalyst pellet from the catalyst selected for this project, it aids in determining the steps necessary to complete the calculation of the effectiveness factor. Pacheco et al. (2003) determined that diffusion into the catalyst pellets fell in the transition regime where both bulk diffusion and Knudsen diffusion occur.

The effective diffusivity when describing both bulk and Knudsen diffusion as written by Pacheco et al. (2003) is as follows:

$$\frac{1}{D_{eff}} = \frac{t}{\theta}\left(\frac{1}{D_k} + \frac{1}{D_m}\right) \tag{6.6}$$

where t = tortuosity

θ = void fraction of the catalyst pellet

D_k = Knudsen diffusion coefficient

D_m = molecular or bulk diffusion coefficient

The tortuosity factor can be described as the ratio of the actual distance a gas molecule travels between two points to the shortest distance between the two points. Although actual tortuosity values vary throughout the catalyst pores, an average value is typically used. A range of tortuosity values in different catalytic systems for various void fractions was reported by Robert (1981). Pacheco et al. (2003) estimated the catalyst void fraction to be 0.19 and therefore used a tortuosity value of 2. For the present study, better estimations of the catalyst void fraction would need to be made before a reasonable tortuosity factor could be predicted. Poling et al. (2001) and Smith (1970) provide the theory necessary to calculate the diffusion coeffients D_k and D_m.

Once all parameters are calculated, estimates of the effectiveness factor can be made assuming that parameters such as tortuosity, catalyst pore radius, and catalyst void fraction are known. This calculation is also dependent on the accuracy of the chemical reaction kinetics to describe the actual chemical reactions occurring. Further investigation into the reaction mechanism employed is necessary determine to determine if changes to the mechanism are required.

As was discussed in section 3.5.1, the chemical reaction mechanism employed by Pacheco et al. (2003) was derived directly from studies conducted by Xu and Froment (1989) on methane steam reforming and by Jin et al. (2000) on methane partial oxidation. Pacheco et al. (2003) performed a data regression analysis on the results of these studies to obtain new pre-exponential factors and equilibrium constants so that numerical modeling results would reflect experimental data results. The ability of a data regression process on the reaction kinetics of a lighter hydrocarbon such as methane to predict the reaction kinetics for autothermal reforming of iso-octane is still uncertain. An obvious issue that has become evident is in the reaction rate equilibrium constant. This can be easily shown considering reaction *iv* in the Pacheco et al. (2003) mechanism:

iv) Steam Reforming B: $C_8H_{18} + 16H_2O \rightarrow 8CO_2 + 25H_2$

Using partial pressures, the equilibrium constant for this reaction would be:

$$K_4^{'} = \frac{p_{H_2}^{25} p_{CO_2}^{8}}{p_{iC_8H_{18}} p_{H_2O}^{16}}$$

The rate expression described by Pacheco et al. (2003) for this reaction is

$$r_4 = \frac{k_4}{p_{H_2}^{3.5}}\left(p_{iC_8H_{18}} p_{H_2O}^{2} - \frac{p_{H_2}^{4} p_{CO_2}}{K_4\left(1 + K_{CO}p_{CO} + K_{H_2}p_{H_2} + K_{iC_8H_{18}}p_{iC_8H_{18}} + K_{H_2O}(p_{CO}/p_{H_2})\right)}\right)$$

At equilibrium $r_4 = 0$. Therefore, the Pacheco et al. (2003) equilibrium constant becomes:

$$K_4 = \frac{p_{H_2}^{4} p_{CO_2}}{p_{iC_8H_{18}} p_{H_2O}^{5}}$$

Although K'_4 and K_4 are broadly similar, they obviously will produce different equilibrium constants. As the reactions proceed closer to equilibrium, the equilibrium constants play a more significant role in the product species concentrations yielding different results.

This discussion was purely meant to highlight some of the areas in which improvements to the model used in this work should be considered. With further information about the catalyst pellet characterisitics, these improvements to the model can be carried out.

Appendix B
Fluent User Input

The summary given in Appendix B is an example of the user input necessary to define the CFD model. The summary describes the models selected, the relaxation factors, the discretization schemes, and the material properties. The user input of the boundary conditions have not been covered in this summary as they can be found in chapter 3. The reaction mechanism was input through a user-defined function and can be found in Appendix C.

FLUENT
Version: axi, dp, segregated, spe, lam (axi, double precision, segregated, species, laminar)
Release: 6.2.16
Title:

Models

Model	Settings
Space	Axisymmetric
Time	Steady
Viscous	Laminar
Heat Transfer	Enabled
Solidification and Melting	Disabled
Radiation	None
Species Transport	Reacting (7 species)
Coupled Dispersed Phase	Disabled
Pollutants	Disabled
Soot	Disabled

Solver Controls

Equation	Solved
Flow	yes
c8h18	yes
o2	yes
co2	yes
n2	yes
co	yes
h2	yes
Energy	yes

Relaxation

Variable	Relaxation Factor
Pressure	0.5
Density	0.6
Body Forces	0.6
Momentum	0.5
c8h18	0.4
o2	0.5
co2	0.5
n2	0.5
co	0.5
h2	0.5
Energy	0.4

Discretization Scheme

Variable	Scheme
Pressure	PRESTO!
Momentum	Second Order Upwind
c8h18	Second Order Upwind
o2	Second Order Upwind
co2	Second Order Upwind
n2	Second Order Upwind
co	Second Order Upwind
h2	Second Order Upwind
Energy	Second Order Upwind

Solution Limits

Quantity	Limit
Minimum Absolute Pressure	1
Maximum Absolute Pressure	5e+10
Minimum Temperature	1
Maximum Temperature	5000

Material Properties

Material: silicon-carbide (solid)

Property	Units	Method	Value(s)
Density	kg/m3	constant	3220
Cp (Specific Heat)	j/kg-k	constant	650
Thermal Conductivity	w/m-k	constant	200

Material: pt-catalyst (solid)

Property	Units	Method	Value(s)
Density	kg/m3	constant	6500
Cp (Specific Heat)	j/kg-k	constant	500
Thermal Conductivity	w/m-k	constant	2

Material: inconel-625 (solid)

Property	Units	Method	Value(s)
Density	kg/m3	constant	8440
Cp (Specific Heat)	j/kg-k	constant	410
Thermal Conductivity	w/m-k	polynomial	(811,17.5) (922,19) (1033,20.8) (1144,22.8) (1255 25.3) (1366,28.2) (1477,31.5)

Material: (hydrogen . n-octane-air) (fluid)

Property	Units	Method	Value(s)
Cp (Specific Heat)	j/kg-k	polynomial	(500,14510) (750,14650) (1000,14980) (1100,15150) (1200,15340) (1400,15770)
Thermal Conductivity	w/m-k	constant	0.1672
Viscosity	kg/m-s	constant	8.411e-06
Molecular Weight	kg/kgmol	constant	2.01594
Standard State Enthalpy	j/kgmol	constant	-1881.377
Standard State Entropy	j/kgmol-k	constant	130579.06
Reference Temperature	k	constant	298.14999
L-J Characteristic Length	angstrom	constant	2.92
L-J Energy Parameter	k	constant	38
Degrees of Freedom		constant	0
Speed of Sound	m/s	none	#f

Material: (carbon-monoxide . n-octane-air) (fluid)

Property	Units	Method	Value(s)
Cp (Specific Heat)	j/kg-k	polynomial	(300,1040) (600,1087) (1000,1185) (1500,1257) (2000,1294) (2500,1315)
Thermal Conductivity	w/m-k	constant	0.025
Viscosity	kg/m-s	constant	1.75e-05
Molecular Weight	kg/kgmol	constant	28.01055
Standard State Enthalpy	j/kgmol	constant	-1.1053956e+08
Standard State Entropy	j/kgmol-k	constant	197531.64
Reference Temperature	k	constant	298.14999
L-J Characteristic Length	angstrom	constant	0
L-J Energy Parameter	k	constant	0
Degrees of Freedom		constant	0
Speed of Sound	m/s	none	#f

Material: (carbon-dioxide . n-octane-air) (fluid)

Property	Units	Method	Value(s)
Cp (Specific Heat)	j/kg-k	polynomial	(300,846) (600,1075) (1000,1234) (1500,1326) (2000,1371) (2500,1397)
Thermal Conductivity	w/m-k	constant	0.0145
Viscosity	kg/m-s	constant	1.37e-05
Molecular Weight	kg/kgmol	constant	44.009949
Standard State Enthalpy	j/kgmol	constant	-3.9353235e+08
Standard State Entropy	j/kgmol-k	constant	213720.2
Reference Temperature	k	constant	298.14999
L-J Characteristic Length	angstrom	constant	3.941
L-J Energy Parameter	k	constant	195.2
Degrees of Freedom		constant	0
Speed of Sound	m/s	none	#f

Material: (n-octane-vapor . n-octane-air) (fluid)

Property	Units	Method	Value(s)
Cp (Specific Heat)	j/kg-k	polynomial	(500,2513) (1000,3805) (1500,4428) (2000,4879)
Thermal Conductivity	w/m-k	constant	0.0178
Viscosity	kg/m-s	constant	6.75e-06
Molecular Weight	kg/kgmol	constant	114.22
Standard State Enthalpy	j/kgmol	constant	-2.09e+08
Standard State Entropy	j/kgmol-k	constant	0
Reference Temperature	k	constant	298.14999
L-J Characteristic Length	angstrom	constant	0
L-J Energy Parameter	k	constant	0
Degrees of Freedom		constant	0
Speed of Sound	m/s	none	#f

Material: (nitrogen . n-octane-air) (fluid)

Property	Units	Method	Value(s)
Cp (Specific Heat)	j/kg-k	polynomial	(300,1045) (600,1075) (1000,1164) (1500,1239) (2000,1283) (2500,1314)
Thermal Conductivity	w/m-k	constant	0.0242
Viscosity	kg/m-s	constant	1.663e-05
Molecular Weight	kg/kgmol	constant	28.013399
Standard State Enthalpy	j/kgmol	constant	0
Standard State Entropy	j/kgmol-k	constant	191494.78
Reference Temperature	k	constant	298.14999
L-J Characteristic Length	angstrom	constant	3.621
L-J Energy Parameter	k	constant	97.53
Degrees of Freedom		constant	0
Speed of Sound	m/s	none	#f

Material: (oxygen . n-octane-air) (fluid)

Property	Units	Method	Value(s)
Cp (Specific Heat)	j/kg-k	polynomial	(300,914) (600,1005) (1000,1084) (1500,1136) (2000,1175) (2500,1215)
Thermal Conductivity	w/m-k	constant	0.0246
Viscosity	kg/m-s	constant	1.919e-05
Molecular Weight	kg/kgmol	constant	31.9988
Standard State Enthalpy	j/kgmol	constant	0
Standard State Entropy	j/kgmol-k	constant	205026.86
Reference Temperature	k	constant	298.14999
L-J Characteristic Length	angstrom	constant	3.458
L-J Energy Parameter	k	constant	107.4
Degrees of Freedom		constant	0
Speed of Sound	m/s	none	#f

Material: (water-vapor . n-octane-air) (fluid)

Property	Units	Method	Value(s)
Cp (Specific Heat)	j/kg-k	polynomial	(300,1858) (600,2020) (1000,2275) (1500,2601) (2000,2833) (2500,2996)
Thermal Conductivity	w/m-k	constant	0.0261
Viscosity	kg/m-s	constant	1.34e-05
Molecular Weight	kg/kgmol	constant	18.015341
Standard State Enthalpy	j/kgmol	constant	-2.418379e+08
Standard State Entropy	j/kgmol-k	constant	188696.44
Reference Temperature	k	constant	298.14999
L-J Characteristic Length	angstrom	constant	2.605
L-J Energy Parameter	k	constant	572.4
Degrees of Freedom		constant	0
Speed of Sound	m/s	none	#f

Material: n-octane-air (mixture)

Property	Units	Method
Mixture Species: (c8h18, o2, co2, n2, co, h2, h2o)		
Reaction: finite-rate		
(reaction-1: 1c8h18 + 12.5o2 --> 8co2 + 9h2o)		
(reaction-2: 1c8h18 + 8h2o --> 8co + 17h2)		
(reaction-3: 1c8h18 + 8co2 --> 16co + 9h2)		
(reaction-4: 1c8h18 + 16h2o --> 8co2 + 25h2)		
(reaction-5: 1co + 1h2o --> 1co2 + 1h2)		
Density	kg/m3	incompressible-ideal-gas
Cp (Specific Heat)	j/kg-k	mixing-law
Thermal Conductivity	w/m-k	mass-weighted-mixing-law
Viscosity	kg/m-s	mass-weighted-mixing-law
Mass Diffusivity	m2/s	user-defined (diffusivity::EF001)
Thermal Expansion Coefficient	1/k	constant

Appendix C

User-defined Functions

The following code was written in C++ and incorporated into the Fluent software compiler to provide the user-defined functions describing the effective diffusivity and reaction rates in the Pacheco et al. (2003) chemical reaction model.

```
/**************************************************************************/
/* Reaction (1) Partial Oxidation                                          */
/*     C8H18 + 12.5O2 ->  8CO2 + 9H20                                      */
/* Reaction (2) Steam Reforming Reaction i                                 */
/*     C8H18 + 8H2O ->  8CO + 9H2O                                         */
/* Reaction (3) Carbon Reforming                                           */
/*     C8H18 + 8CO2 ->  16CO + 9H2                                         */
/* Reaction (4) Steam Reforming Reaction ii                                */
/*     C8H18 + 16H2O ->  8CO2 + 25H2                                       */
/* Reaction (5) Water-Gas Shift Reaction                                   */
/*     CO + H2O -> CO2 + H2                                                */
/**************************************************************************/

#include "udf.h"


/*This function defines the effective diffusivity term in equation 3.14*/

DEFINE_DIFFUSIVITY(diffusivity, c, t,i)
{
#define d_inf 0.000001

real D_eff;
real u = C_U(c, t);
real v = C_V(c, t);

D_eff=.000625*sqrt(u*u+v*v);

  return D_eff;
}


/* This function defines the volumetric rate of reaction of the Pacheco et al. (2003) mechanism*/

DEFINE_VR_RATE(rate,c,t,r,wk,yk,rate,rr_t)
{
```

```
/*Pre-exponential factors and Activation energies.  The pre-exponential factors are multiplied by
the density of the catalyst multiplied by the effectiveness factor*/
#define A1 2.58e8*1400*.001
#define A2 2.61e9*1400*.001
#define A3 2.78e-5*1400*.001
#define A4 1.52e7*1400*.001
#define A5 1.55e1*1400*.001
#define E1 166e3
#define E2 240.1e3
#define E3 23.7e3
#define E4 243.9e3
#define E5 67.1e3

/*Heats of adsorption (J/kmol) - taken from Xu (1989)*/
#define HCO -70.65e3
#define HH2 -82.9e3
#define HC8 -38.28e3
#define HH2O 88.68e3

/*Universal Gas Constant (J/mol*K) */
#define UGC 8.314

/*Adsorption pre-exponential constants (bar-1) - taken from Xu (1989) except H2O, taken from
 Pacheco et al. (2003)*/
#define ACO 8.23e-5
#define AH2 6.12e-9
#define AC8 6.65e-4
#define AH2O 1.57e4

/*Adsorption coefficient */
real KCO=ACO*exp(-HCO/(UGC*C_T(c,t)));
real KH2=AH2*exp(-HH2/(UGC*C_T(c,t)));
real KC8=AC8*exp(-HC8/(UGC*C_T(c,t)));
real KH2O=AH2O*exp(-HH2O/(UGC*C_T(c,t)));

/*Mass fractions*/
real mC8=C_YI(c,t,0);
real mO2=C_YI(c,t,1);
real mCO2=C_YI(c,t,2);
real mN2=C_YI(c,t,3);
real mCO=C_YI(c,t,4);
real mH2=C_YI(c,t,5);
real mH2O=C_YI(c,t,6);

/*Partial pressures*/
real pOp=1.01;                  /*operating pressure (bar)*/
real sum=(mC8/114+mO2/32+mCO2/44+mN2/28+mCO/28+mH2/2+mH2O/18);
real pC8=mC8/114/sum*pOp;
real pO2=mO2/32/sum*pOp;
real pCO2=mCO2/44/sum*pOp;
real pN2=mN2/28/sum*pOp;
real pCO=mCO/28/sum*pOp;
```

```
        real pH2=mH2/2/sum*pOp;
        real pH2O=mH2O/18/sum*pOp;

        /*Denominator variable "DET" used in rate expressions*/
        real DET=(1+KCO*pCO+KH2*pH2+KC8*pC8+KH2O*pH2O/(pH2));


        /* Initialize equilibrium constants */
        real K2;
        real K3;
        real K4;
        real K5;


        if (!strcmp(r->name, "reaction-2"))
        {K2=5.75e12*exp(-11476/((C_T(c,t))));
        *rate=A2*exp(-E2/(8.314*(C_T(c,t))))/pow((pH2),2.5)*(pC8*pH2O-
        (pH2*pH2*pH2*pCO/K2))/(DET*DET);}

        else if (!strcmp(r->name, "reaction-1"))
        {*rate=A1*exp(-E1/(8.314*(C_T(c,t))))*pC8*pO2;}

        else if (!strcmp(r->name, "reaction-3"))
        {K3=exp(-30782/C_T(c,t)+38.9)/(100*100);
        *rate=A3*exp(-E3/(8.314*(C_T(c,t))))*pC8*pCO2*(1-
        (pCO*pCO*pH2*pH2)/(K3*(pC8*pCO2)));}

        else if (!strcmp(r->name, "reaction-4"))
        {K4=7.24e10*exp(-21646/((C_T(c,t))));
        *rate=A4*exp(-E4/(8.314*(C_T(c,t))))/pow((pH2),3.5)*(pC8*pH2O*pH2O-
        pH2*pH2*pH2*pH2*pCO2/K4)/(DET*DET);}

        else if (!strcmp(r->name, "reaction-5"))
        {K5=.009475*exp(4804/(C_T(c,t)));
        *rate=A5*exp(-E5/(8.314*(C_T(c,t))))/pH2*(pCO*pH2O-pH2*pCO2/K5)/(DET*DET);}

        if (*rate>10) /* stops reaction rate from becoming unreasonable high; facilitates convergence */
        {*rate=10;}
        else if (*rate<-10)
        {*rate=-10;}


        *rr_t=*rate;
}
```